Juryboekje

studentenSTAALprijs 2021

Bachelor

B01

Saskia van der Velden

Circulair construeren, en nu?

KORTE OMSCHRIJVING VOOR EXPOSITIE:

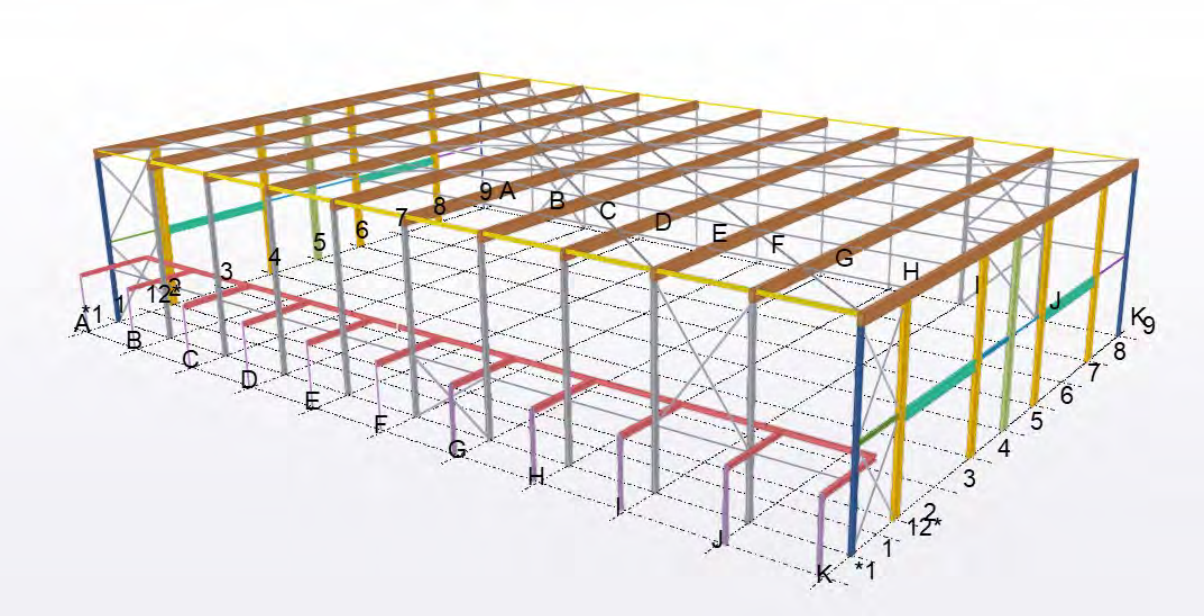

Door invoering van het VN-Klimaatakkoord[Parijs, 2016] dient de bouwbranche op verschillende vlakken te innoveren. Het onderzoek *"Circulair construeren, en nu?"* besteed aandacht aan het controleerbaarder maken van een circulair ontwerp voor een hoofddraagconstructie. Om dit te bereiken is een checklist met richtlijnen en/of eisen opgesteld. Deze is getoetst bij een lopend project om te inventariseren of de procedure uitvoerbaar is.

KORTE OMSCHRIJVING VOOR DE JURY:

Nederland heeft besloten in het kader van het VN-Klimaatakkoord van Parijs uit 2016 om in 2030 49% en in 2050 95% minder broeikasgassen uit te stoten ten opzichte van 1990. Verder is in januari 2017 het Grondstoffenakkoord ondertekend. Daarin is beschreven dat in Nederland in 2030 50% minder grondstoffen worden gebruikt en dat er in 2050 een economie is zonder afval en alles volledig draait op het hergebruik van grondstoffen. Om de doelen uit de akkoorden te behalen zijn er noodzakelijke veranderingen binnen de bouwbranche, maar hoe?

De bouwbranche houdt zich, net zoals IMd Raadgevende Ingenieurs, al langere tijd bezig met het ontwikkelen van duurzame methodes in de bouw. Op dit moment beschikt de bouwbranche nog niet over de juiste procedures om goed aan de slag te kunnen gaan met circulair construeren. Daarbij mist de informatie om circulaire constructies gedurende het ontwerpproces te controleren en toetsen, omdat er nog niet genoeg is gestandaardiseerd en gestructureerd.

Een eventuele oplossing is het opstellen van een procedure met richtlijnen en eisen voor het ontwerpen van circulaire constructie. De onderzoeksvraag van dit onderzoek luidt: "*Hoe kan de procedure van een circulaire constructie worden gedefinieerd, zodat deze manier van ontwerpen meer controleerbaar wordt voor de betrokken stakeholders, in specifiek de opdrachtgever IMd Raadgevende Ingenieurs?*".

Om de procedure goed op te kunnen zetten is gebruik gemaakt van kwalitatief onderzoek, bestaande uit literatuuronderzoek, onderzoeksprojecten en interviews met werkvelddeskundigen.

Om te beoordelen of de opgestelde procedure uitvoerbaar is in de praktijk wordt deze getest door het toe te passen bij een project. Om de procedure zoveel mogelijk te kunnen uitvoeren waren twee verschillende projecten nodig: een gebouw wat gebruikt mag worden als donorstaal en een nieuw te bouwen gebouw.
Voor het nieuw te bouwen gebouw heeft IMd Raadgevende Ingenieurs informatie verstrekt over een Nieuwbouw Sportaccommodatie te Waddinxveen. Dit betreft een sporthal voor een plaatselijke voetbalvereniging en voor basisscholen in de omgeving. Voor dit project is, voor het gebruik van donorstaal, een ander te demonteren pand beschikbaar gesteld. Dit pand betreft het P.T.T. V.C. gebouw te Waddinxveen.

Zoals eerder benoemd is de noodzaak van een procedure voor circulair construeren binnen de bouwbranche hoog. Dit om het ontwerpproces van circulaire constructies te structureren en standaardiseren voor betere controle en toetsing.
Uit onderzoek is gebleken dat de procedure die opgesteld kan worden aan de hand van richtlijnen en eisen. Hiervoor dienen de juiste technieken, methoden en middelen beschreven te worden, zoals demontabel verbinden, gebruiken van donorstaal en een LCA-berekening.
Door juiste communicatie en samenwerking tussen de 'uitvoerende partijen' en de overheid is het mogelijk om het doel te behalen waarbij het ontwerpproces voor circulair construeren controleerbaarder wordt.
Om het resultaat uit het onderzoek correct toe te passen in de praktijk is een checklist voor de uitvoering van de procedure gemaakt. Hierbij is bij elke stakeholder benoemd welke richtlijnen en eisen in het (werk)proces geïmplementeerd kunnen worden.

Verbindingen:

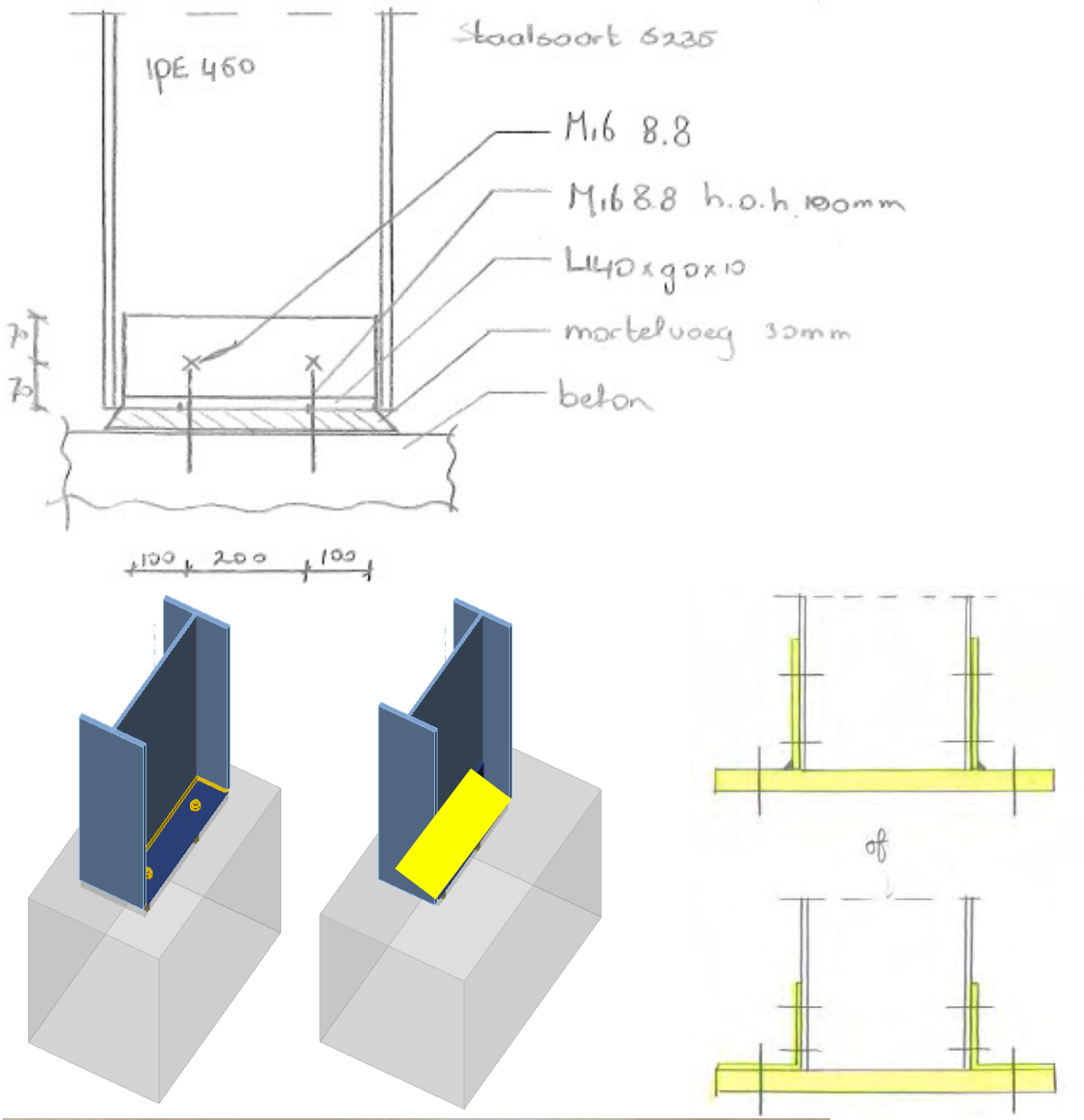

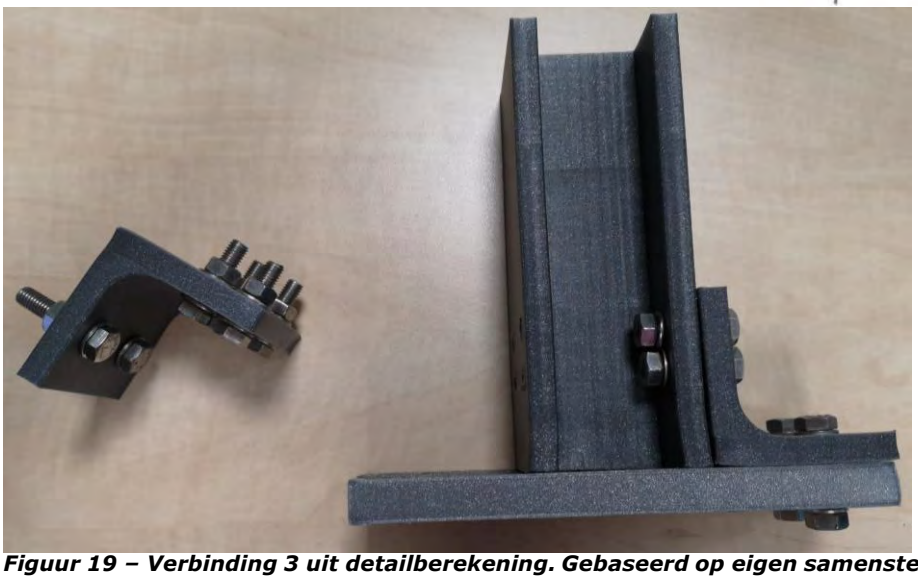

Figuur 19 – Verbinding 3 uit detailberekening. Gebaseerd op eigen samenstelling.

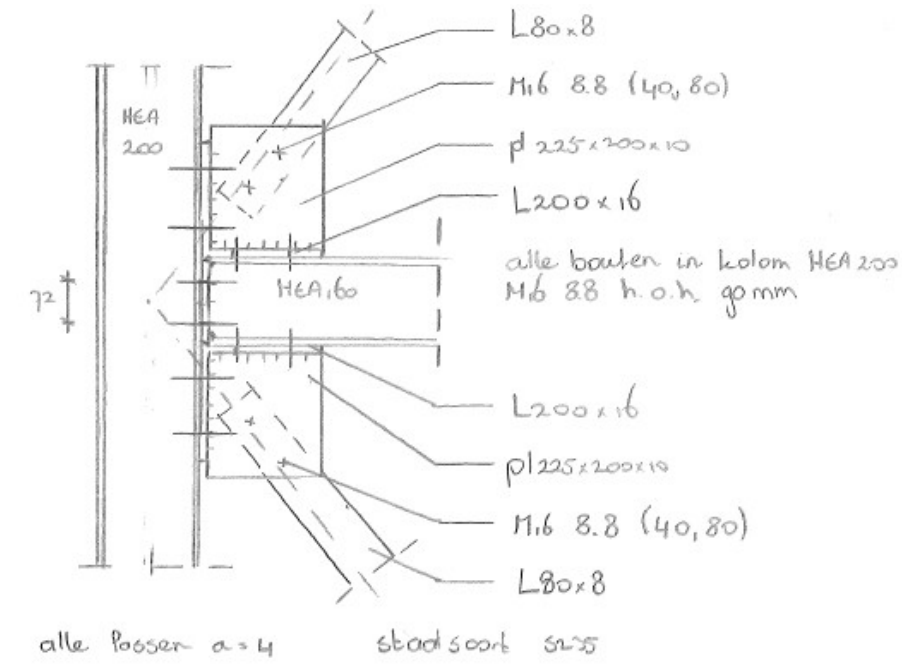

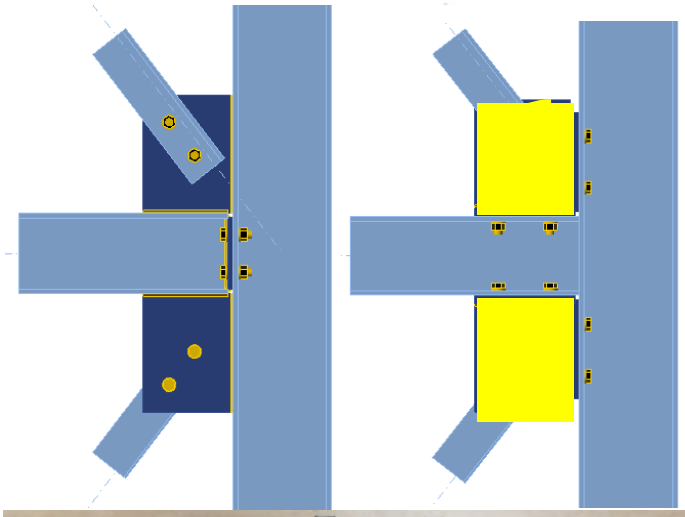

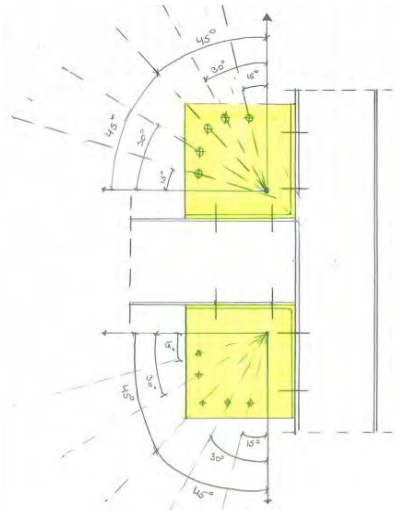

Figuur 20 – Verbinding 5 uit detailberekening. Gebaseerd op eigen samenstelling.

Andere verbindingen staan in bijlage 11.5 – detailberekeningsrapport.
Dit document is te vinden in het bijlage boek van pagina 774 tot pagina 931.

B02

Taylyan Orlinov

Hotel, spa en casino op het Katendrechtse Hoofd

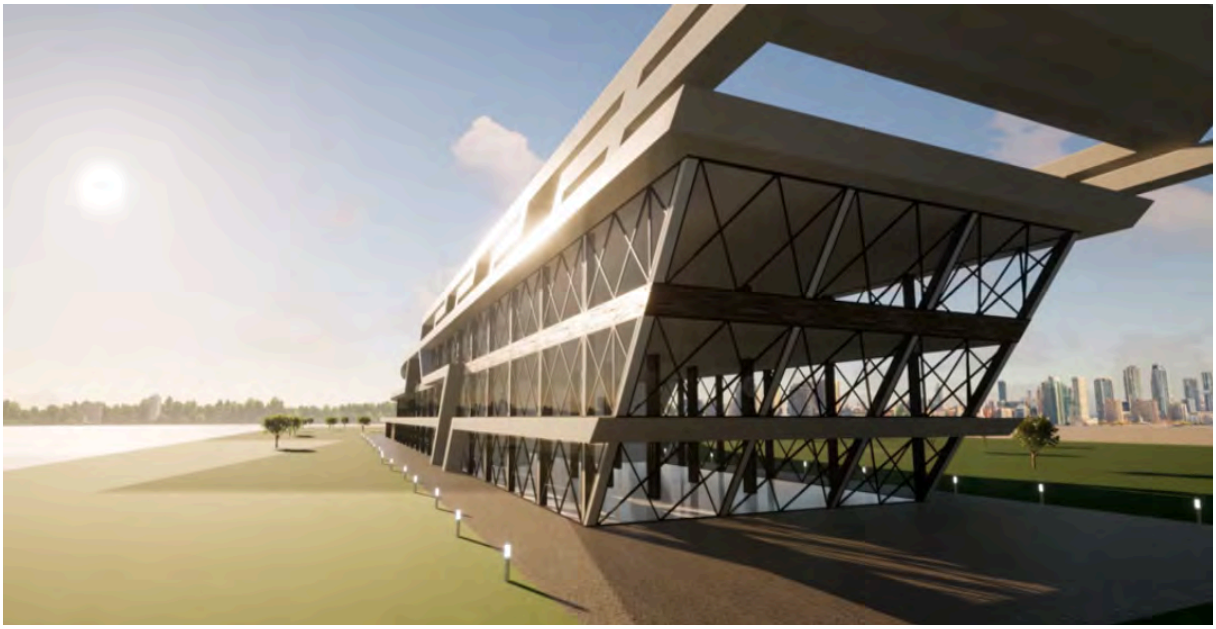

Elk jaar zit er een afstudeerproject bij, dat de jury van de staalSCHOOLprijs verrast en soms zelfs omverblaast. Dit jaar is dat het hotel, spa en casino van Taylyan Orlinov. Een prachtig gebouw, dat zijn inspiratie haalt bij het oeuvre van de helaas te vroeg gestorven Britse architecte Zaha Hadid. Met zijn soepele vormen en dynamisch lijnenspel hint Taylyan op de sensuele welvingen van de Evelyn Grace Academy in Londen. Het drielaagse gebouw slingert over het Katendrechtse Hoofd door een relaxed parklandschap en richt aan de Maas zijn kop op naar Rotterdam-Noord.

Niet alleen stedenbouwkundig, ook architectonisch zijn intelligente keuzes gemaakt. Bijvoorbeeld door de slingers die de lange gevels maken, verschillend te maken. Daardoor is het gebouw smal bij de ondiepe hotelkamers met middengang. En dik aan het andere einde bij het café met terras en het restaurant. Daartussen is er een verdikking die plaats biedt aan het kuuroord met zwembad, het casino en de luxe hotelkamers.

Daarbij is de keuze voor een staalskelet een logische. Want het diverse en complexe programma vindt soepel zijn plek tussen de ranke kolommen. Door in het slingerende deel het kolommenraster een kwartslag te draaien, past het programma van eisen helemaal makkelijk.

Bij de keuze en de detaillering van het vloersysteem ziet de jury verbeterpunten. Want de gekozen vloer met betonnen kanaalplaten is wel heel goed in rechthoeken maken. Maar bij driehoeken, ronde of andere onregelmatige vormen is het beter om een staalplaat-beton vloer te kiezen. Daarnaast is het klemmen van de vloer onder de bovenflens van het staalprofiel uitvoeringstechnisch niet mogelijk.

Desondanks was het voor de jury duidelijk, dat er dit jaar maar één winnaar kan zijn. Vanwege de prachtige ligging op de locatie, het doordachte concept, de intelligente toepassing van staal en de bijzonder fraaie architectuur, roept de jury Taylyan Orlinov unaniem uit tot winnaar van de studentenSTAALprijs MBO 2021!

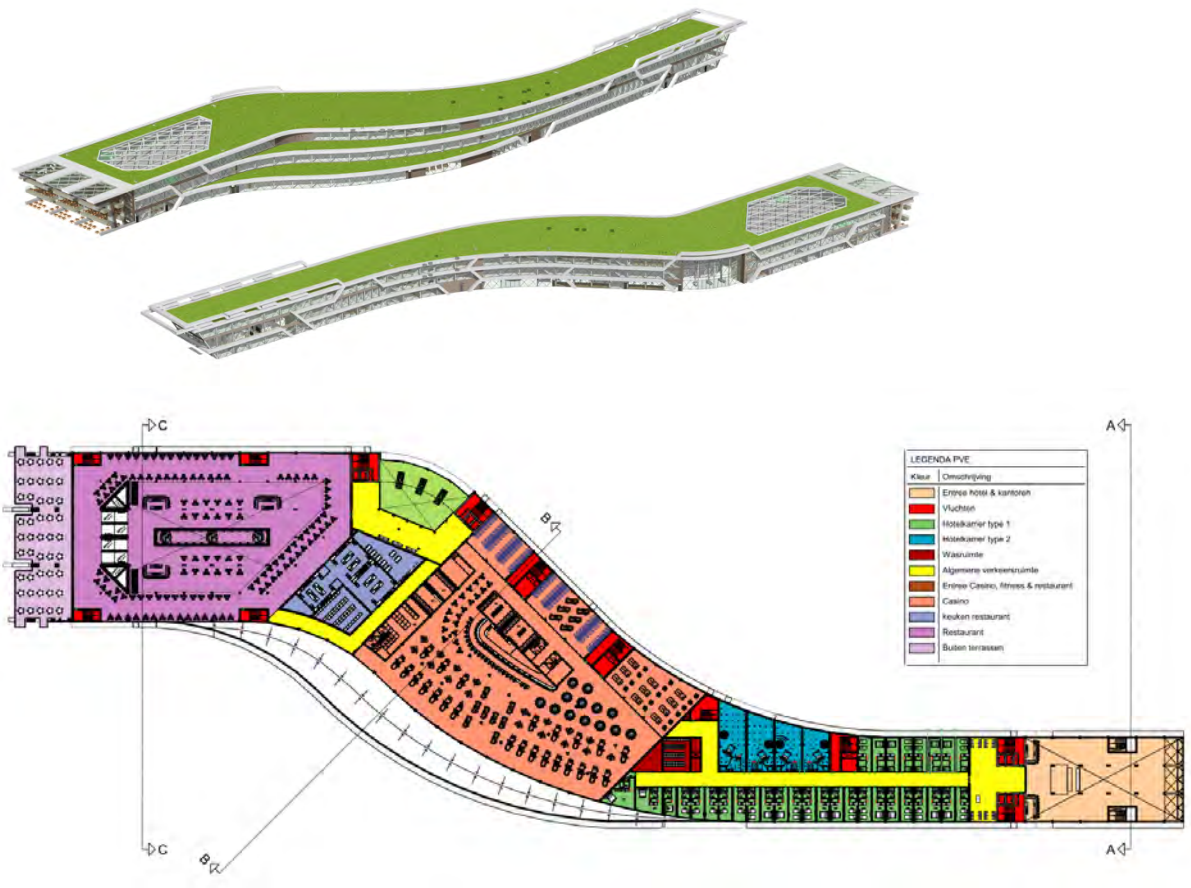

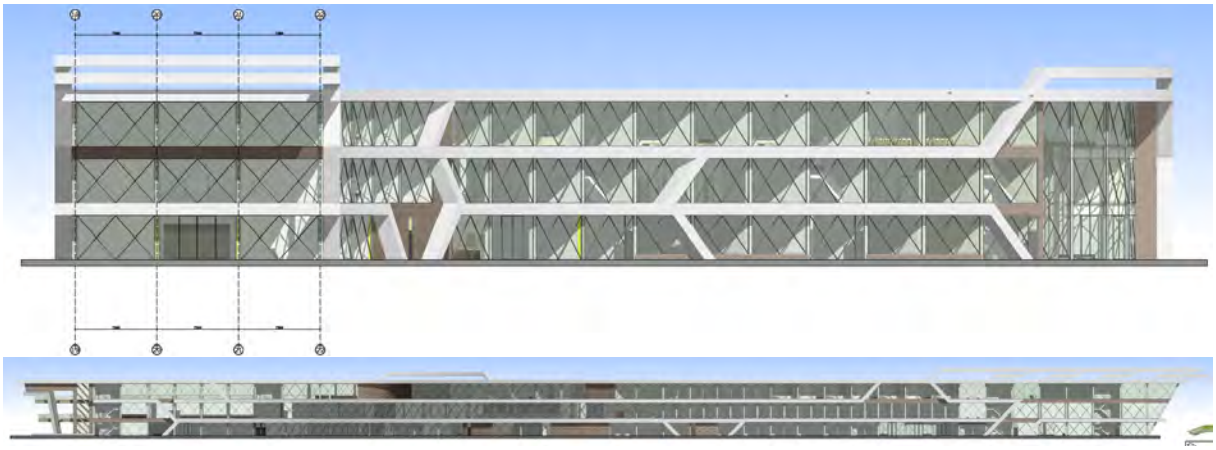

B03

Luc de Wit

Protocol voor materiaalkundige beoordeling van de herbruikbaarheid van utilitair constructiestaal

Omschrijving Project L. de Wit

Uit een algemene inventarisatie van zusteronderneming SGS Search is rond juni 2020 naar voren gekomen dat staalconstructies zeer geschikt zijn voor hoogwaardig hergebruik in een
2e of 3e levenscyclus. Voortkomend uit deze sessies is vanuit SGS INTRON het idee ontstaan een nieuwe dienst op te richten om staalconstructies op herbruikbaarheid te kunnen beoordelen middels een protocol. Een protocol geeft de markt meer zekerheid, waarmee hergebruik, als belangrijke strategie voor circulair bouwen, wordt gestimuleerd.

Het doel van dit onderzoek was het opstellen van een marktconform (toetsings-)protocol waarmee de herbruikbaarheid van utilitaire staalconstructies op uniforme wijze wordt beoordeeld en SGS INTRON deze als TIC-dienst (dienst voor Toetsing, Inspectie en Certificering) aan kan bieden.

Voor de structuurbepaling van het beoordelingsproces zijn drie gelijksoortige TIC-protocollen voor hergebruik van constructieve bouwelementen geanalyseerd op de beoordelings- structuur. Aan de hand van deze resultaten is een geschematiseerd beoordelingsproces opgesteld om de beoordelingsstructuur te visualiseren. Dit geschematiseerd beoordelingsproces is als leidraad gebruikt en afgestemd op de werkmethode van SGS INTRON. Daarbij zijn drie eerder door SGS INTRON uitgevoerde inspecties geanalyseerd en experts geïnterviewd, actief in verschillende fasen van het beoordelingsproces. Een
belangrijk aspect is dat het beoordelingsproces is afgestemd op het circulaire bouwproces. Hiervoor is het geschematiseerd beoordelingsproces uitgezet op een tijdrekenkundige weergave van het circulaire bouwproces. Dit heeft geleid tot inzichten, waar in het circulaire bouwproces, de verschillende processtappen uit het geschematiseerde beoordelingsproces actief zijn en welke stakeholders belang hebben bij het protocol.

Om tot een bruikbaar beoordelingsprotocol te komen is het geschematiseerde beoordelingsproces per processtap verder uitgewerkt. Hierbij zijn onder andere de minimaal benodigde vast te stellen materiaaleigenschappen, verschillende verwerkingsscenario’s en non- en destructieve inspectiemethoden gedefinieerd. Dit heeft geresulteerd in:

1. Definitie vier primaire verwerkingsscenario's voor CE-markering bij hergebruik: Door onderscheid te maken tussen vier primaire verwerkingsscenario's voor hergebruik van constructieve staalelementen, is per verwerkingsscenario inzichtelijk wanneer constructieve staalelementen van een CE-markering dienen te worden voorzien.

2. Model voor classificatie constructieve staalelementen in hergebruikklassen: Het beoordelingsproces voor hergebruik van constructieve staalelementen is vastgelegd in een model van hergebruikklassen (klasse A t/m G). Hierdoor ontstaat een transparant en uniform beoordelingsproces doordat per verwerkingsscenario de benodigde gegevens en materiaalkundige beoordeling zijn gedefinieerd en uitgezet in een beslissingstabel. Afwijkingen en vrije inttrepetatrie in het beoordelingsproces worden hiermee voorkomen.

Het eindproduct is een beoordelingsprotocol waarmee constructiestaal, teruggewonnen uit utilitaire bouwwerken, met zekerheid kan worden hergebruikt door een transparante en uniforme toetsing, inspectie en certificering. Het protocol is vooralsnog bestemd voor intern gebruik voor SGS INTRON. Er wordt geen definitief certificeringssysteem ontwikkeld omdat daarvoor ook andere bijkomende zaken moeten worden onderzocht, zoals aansprakelijkheid bij certificering en marktpotentie voor een commerciële dienst, die buiten het onderzoek vallen. SGS INTRON heeft wel voornemens het onderzoek op een geschikt moment om te zetten naar een commerciële dienst.

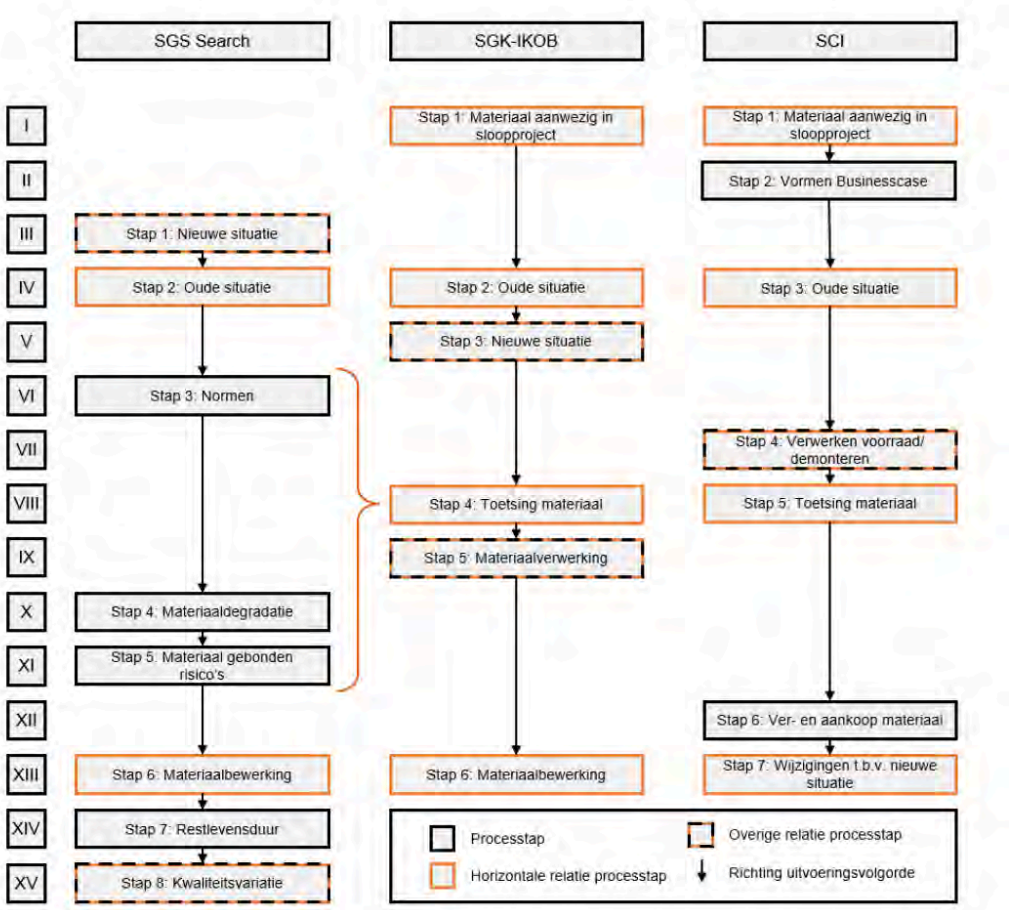

Figuur 3-4: Schematische vergelijking van de drie beoordelingsprocessen

Lucas de Wit

Digitaal onderteken d door Lucas de Wit
Datum: 2021.09.05 13:12:37 +02'00'

SGS

PROTOCOL VOOR MATERIAALKUNDIGE BEOORDELING VAN DE HERBRUIKBAARHEID VAN UTILITAIR CONSTRUCTIESTAAL

SGS INTRON

17 Mei 2021
Sittard

Auteur:
Lucas de Wit

Versie: Definitief
Project nr. 17052021

4 STAPPENPLAN

Om te bepalen of constructieve staalelementen geschikt zijn voor hergebruik, dienen de volgende processtappen te worden doorlopen, zie figuur 4-1. Ter vergemakkelijking van het beoordelingsproces zijn in bijlage E aanvullende beslissingsschema's opgenomen.

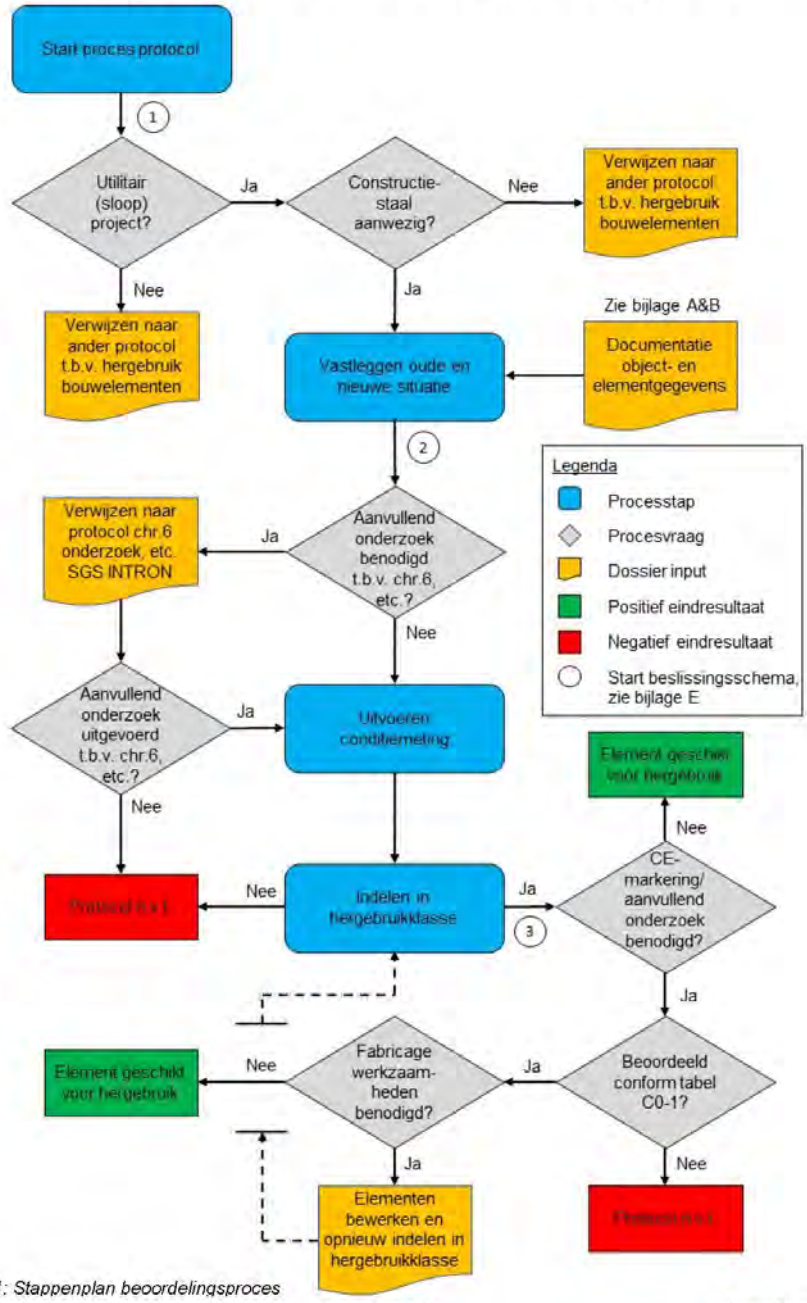

Figuur 4-1: Stappenplan beoordelingsproces

Beslissingsschema 2:

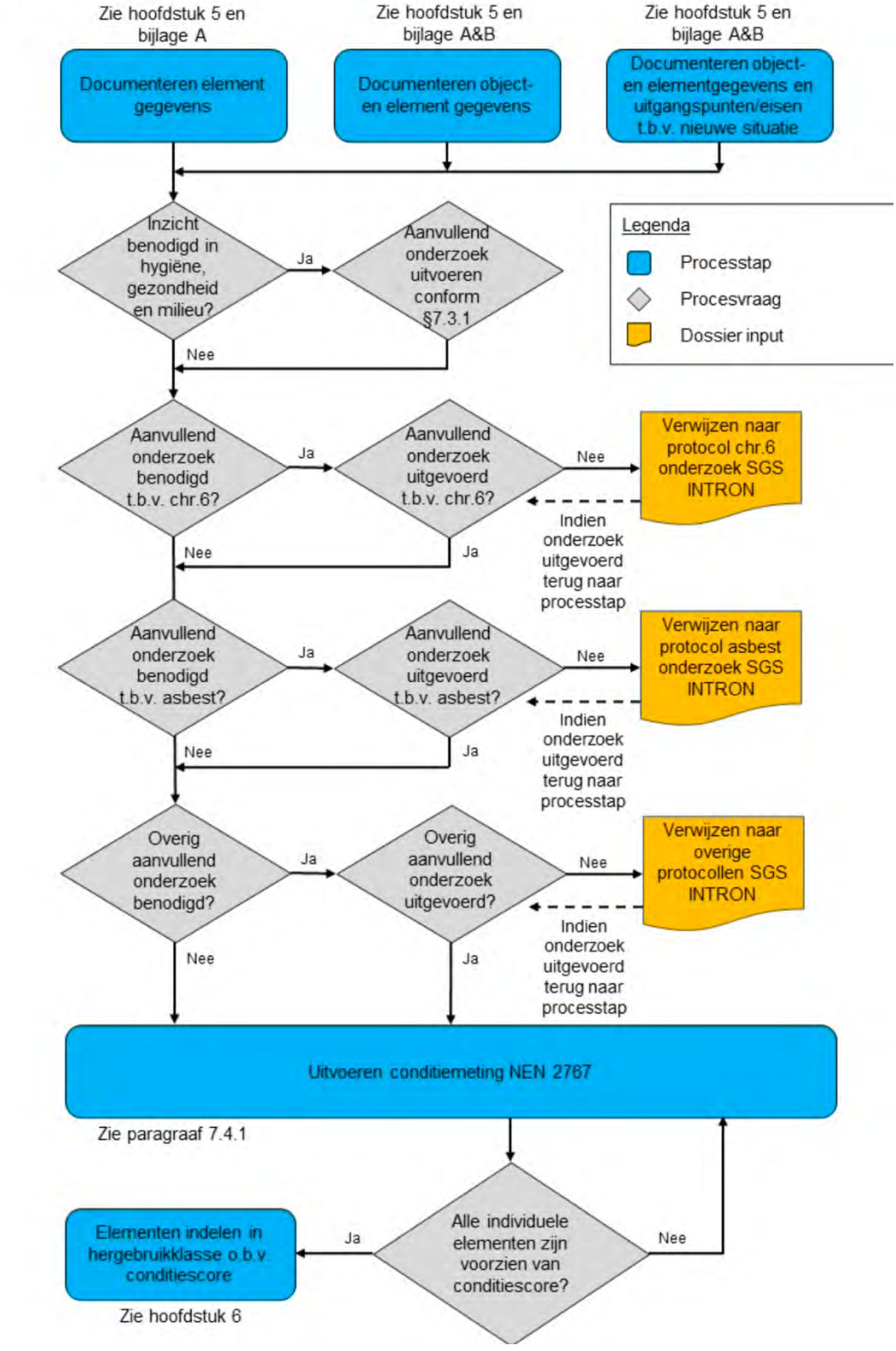

Master

M01

Dirk van der Laan

Structural Optimization of Stiffened Plates Application on an Orthotropic Steel Bridge Deck

Structural Optimization of Stiffened Steel Plates

Application on an Orthotropic Steel Deck

Samenvatting expositie (69 woorden)

Door het ontwerp van een orthotroop stalen brugdek (OSD) wiskundiger aan te pakken, kon de optimalisatie ervan grotendeels geautomatiseerd worden. Hieruit bleek dat een gewichtsbesparing van ruim zeventien procent mogelijk is door de dikte van de dekplaat te halveren en de trogbreedte sterk te verkleinen. Dit betekent een duidelijke breuk met het conventionele ontwerp van OSD's, waarin al sinds de jaren '50 een trogbreedte van 300 mm wordt gebruikt.

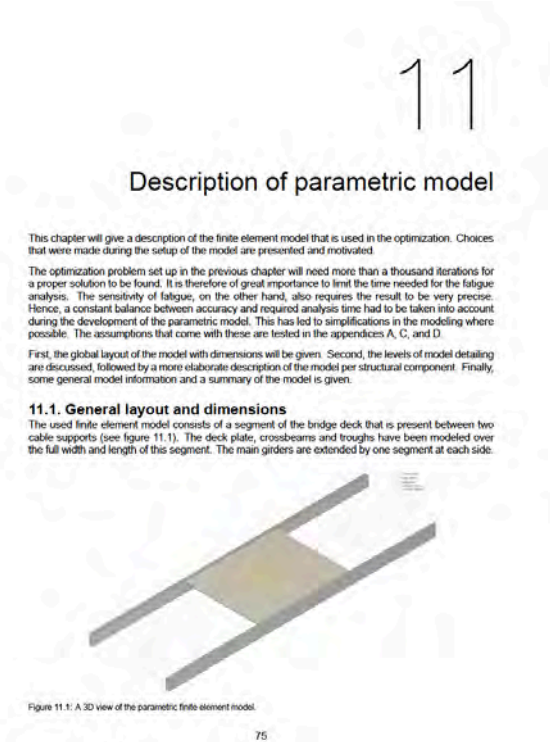

11

Description of parametric model

This chapter will give a description of the finite element model that is used in the optimization. Choices that were made during the setup of the model are presented and motivated.

The optimization problem set up in the previous chapter will need more than a thousand iterations for a proper solution to be found. It is therefore of great importance to limit the time needed for the fatigue analysis. The sensitivity of fatigue, on the other hand, also requires the result to be very precise. Hence, a constant balance between accuracy and required analysis time had to be taken into account during the development of the parametric model. This has led to simplifications in the modeling where possible. The assumptions that come with these are tested in the appendices A, C, and D.

First, the global layout of the model with dimensions will be given. Second, the levels of model detailing are discussed, followed by a more elaborate description of the model per structural component. Finally, some general model information and a summary of the model is given.

11.1. General layout and dimensions

The used finite element model consists of a segment of the bridge deck that is present between two cable supports (see figure 11.1). The deck plate, crossbeams and troughs have been modeled over the full width and length of this segment. The main girders are extended by one segment at each side.

Figure 11.1: A 3D view of the parametric finite element model.

75

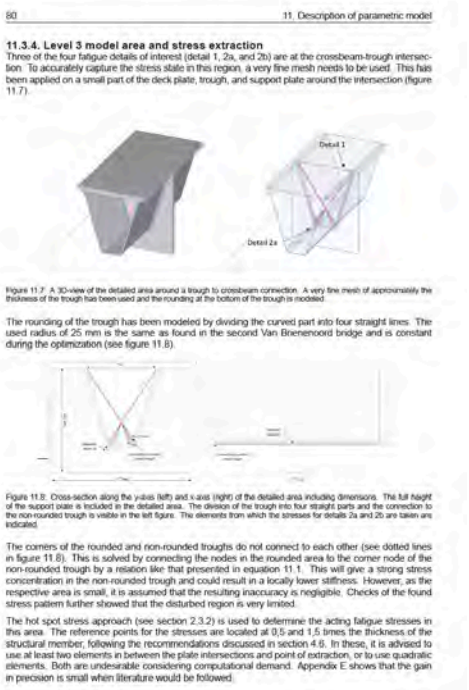

80 11. Description of parametric model

11.3.4. Level 3 model area and stress extraction

Three of the four fatigue details of interest (detail 1, 2a, and 2b) are at the crossbeam-trough intersection. To accurately capture the stress state in this region, a very fine mesh needs to be used. This has been applied on a small part of the deck plate, trough, and support plate around the intersection (figure 11.7).

Detail 1

Detail 2a

Figure 11.7: A 3D-view of the detailed area around a trough to crossbeam connection. A very fine mesh of approximately the thickness of the trough has been used and the rounding at the bottom of the trough is modeled.

The rounding of the trough has been modeled by dividing the curved part into four straight lines. The used radius of 25 mm is the same as found in the second Van Brienenoord bridge and is constant during the optimization (see figure 11.8).

Figure 11.8: Cross-section along the y-axis (left) and x-axis (right) of the detailed area including dimensions. The full height of the support plate is included in the detailed area. The division of the trough into four straight parts and the connection to the non-rounded trough is visible in the left figure. The elements from which the stresses for details 2a and 2b are taken are indicated.

The corners of the rounded and non-rounded troughs do not connect to each other (see dotted lines in figure 11.8). This is solved by connecting the nodes in the rounded area to the corner node of the non-rounded trough by a relation like that presented in equation 11.1. This will give a strong stress concentration in the non-rounded trough and could result in a locally lower stiffness. However, as the respective area is small, it is assumed that the resulting inaccuracy is negligible. Checks of the found stress pattern further showed that the disturbed region is very limited.

The hot spot stress approach (see section 2.3.2) is used to determine the acting fatigue stresses in this area. The reference points for the stresses are located at 0,5 and 1,5 times the thickness of the structural member, following the recommendations discussed in section 4.6. In these, it is advised to use at least two elements in between the plate intersections and point of extraction, or to use quadratic elements. Both are undesirable considering computational demand. Appendix E shows that the gain in precision is small when literature would be followed.

Samenvatting juryrapport (316 woorden)

Een orthotroop stalen dek (OSD) bestaat uit een stalen plaat verstijfd door constructieve elementen in twee richtingen die loodrecht op elkaar staan. Door de hoge efficiëntie van het systeem is het een veelgebruikte oplossing voor bruggen met een grotere overspanning, waar het grootste deel van de belasting op de constructie wordt veroorzaakt door het eigen gewicht. OSD's zijn echter ook erg gevoelig voor vermoeiing, waardoor de constructieve analyse van dit soort dekken complex en tijdrovend is. Optimalisatie van het ontwerp op conventionele wijze is hierdoor praktisch onmogelijk.

In dit onderzoek is daarom gebruik gemaakt van de meer wiskundig georiënteerde technieken vanuit *Structural Optimization* om het eigen gewicht van een orthotroop dek te minimaliseren, terwijl de eisen voor vermoeiing worden gerespecteerd. Het renovatieontwerp van de Van Brienenoordbrug is hierbij gebruikt als case study. In het eerste deel van het onderzoek is *parametrische optimalisatie* beschouwd en werd een workflow ontwikkeld die automatisch de optimale afmetingen voor een OSD kan bepalen. Het tweede deel richtte zich op *topologieoptimalisatie*, waarmee getracht werd een verbeterde plaatsing van verstijvende elementen te vinden.

De parametrische optimalisatie uit het eerste deel leidde uiteindelijk tot een gewichtsbesparing van ruim zeventien procent (280 kg/m² in plaats van 339 kg/m²). Deze reductie werd bereikt door de dikte van de dekplaat te halveren, wat mogelijk werd gemaakt door de afstand tussen en de breedte van de verstijvende troggen sterk te verkleinen. Hiervoor wordt al sinds de introductie van OSD's in de jaren '50 een waarde van 300 mm voor gebruikt. Deze keuze is toentertijd echter gebaseerd op statische capaciteit, niet op vermoeiing. Een schatting van kosten liet bovendien zien dat de prijs van het geoptimaliseerde ontwerp vergelijkbaar is met het originele ontwerp van de case study.

Uit de topologieoptimalisaties van het tweede deel bleek dat de conventionele loodrechte plaatsing van verstijvende elementen de voorkeur houdt. Meer onderzoek is echter nodig voordat deze conclusie als definitief kan worden gezien.

M02

Marc Nijenhuis

Penetrated CHS X-joints in steel

Penetrated CHS X-joints are widely applied in civil industry. This joint is characterized by penetration of the chord by the brace member. Although EC design rules are available for standard non-penetrated X-joints, there are no specific design rules for their penetrated equivalents and therefore the structural behavior of these joints and the possible differences with non-penetrated joints are studied. A FE analyses with extensive
parameter study is conducted from which a clear and uniform set of design rules for penetrated CHS X-joints is developed.

C.2.2 Single-sided compression (F_x) – β 0.2

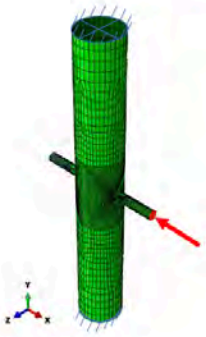

Eurocode results:

1 Brace cross-section fail.:	$N_{pl,Rd}$ Design plastic resistance	
2δ 10	2331	kN
2δ 30	835	kN
2δ 50	508	kN

2 Chord face failure:	$N_{pl,Rd}$ Design plastic resistance	
2γ 10	9579	kN
2γ 30	1326	kN
2γ 50	529	kN

1 Chord bending moment:	$N_{pl,Rd}$ Design plastic resistance	
2γ 10	21632	kN
2γ 30	8288	kN
2γ 50	5110	kN

2 Chord punching shear:	$N_{pl,Rd}$ Design plastic resistance	
2γ 10	7478	kN
2γ 30	2493	kN
2γ 50	1496	kN

Finite element results:

β 0.2 – 2γ 10

Model	Yield Load (kN)	RF1.1 (kN)	RF1.2 (kN)	RF1 (kN)
2δ 10	2336.7	2869.9	Not reached	2869.9
2δ 30	834.8	894.4	Not reached	894.4
2δ 50	508.4	513.8	Not reached	513.8

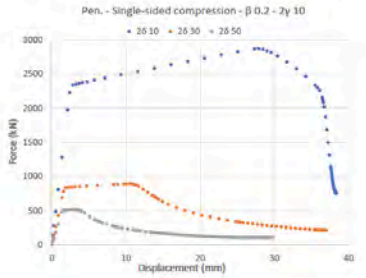

β 0.2 – 2γ 30

Model	Yield Load (kN)	RF1.1 (kN)	RF1.2 (kN)	RF1 (kN)
2δ 10	2333.4	2757.1	Not reached	2757.1
2δ 30	837.6	882.7	Not reached	882.7
2δ 50	509.4	509.4	Not reached	509.4

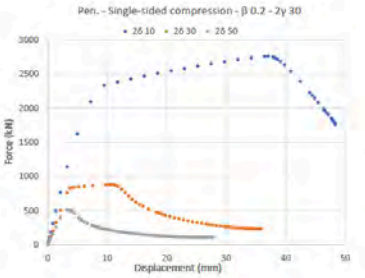

β 0.2 – 2γ 50

Model	Yield Load (kN)	RF1.1 (kN)	RF1.2 (kN)	RF1 (kN)
2δ 10	1165.5	2846.9	2693.1	2693.1
2δ 30	822.3	856.5	Not reached	856.5
2δ 50	504.0	504.0	Not reached	504.0

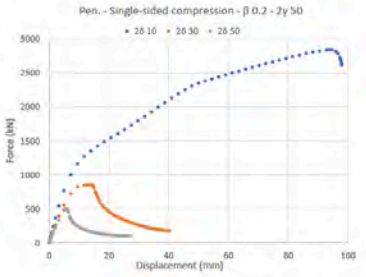

C.2.2.3 *Penetrated model – Single-sided compression – β 0.2 – 2γ 50*

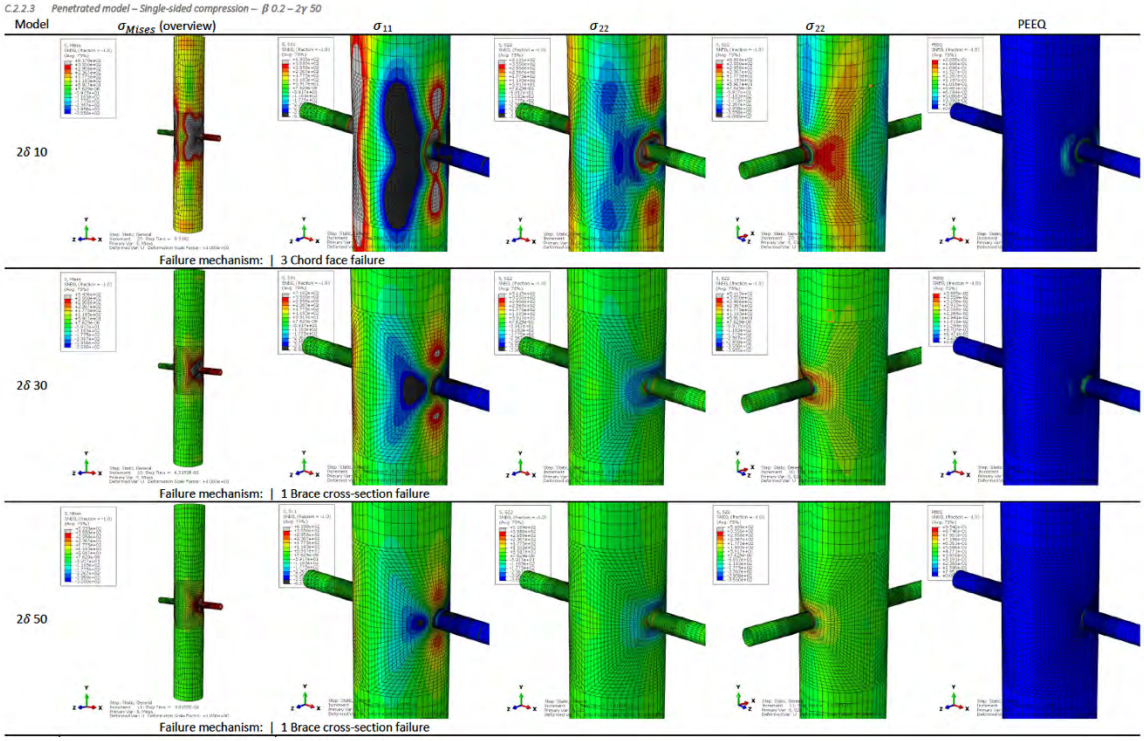

5.6.4 Case study | Mooring bollard Witteveen+Bos

To be able to check the mooring bollard of Witteveen+Bos, as shown in Figure 52, the calculation sheet has been adjusted to allow for eccentricities in the Y- and Z-direction (e_y = 375mm, and e_z = 450mm). Due to these eccentricities, the additional bending and torsional moments are introduced in the joint. Figure 53 elaborates on the calculation of these additional bending and torsional moments. Eventually, the following forces & moments that are acting on the brace, have to be taken into account:

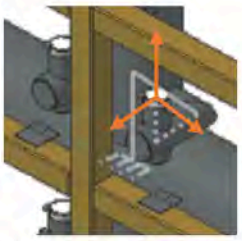

Figure 52: Model Witteveen+Bos

- Single-sided tension/compr. (F_x)
  - N_{Ed}
  - $M_{z,Ed}$ ($F_{x,Ed}*e_y$)
  - $M_{y,Ed}$ ($F_{x,Ed}*e_z$)
- Shear F_y (chord bending moment)
  - $V_{y,Ed}$
  - $M_{x,Ed}$ ($V_{y,Ed}*e_z$)
- Shear F_z (chord torsional moment)
  - $V_{z,Ed}$
  - $M_{x,Ed}$ ($V_{z,Ed}*e_y$)

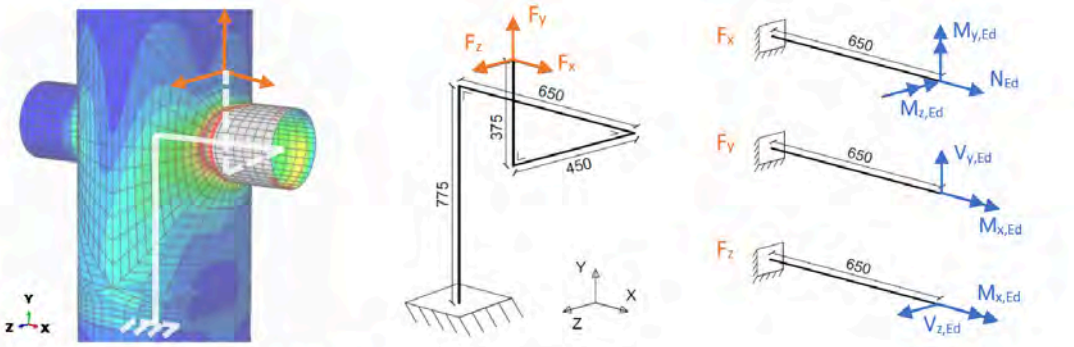

Figure 53: Mechanical scheme and acting forces

Table 51: Design checks – joint failures method 1 & 2

Joint failures method 1		
Chord face failure tension (F_x)		
N_{Ed}		Input (N_{Ed})
$Pen_{Cff,x}$		$1.1*(k_p*f_{y0}*t_0*d_1*f_\delta*f_\beta)/\sin\theta_1/\gamma_{M5}$
f_δ		$1+(50-2\delta)/200$
f_β		$(\sin(0.65*\beta*\pi)-\beta+0.8)$
	$UC_{Cff,x}$	$N_{Ed}/Pen_{cff,x}$
Chord face failure shear F_y		
$V_{y,Ed,1}$		Input ($V_{y,Ed}$)
$V_{y,Ed,2}$		$F_{X,Ed}*e_y/e_x$
$V_{y,Ed,tot}$		$V_{y,Ed,1}+V_{y,Ed,2}$
$Pen_{Cff,y}$		$3*(k_p*f_{y0}*t_0*d_1*d_0)/(L_1*\sin\theta_1)/\gamma_{M5}$
	$UC_{Cff,y}$	$V_{y,Ed,tot}/Pen_{cff,y}$
Chord face failure shear F_z		
$V_{z,Ed,1}$		Input ($V_{z,Ed}$)
$V_{z,Ed,2}$		$F_{X,Ed}*e_z/e_x$
$V_{z,Ed,tot}$		$V_{z,Ed,1}+V_{z,Ed,2}$
$Pen_{Cff,z}$		$1.7*(k_p*f_{y0}*t_0*d_1*d_0)/(L_1*\sin\theta_1)/\gamma_{M5}$
	$UC_{Cff,z}$	$V_{z,Ed,tot}/Pen_{cff,z}$
Chord bending moment (torsional moment brace)		
T_{Ed}		Input (M_x)
$M_{T,pl,Rd}$		$W_{pl}*f_{y0}$
	UC_{Cbm}	$T_{Ed}/M_{T,pl,Rd}$
Combination		
	UC	$UC_{Cff,x}+(UC_{Cff,y})^2+UC_{Cff,z}+UC_{Cbm,x}$
$UC_{joint\ failures}$		

Joint failures method 2		
Chord face failure tension (F_x)		
N_{Ed}		Input (N_{Ed})
$Pen_{Cff,x}$		$1.1*(k_p*f_{y0}*t_0*d_1*f_\delta*f_\beta)/\sin\theta_1/\gamma_{M5}$
f_δ		$1+(50-2\delta)/200$
f_β		$(\sin(0.65*\beta*\pi)-\beta+0.8)$
	$UC_{Cff,x}$	$N_{Ed}/Pen_{cff,x}$
Chord face failure shear F_y		
$V_{y,Ed}$		Input ($V_{y,Ed}$)
$Pen_{Cff,y}$		$3*(k_p*f_{y0}*t_0*d_1*d_0)/(L_1*\sin\theta_1)/\gamma_{M5}$
	$UC_{Cff,y}$	$V_{y,Ed}/Pen_{cff,y}$
Chord face failure shear F_z		
$V_{z,Ed}$		Input ($V_{z,Ed}$)
$Pen_{Cff,z}$		$1.7*(k_p*f_{y0}*t_0*d_1*d_0)/(L_1*\sin\theta_1)/\gamma_{M5}$
	$UC_{Cff,z}$	$V_{z,Ed}/Pen_{cff,z}$
Chord bending moment M_x (torsional moment brace)		
T_{Ed}		Input (M_x)
M_{pl}		$W_{pl}*f_{y0}$
	$UC_{Cbm,x}$	T_{Ed}/M_{pl}
Chord bending moment M_z (F_x*e_y)		
$M_{z,Ed}$		$F_{X,Ed}*e_y$
M_{pl}		$W_{pl}*f_{y0}$
	$UC_{Cbm,z}$	$M_{z,Ed}/M_{pl}$
Chord torsional moment M_y (F_x*e_z)		
$M_{y,Ed}$		$F_{X,Ed}*e_z$
$T_{pl,Rd}$		W_T*f_y
	$UC_{Ctm,y}$	$M_{z,Ed}/T_{pl,Rd}$
Combination		
	UC	$UC_{Cff,x}+(UC_{Cff,y})^2+UC_{Cff,z}+UC_{Cbm,x}+(UC_{Cbm,z})^2+UC_{Ctm,y}$
$UC_{joint\ failures}$		

ABSTRACT

Steel circular hollow sections (CHS) are widely used for structures in the civil industry, such as mooring and off-shore structures. A common joint in these structures is the X-joint, in which two coaxial braces are connected to either side of the chord, the main structural element. In most cases, the braces are welded to the chord, without penetrating it at the intersection. However, in civil structures, another type of X-joint for circular hollow sections is frequently used. These joints are referred to as penetrated CHS X-joints in which the brace passes through the chord. Although penetrated CHS X-joints are frequently applied by Dutch engineering firms in civil structures and extensive guidelines and rules are available for non-penetrated X-joints, there are no specific design rules available for penetrated CHS X-joints and available research into these joints is limited.

This research focused on gaining insight into and predicting the behavior of penetrated CHS X-joints. Since very limited research has been done into this type of CHS X-joints, literature and existing research into a comparable penetrated connection, plate-to-structural hollow sections (SHS), has been studied. Analogous to the penetrated CHS X-joints and their non-penetrated equivalents, the behavior of through plate joints is compared with their corresponding branched plate equivalents. It has been found that the former has a capacity of more than double till even three times the capacity of their equivalent branched plate joints.

A similar increase in capacity is expected for penetrated CHS X-joints. To gain insight into the structural behavior of the penetrated joints and the possible differences with respect to their non-penetrated equivalents, a parameter study consisting of 388 finite element (FE) analyses is conducted in which applied loads and geometrical dimensions are varied. For this purpose a FE model is created using a python script. The script is imported in the FE software ABAQUS, which is used to perform a geometrical and material non-linear FE analysis. An elastic-plastic material model with linear strain hardening, as provided in Eurocode (EC) EN 1993-1-5 is adopted.

In the parameter study for several load cases the geometrical parameters, the brace width-to-chord width ratio β, the chord diameter to thickness ratio 2γ, and the brace diameter to thickness ratio 2δ are varied within a certain range that is common for applicantions in civil structures. The parameter study is performed for penetrated, as well as for non-penetrated, CHS X-joints. Initially only the boundary values of the geometrical parameters are simulated to identify the critical areas for which the current set of design rules insufficiently describe the behavior of the joint and the capacity of the penetrated CHS X-joint is underestimated significantly. Based on these results, additional parameter configurations have been evaluated using finite element analysis (FEA). The parameter study is performed for the load cases "Double-sided compression and tension (F_x)", "Single-sided compression and tension (F_x)", "Bending moment about the Y-axis (M_y)", "Bending moment about the Z-axis (M_z)", "Shear F_y (chord bending moment)", and "Shear F_z (chord torsional moment)".

It appears that for several load cases, the design rules for non-penetrated CHS X-joints, as provided in the EN 1993-1-8, do not suffice for penetrated CHS X-joints in those critical areas. The critical areas are identified and evaluated and based on the FEA results, improved and new design rules for penetrated joints are created for the load cases for which this is required: "Single-sided compression and tension (F_x)", "Shear in the Y-direction (F_y)", and "Shear in the Z-direction (F_z). For the load cases "Double-sided compression and tension (F_x)" and "Bending moment about the Y- (M_y) and Z-axis (M_z)" the behavior can be approximated accurately with the basic cross-section design rules from the EC, and therefore, the EC design rules for non-penetrated joint failures should for penetrated geometries in these load cases, be omitted while calculating the governing failure mechanisms and the corresponding plastic design resistances. The new sets of design rules for penetrated CHS X-joints are evaluated and the behavior of penetrated CHS X-joints subjected to the aforementioned failure mechanisms can be described well. Additionally, the application of the new design rules for penetrated CHS X-joints is validated for combined load cases. The research is concluded with a clear and uniform set of design rules that can be used for the calculation of penetrated CHS X-joints.

M03

Christiaan Jilderda

Fatigue in Tubular Structures

Project description for student STEEL award 2021

Exhibition description (approximately 60 words)

The fatigue assessment for tubular structures can become a very complex and time-consuming process. In order to gain insight in this process, a design tool was created in Grasshopper, that can analyze and optimize the fatigue performance of tubular structures in a parametric way, very early in the design process.

Contents

- Problem statement
- Fatigue theory
- Fatigue assessment
- Design tools
- Case studies
- Conclusion

Description for the jury

Fatigue is a material failure mechanism that might lead to problems when it is not considered in the design phase. There seems to be a trend that fatigue assessment is becoming more important in structural engineering. For tubular structures, fatigue assessment is generally done by using analytical formulas to determine the hot-spot stress. These formulas are complex and the design parameters are intertwined in multiple components of the fatigue assessment, which makes it
hard for an engineer to estimate the impact of his design choices.

To gain insight in these parameters, one design tool is developed from scratch, and two existing software tools are programmed to perform fatigue calculations. The new design tool, called Fatigue Design & Assessment tool, is made in Excel. The two existing tools are Smart Synthesis Tool and Grasshopper. Two case studies are performed to analyze how the design tools can be used to optimize the fatigue characteristics of a design.

Each of the software tools provides insight in the design parameters, but all on a different level. The FDA tool can exactly tell how changing one certain parameter affects the outputs. The SST provides insight by creating and comparing many solutions within the solution space. The Grasshopper software offers an engineer insight in the fatigue performance while he is still creating the initial shape of the structure. A great advantage of Grasshopper is that no external software is needed to perform the structural analysis, which is input for the fatigue assessment.

The case studies have shown that with the insight provided by the design tools, an engineer is able to improve his design with regard to fatigue life, structure mass, weld volume or combined costs of materials and welding. In the first case study, one proposed concept shows a possible increase in fatigue life of 20%. A different concept shows that a mass reduction of 24% can be achieved, while maintaining the original fatigue life of 50 years.

In the second case study a concept is created in Grasshopper with a slightly different overall geometry. With this concept an improvement in fatigue life of 286% compared to the original design is achieved. The results from both case studies proof that the design tools are most effective when they are deployed early in the design process, or in a design where it is allowed to optimize many parts separately.

The research shows that by means of the analytical formulas, a hot-spot stress fatigue assessment can fairly easily be programmed in different software applications, and that it pays off to do so. The fact that the hot-spot stress method is not limited to tubular joints means that results similar to this research can be achieved for any type of welded joint.

In the end, the choice of fatigue assessment type is discussed. The hot-spot stress method with analytical formulas is an often used and accepted method, but also Finite Element Analysis could have been the basis for a parametric design tool. FE-based design tools are the only way to include any type of joint, since no analytical formulas exist for other than tubular joints.

Assessment environment

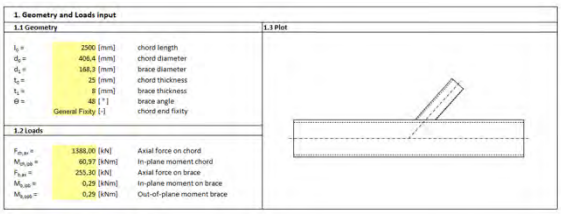

1. Geometry and Loads input

1.1 Geometry

l_0 =	2500	[mm]	chord length
d_0 =	406,4	[mm]	chord diameter
d_1 =	168,3	[mm]	brace diameter
t_0 =	25	[mm]	chord thickness
t_1 =	8	[mm]	brace thickness
Θ =	48	[°]	brace angle
	General Fixity	[-]	chord end fixity

1.2 Loads

$F_{ch,ax}$ =	1388,00	[kN]	Axial force on chord
$M_{ch,ipb}$ =	60,97	[kNm]	In-plane moment chord
$F_{b1,ax}$ =	255,30	[kN]	Axial force on brace
$M_{b1,ipb}$ =	0,29	[kNm]	In-plane moment on brace
$M_{b1,opb}$ =	0,29	[kNm]	Out-of-plane moment brace

1.3 Plot

2. Stress concentration factor calculation

2.1 Joint geometry ratios

α =	12,303	[-]	Relative chord length	$= 2\,l_0 / d_0$
β =	0,414	[-]	Width ratio	$= d_1 / d_0$
γ =	8,128	[-]	Chord slenderness	$= d_0 / 2\,t_0$
τ =	0,320	[-]	Wall thickness ratio	$= t_1 / t_0$

Validity conditions

α =	Valid	$4 \le \alpha \le 40$	[1] / par. 9.1.6
β =	Valid	$0{,}2 \le \beta \le 1{,}0$	[1] / par. 9.1.6
γ =	Valid	$15 \le 2\gamma \le 64$	[1] / par. 9.1.6
τ =	Valid	$0{,}2 \le \tau \le 1{,}0$	[1] / par. 9.1.6
Θ =	Valid	$30° \le \Theta \le 90°$	[1] / par. 9.1.6

[1] / Symbols and abbreviated terms

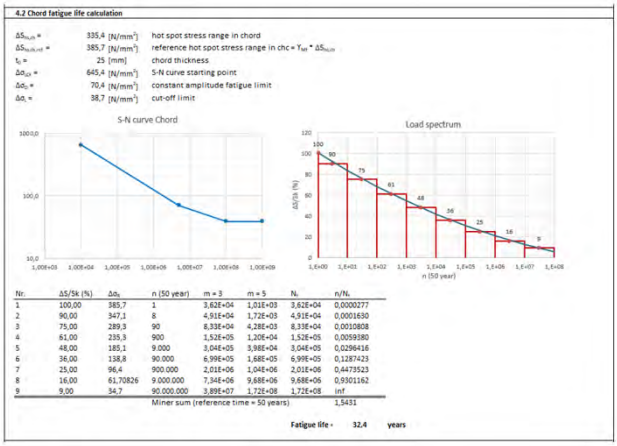

4.2 Chord fatigue life calculation

$\Delta S_{hs,ch}$ =	335,4	[N/mm²]	hot spot stress range in chord
$\Delta S_{hs,ch,ref}$ =	385,7	[N/mm²]	reference hot spot stress range in chc = $\gamma_{Mf} * \Delta S_{hs,ch}$
t_0 =	25	[mm]	chord thickness
$\Delta\sigma_{c1}$ =	645,4	[N/mm²]	S-N curve starting point
$\Delta\sigma_c$ =	70,4	[N/mm²]	constant amplitude fatigue limit
$\Delta\sigma_l$ =	38,7	[N/mm²]	cut-off limit

S-N curve Chord

Load spectrum

Nr:	Δσ/σk (%)	$\Delta\sigma_k$	n (50 year)	m = 3	m = 5	N_i	n/N_i
1	100,00	385,7	1	3,62E+04	1,01E+03	3,62E+04	0,0000277
2	90,00	347,1	8	4,91E+04	1,72E+03	4,91E+04	0,0001630
3	75,00	289,3	90	8,33E+04	4,28E+03	8,33E+04	0,0010808
4	61,00	235,3	900	1,52E+05	1,20E+04	1,52E+05	0,0059380
5	48,00	185,1	9.000	3,04E+05	3,98E+04	3,04E+05	0,0296416
6	36,00	138,8	90.000	6,99E+05	1,68E+05	6,99E+05	0,1287423
7	25,00	96,4	900.000	2,01E+06	1,04E+06	2,01E+06	0,4473523
8	16,00	61,70826	9.000.000	7,34E+06	9,68E+06	9,68E+06	0,9301162
9	9,00	34,7	90.000.000	3,89E+07	1,72E+08	1,72E+08	inf

Miner sum (reference time = 50 years): 1,5431

Fatigue life = 32,4 years

TUBULAR JOINT FATIGUE OPTIMIZATION TOOL

Geometry (Check box makes value equal to brace 1)			
Joint type		T-Joint	
Chord length	l_0	2500	[mm]
Brace length	l_1	800	[mm]
Chord diameter	d_0	406,4	[mm]
Chord thickness	t_0	25	[mm]
Brace diameter	d_1	168,3	[mm]
Brace thickness	t_1	8	[mm]
Brace angle	θ_1	48	[°]

Section forces			
Axial force on chord	$F_{ch,ax}$	1388	[kN]
In-plane moment chord	$M_{ch,ipb}$	60,97	[kNm]
Axial force on brace	$F_{b1,ax}$	255,3	[kN]
In-plane moment on brace	$M_{b1,ipb}$	0,2862	[kNm]
Out-of-plane moment brace	$M_{b1,opb}$	0,2862	[kNm]

Chart control			
Input	Update	Chord diameter	406,4
Output		Fatigue life chord	403

Joint number	Reset	6
Node		4
Element		79
Wind direction		150

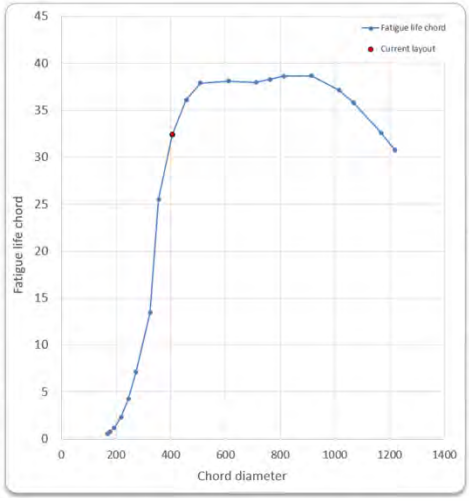

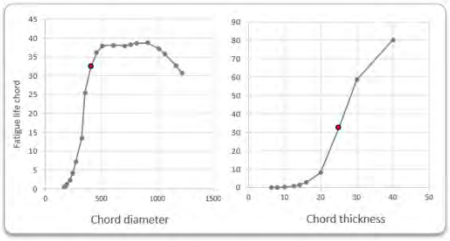

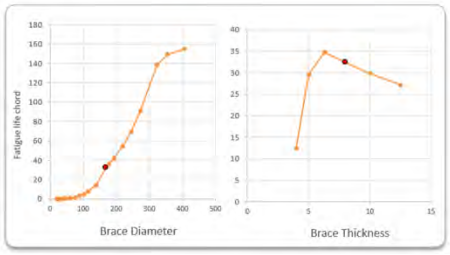

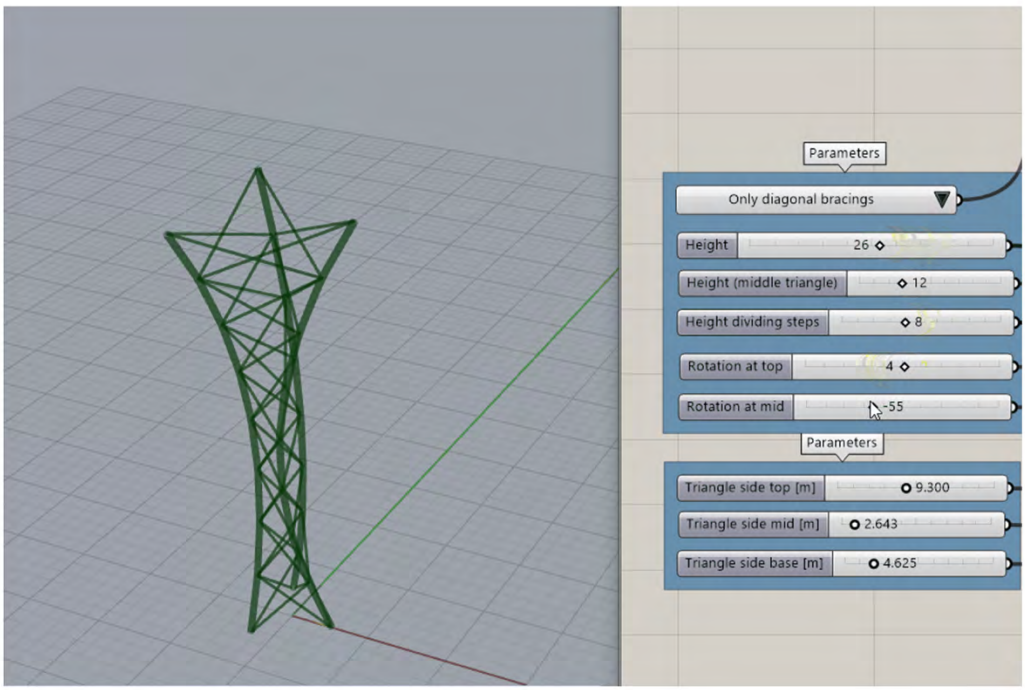

M04

Milco Hahury

Experiment design and numerical study of a new type of plug-and-play joint

The behaviour of the plug-and-play joint is characterized, in terms of strength, stiffness and rotation capacity, following the EN1993-1-8 component method. An experimental and numerical study are performed using the component test; T-plug bending around weak axis. The component interaction is established by proposing a physical spring model and a Eurocode aligned component model for practical use in design standards.

Abstract

Explicit rules for safety verification of open cold-formed lightweight beam-to-tubular column joints are missing in the current EC3-1-8. By developing economical detailing, with design guidance based on Eurocodes, the market share for new buildings, renovation and for additional storeys on existing buildings will increase. Within the INNO3DJOINTS project an innovative plug-and-play joint is developed, allowing for modularity and industrialization for low to mid-rise buildings. This solution will increase the competitiveness and sustainability of steel construction. The goal of this MSc thesis is to characterize the behaviour of the plug-and-play joint using the component test; T-plug bending around weak axis. The strength, stiffness and deformation capacity following the EC3-1-8 component method approach are investigated.

An experiment is designed for testing in the Stevin-II laboratory at Delft University of Technology. This work includes both the design of the set of test specimens and laboratory set-up. Secondly, a numerical study is performed to predict the experimental results and an extending parametric study is performed to derive new components, using the finite element software of ABAQUS. The influence of geometrical properties; thickness ratio (reverse channel vs. T-plug web), use of stiffeners, use of tubular sections and length of the T-plug web, is studied for a steel grade S355. The numerical study is validated for three configurations using the component test; T-plug in tension, provided by the INNO3DJOINTS project. As the parametric study is based on an elasto-plastic material model, these numerical results are directly used to derive new analytical expressions/models and characterize new components and component interactions for design verification.

The numerical study resulted in the identification of seven active components for the plug-and-play joint, consisting of basic EC3-1-8 components and tubular components from the CIDECT report 16F: *Component method for tubular joints*. In addition, two new components are introduced namely, the reverse channel in bending and T-plug in bending. Based on a total of 127 unique joint configurations, new analytical expressions are derived to characterize the behaviour of the new components for resistance and stiffness. The component interaction is established by proposing a physical spring model and a component model suitable for Eurocode implementation. This results in the characterization of the joint behaviour for the experimental configuration C-SHS200 with a 7.5% deviation on the resistance and a 20.5% deviation on the stiffness compared to the numerical result.

The accuracy of the joint stiffness can be improved if the component stiffness derivation also includes non-governing configurations and a wider range of parameters is studied, such as the position of the bolt holes along the net-section and the use of tubular section. The results, derivations and the physical spring model contribute to the INNO3DJOINTS project and could be used for implementation in the software tool, to be developed by the French Institute CTICM. Besides, the Eurocode aligned component model is recommended for practical use in design standards, but further research should be performed on the verification of the rotational stiffness on the joint level.

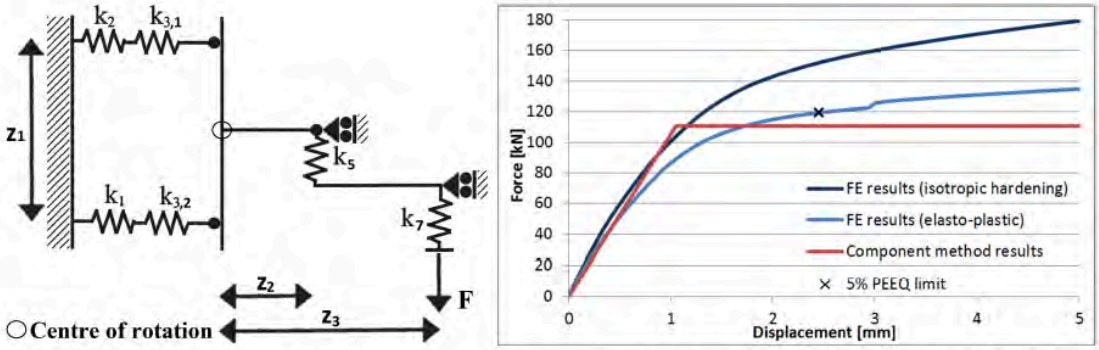

(a) Physical spring model (b) Verification of experimental configuration C-SHS200

Figure 6.1: Characterization of the joint behaviour

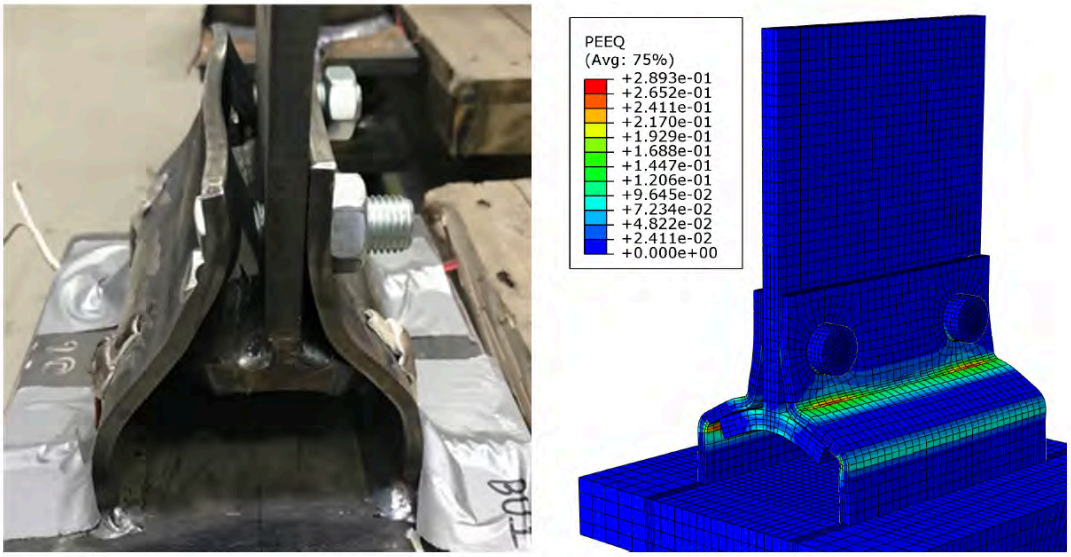

(a) Experiment result (UC) (Da Silva et al., 2019) (b) Numerical result

Figure A.8: Final deformed shape tension validation for test specimen: B-RP

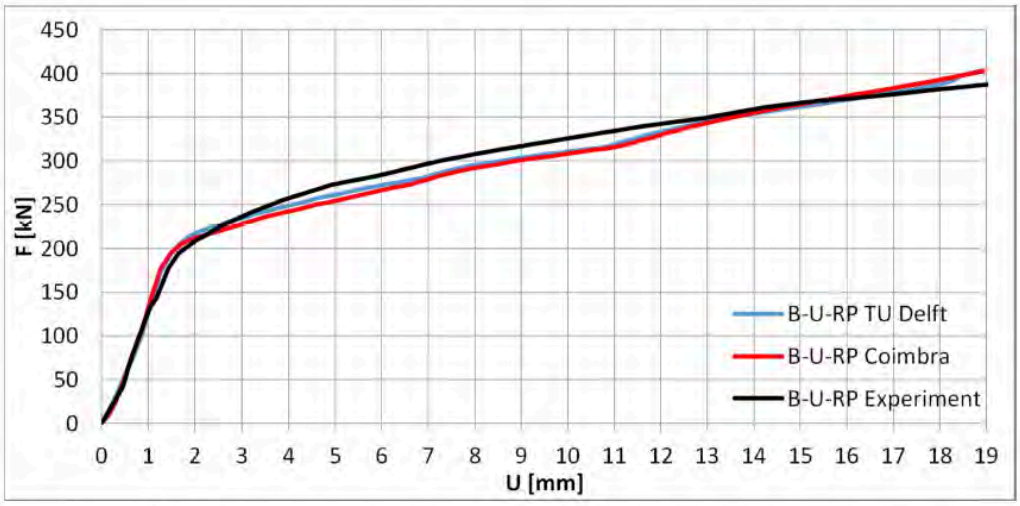

Figure A.9: Force-displacement tension validation of test specimen: B-U-RP

M05

Marije Deul

Fatigue damage accumulation in steel welded joints, subject to (random) variable amplitude loading conditions

Om overtollig staalgewicht in een scheepsconstructie te beperken is er onderzocht hoe de onzekerheden in de vermoeiingsberekening kunnen reduceren. Een significant deel van de onzekerheid over de vermoeiingsweerstand komt uit het spannings-criterium en de schade-accumulatie; de huidige aanpak (Palmgren-Miner met Hot Spot Stress) bewijst zich conservatief voor breedbandige spectra en on-conservatief voor smalle spectra. Als alternatief wordt de non-lineaire schaderegel (Leonetti, 2020) succesvol gecombineerd met het Effective Notch Stress Concept. De levensduur-spreidingsindex neemt af van 1:1.28 tot 1:1.13.

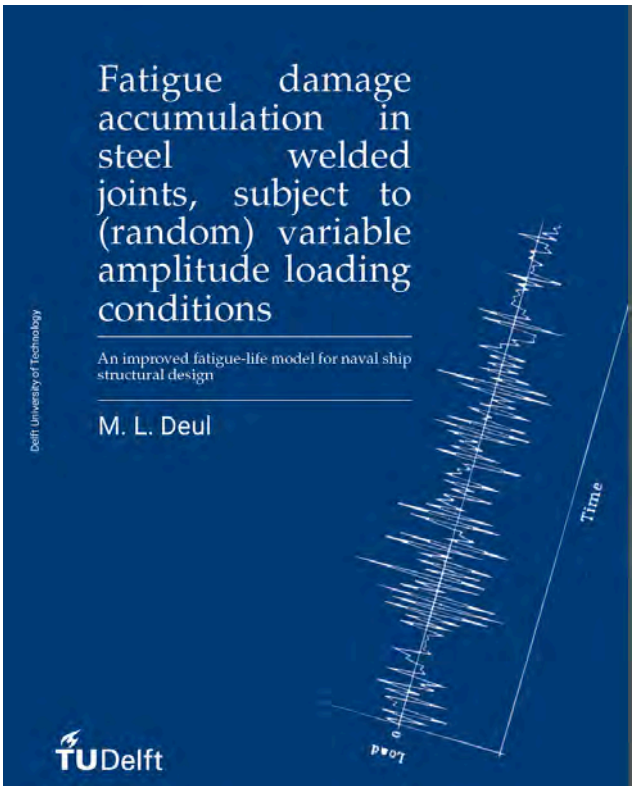

Bouwen met Staal: studentenSTAALprijs 2021 inzending

MSc Afstudeeronderzoek Marije Deul

Schepen worden van oudsher geconstrueerd uit, en gebouwd met, staal. Dit komt onder andere voort uit de relatieve lage kosten en de vertrouwdheid in de sector met het materiaal. Voor scheepsconstructies is de vermoeiingslevensduur een leidende limit-state: de geometrie wordt aangepast of het plaatmateriaal wordt opgedikt om lokale spanningsconcentraties te verlagen tot onder de kritische grens wanneer de voorspelde levensduur niet toereikend is. Echter blijkt deze analyse onderhevig aan veel onzekerheid (fig 1). Deze onzekerheid wordt vertaald naar conservatisme en zodoende naar zwaardere constructies. Omdat voor schepen het gewicht invloed heeft op de beladingscapaciteit en stabiliteit is een sterk conservatieve benadering ongewenst.

Twee bronnen van onzekerheid die nauw verbonden zijn, zijn de spanningsberekening (Fatigue Damage Criterion) en de schadeaccumulatieregel, tevens het onderwerp van deze masterthesis.

Probleemanalyse

De schadeaccumulatieregel van Palmgren en Miner is breed geaccepteerd in de standaarden. Het gebrek van deze regel ligt in de onkunde om het effect van de belastingshistorie op de toekomstige schade te beschrijven. Er wordt aangenomen dat de schade zich met een constante snelheid ontwikkelt, hetgeen door experimenten (en breukmechanica) wordt tegengesproken. Het voordeel van de regel is dat het relatief eenvoudig te implementeren is en een lineaire veiligheidsfactor (soms tot een factor 5 reducerend) toelaat. Figuur 2 toont dat, voor een variatie aan geometrieën, belastinghistories, datasets en staalsoorten (allen constructie staal), de spreiding bij het gebruik van deze regel groot is. In deze referentiecasus is het Hot Spot Structural Stress Concept gebruikt om de spanningsconcentratiefactor te bepalen. Dit concept gebruikt beperkt de lokale informatie over de lasgeometrie.

Als verbetering wordt een non-lineair schade accumulatiemodel (Leonetti, 2020) gecombineerd met het Effective Notch Stress Concept (semi-analytisch; den Besten, 2015). Dit accumulatiemodel beschrijft een afnemende vermoeiingslimiet: hoe meer schade er is, hoe gevoeliger het detail is voor lagere amplitudes en hoe sneller de schade ontwikkelt. Hiernaast modelleert het Effective Notch Stress Concept de lokale geometrie en dus het effect van plaatdikte, lashoek, keelhoogte etc. Het resultaat ziet u in Figuur 3: de spreiding is significant afgenomen. De levensduur-spreidingsindex neemt af van 1:1.28 tot 1:1.13.

Scheepsconstructies als subset van staalconstructies

Binnen het onderzoek lag de focus op belastings-histories die typisch zijn voor scheepsconstructies. Immers, de onzekerheden in de analyse staan los van de onzekerheden in de invoer (zie ook de vele standaarden die generiek geschreven zijn voor stalen constructies). Met het gebruiken van een andere belastings-historie is het werk uitstekend toepasbaar voor een grote variëteit aan variabel belaste stalen constructies!

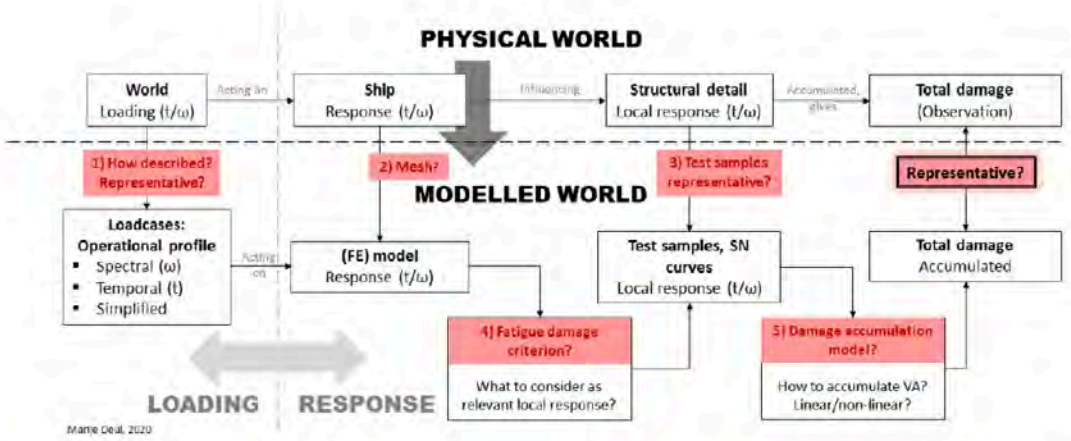

Figure 1: Schematisch overzicht van de bronnen van onzekerheid in de vermoeiingsanalyse, uitgedrukt aan de hand van de vertaling van de fysieke naar de gemodelleerde wereld.

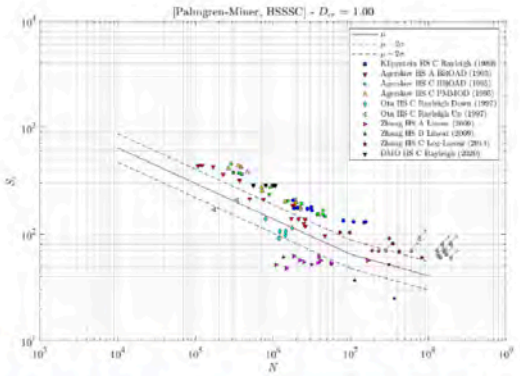

Figure 2: De VA database zoals geanalyseerd met de referentiemethode (Hot spot structural stress met Palmgren-Miner Lineaire schaderegel), vergeleken met de S-N curve van DNV.

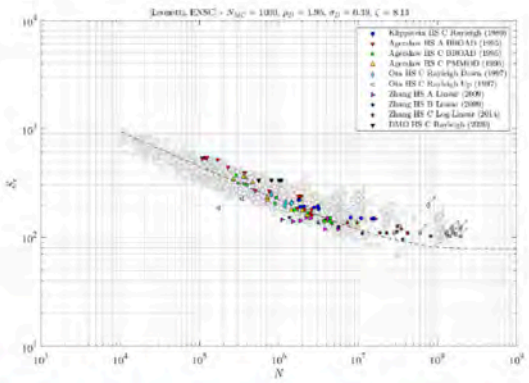

Figure 3: De VA database zoals geanalyseerd met de verbeterde methode (Effective notch stress met de non-lineaire schaderegel van Leoneti (2020)), vergeleken met de referentiedata van Qin (2021)

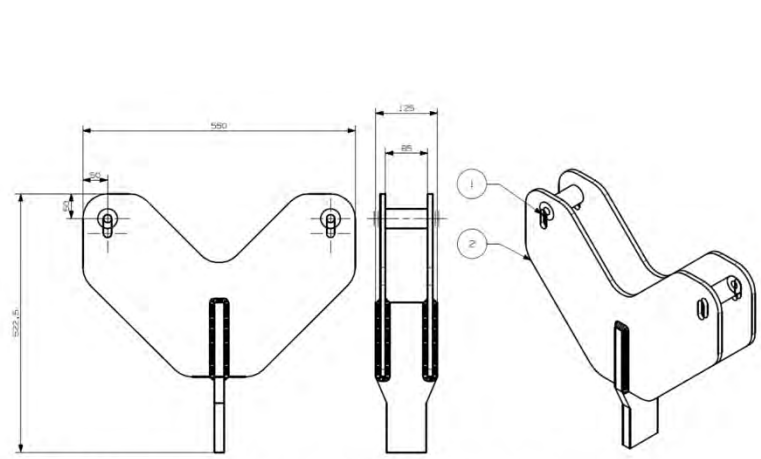

(a) Drawing of the accessory as used to insert the specimen in the testing setup.

(b) Photo of the testing setup, including the accessory.

Figure 6.2: Layout of the test setup and the accessory.

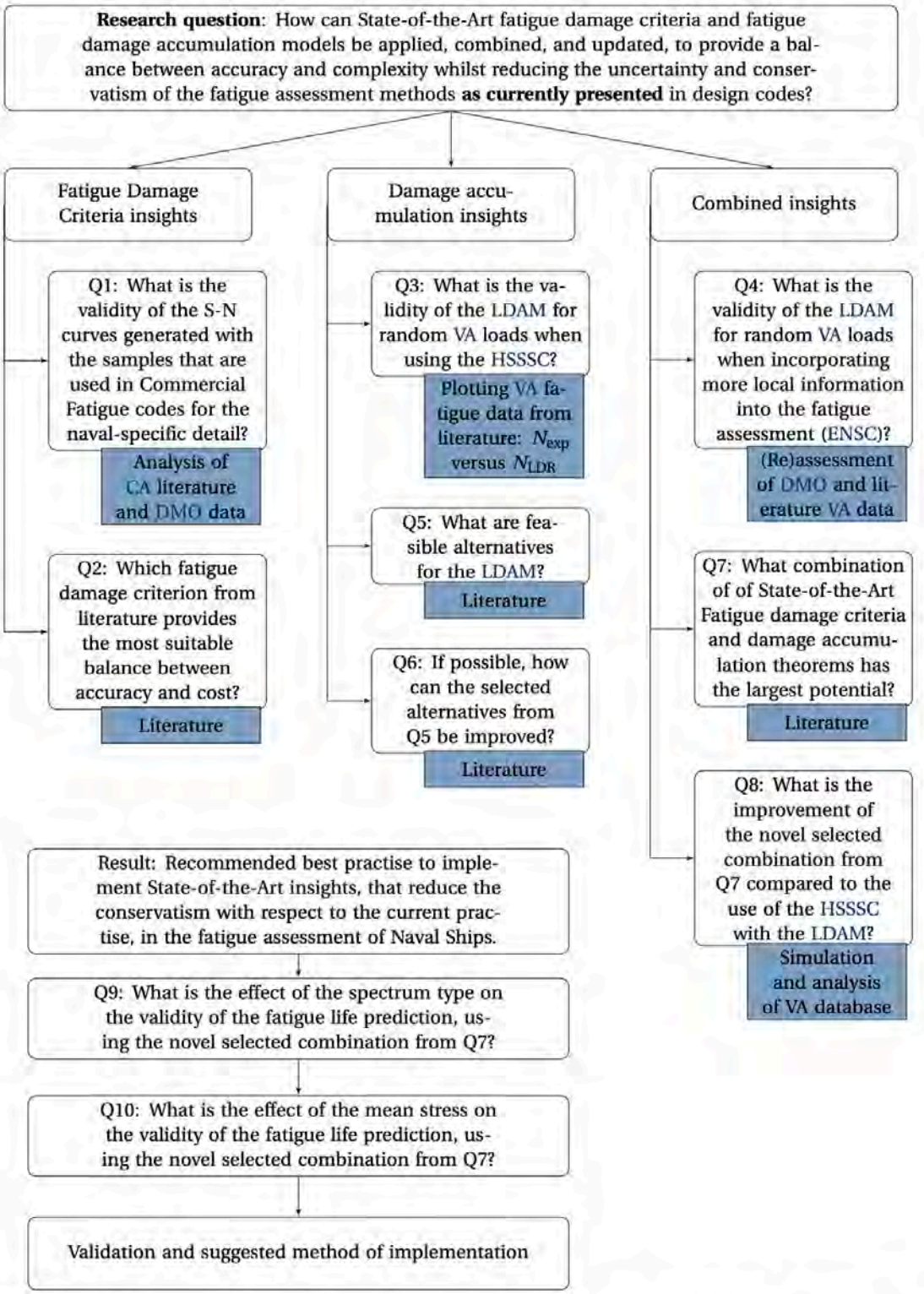

Figure 5.1: Research roadmap. The blue boxes indicate the means that are used to formulate the answer to the respective questions.

M06

Berend Meijer

Impact forces on bridge piers in the event of ship collisions

A research is initiated to study the impact forces of ships on bridge piers. Since the impact forces are developed by plastic deformation of the ship bow, the research is about energy dissipation of the steel ship bow. A formula is established to determine the impact force on bridge piers based on the energy dissipation profile of different steel bows.

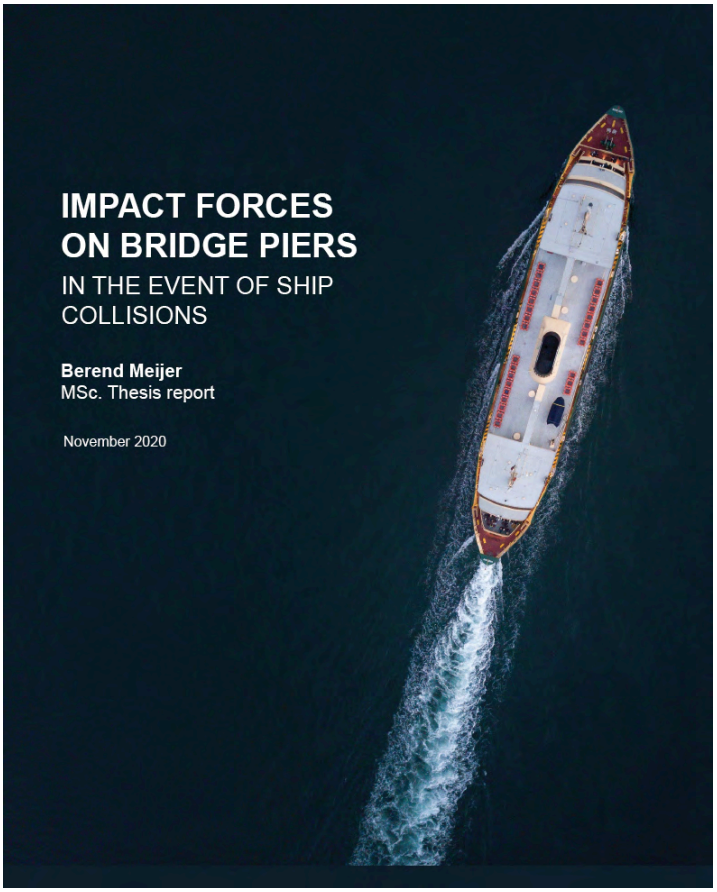

Abstract

The aim of this thesis is to propose a simple technique to estimate the maximum impact forces acting on bridge piers in the event of ship collisions. This technique is determined for Dutch commercial inland wa- terway ships (CEMT classes) and set up to be applied by bridge engineers to determine the required bridge pier strength. Many collision events on bridge piers have occurred in history where some led to a major fail- ure of the bridge deck due to insufficient strength of the bridge pier. The accuracy of the Dutch guideline on calculating these impact forces (ROK 1.4) is questioned, mainly regarding the generalisation of the guideline to different ship types. Therefore, an investigation on this topic has been initiated to provide more accuracy in the estimations on bridge pier impact forces in the event of ship collisions.

The background of the collision event is explained to provide basic knowledge and understanding of the origination of the impact forces. A dynamic nonlinear finite element model has been created using ABAQUS/Explicit to simulate the ship-bridge pier collision event. The bridge pier is assumed to be rigid and fixed, while the ship structure is assumed to dissipate all initial kinetic energy through plastic deformation (crushing of the structure). Material properties have been obtained from a test database and include rate effects. The output of the simulations is presented in the form of impact force versus penetration depth.

Existing analytical calculation methods on the crushing strength of a ship's bow structure are presented and studied for the verification of the numerical finite element model. A sensitivity analysis was performed and showed expected behaviour with no singularities. The correlation between the results of numerical simula- tions and analytical calculation methods showed good agreement. It has been concluded that the numerical calculation model is verified as stable, and results are in agreement with existing calculation methods.

Numerical simulations have been performed on one class IV and two class V ship's bow structures. The de- formation process resulting from these simulations showed visually comparable failure behaviour with a real case. Moreover, a thorough analysis of the reaction forces per structural element of the ship's bow was per- formed where local forces are compared with deformation processes. This showed good correlation.

A relationship between initial kinetic energy levels and maximum impact force has been developed based on the results of the numerical calculations. The global form of the relationship was determined by analysing the results and using found relationships. This form was fitted on the result data through curve fitting techniques. With the established expression, the estimated impact force can be calculated for the event of a ship collision, given an initial kinetic energy level involved in the collision event.

Using this expression, maximum impact force values have been presented for different ship classes. For ships smaller than a medium-sized ship (CEMT IV), the impact force values are higher than is found in the current Dutch guideline. However, lower impact forces are estimated for ships larger than this medium-sized ship. This difference mainly originate from the relatively stiff response of the frontal part of the analysed ship's bows, compared to the ship's bow structure that led to the current Dutch guideline.

With the proposed impact force expression, the maximum impact force on bridge piers in the event of ship collisions could be estimated with increased accuracy.

Nr.	Event
1	Stringer activation by failure of frontal elements
2	Front girder failure and maingirder buckling → more force to deck
3	Collision of lower deck, force distribution to hull
4	Deck buckling followed by activation of radial stiffeners, increase in hull force because of stiffness stringer and lower deck
5	Stringer support buckling, introduction of bending moment on main girder
6	Buckling of lower hull followed by main girder+deck folding
7	Frontal bow part completely crushed → lowerdeck activation
8	Buckling of lower side hull behind stiff section
9	Lowerdeck buckling
10	Folding of front structure into back structure
11	Kinetic energy is equal to zero and fully dissipated into the structure

Table G.1: Failure events during the collision

Figure G.5: Deformation of class IV ship during collision process at t=0.27 s.

Figure G.6: Deformation of the ship Eemshorn after collision with bridge pier.

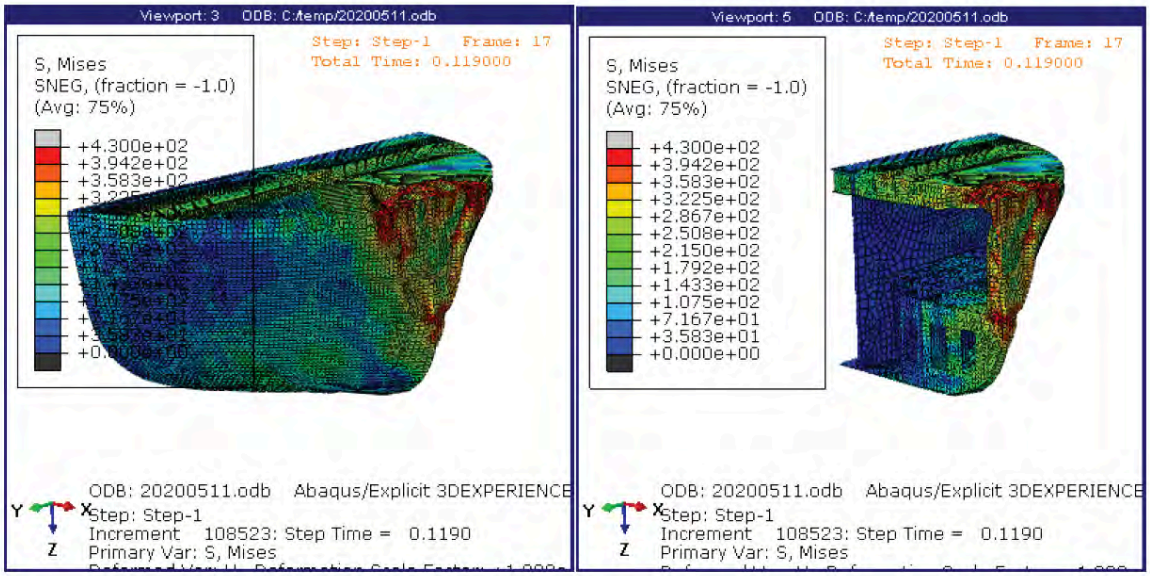

Figure E.1: CEMT IV simulation t = 0.119 s

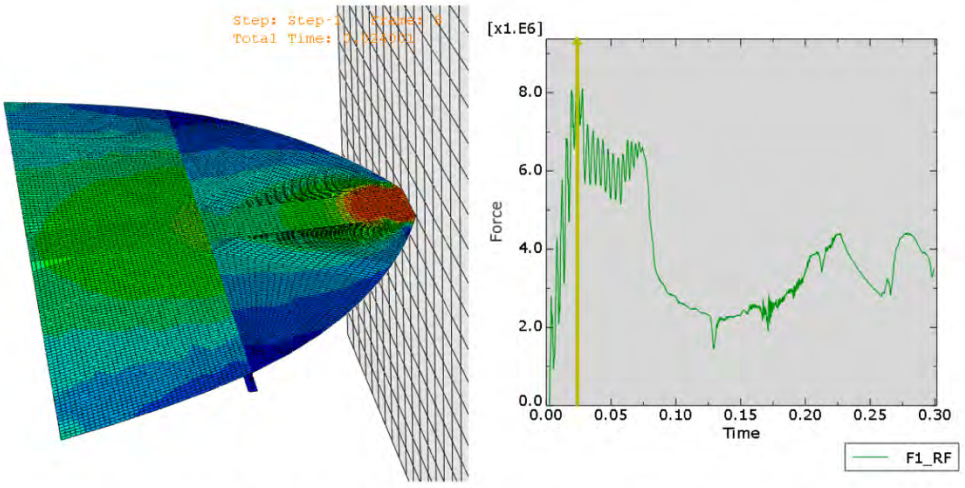

(a) Simulation F1 with reaction forces over time at t = 0.024s

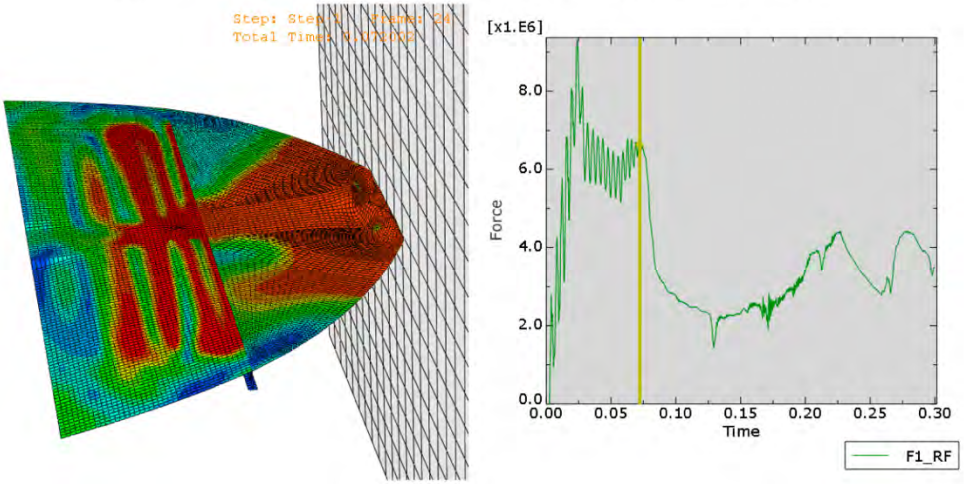

(b) Simulation F1 with reaction forces over time at t = 0.072s

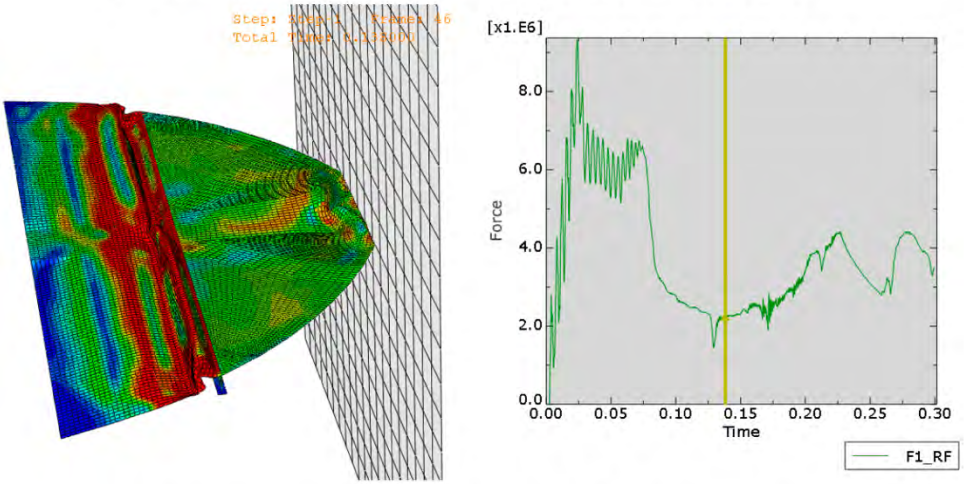

(c) Simulation F1 with reaction forces over time at t = 0.14s

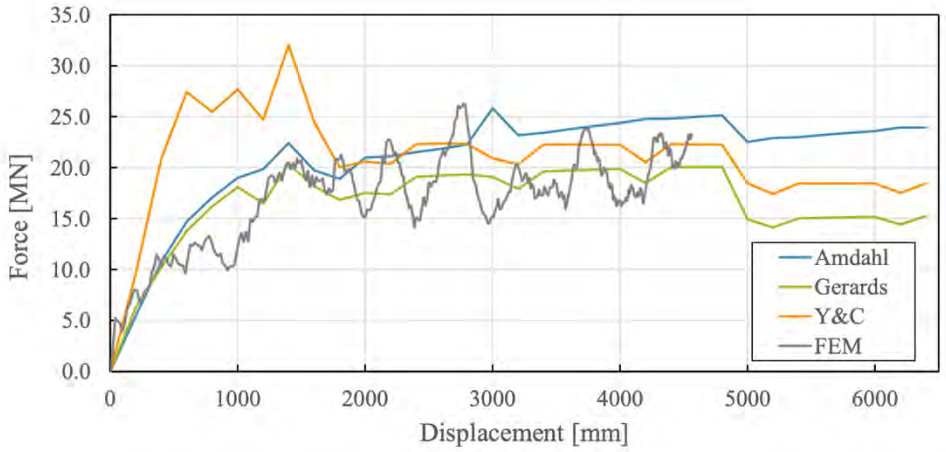

Figure 7.16: Force-displacement graph for Sietske from NLFEA and hand calculations.

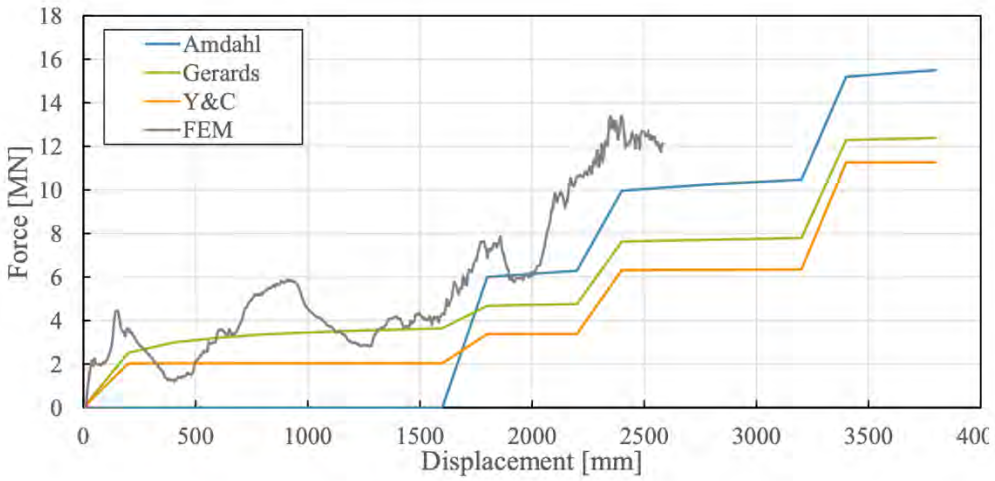

Figure 7.23: Force-displacement graph for Berdina from NLFEA and hand calculations.

M07

Tibo van de Velde

Design of slender steel pedestrian bridges: Applying a moving jogger load model including Human-Structure Interaction

Steel pedestrian bridges can statically be designed slender, but will often have an eigenfrequency within the step frequency range of humans. This can lead to uncomfortable vibrations of the structure. By including the Human-Structure Interaction this research aspires to reduce conservatism in steel bridge design. It shows a significant decrease in maximum acceleration, but unfortunately not in required structural height.

Developments in structural engineering give rise to the ability of increasing the slenderness within the design of steel footbridges. However, this often results in a fundamental eigenfrequency which coincides with the step frequency range of humans on the bridge. This can lead to uncomfortable vibrations of the structure. In order to maintain the comfortability, the Dutch national annex of the Eurocode prescribes to consider a dynamic jogger load case, which is often governing for the slenderness of a design. In this thesis, a moving model for the dynamic jogger load case with the addition of human-structure interaction (HSI) in vertical direction is considered in order to reduce conservatism. Using a simplified 1-dimensional Finite Element representation of a footbridge consisting of 4 HEA320 profiles, a comparison is made between a moving force (MF) and a moving mass--spring-dashpot (MSD) model representing the jogger. Different analyses of a single jogger case are made to investigate the influence of the following simplifications: 1) applying a stationary instead of a moving dynamic load, 2) applying a load model neglecting the separation between jogger and bridge and 3) neglecting the subject variability. The Dutch national annex prescribes the use of multiple joggers during the load case. Therefore, an initial research is done on the effect of HSI on a multiple jogger case. It is found that the HSI results in a decrease of the maximum accelerations for all load cases. The effect increases when the joggers-to-bridge mass ratio increases. The same holds for the influence of separation. The results show that reduction of the maximum acceleration due to the addition of the HSI is generally not large enough to result in an increase of the maximum slenderness of steel pedestrian bridges.

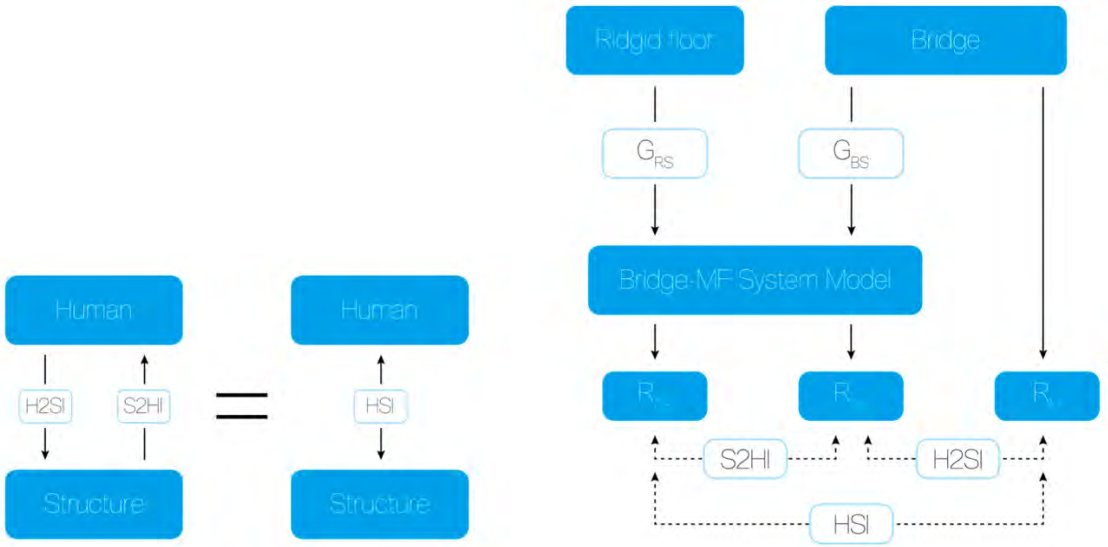

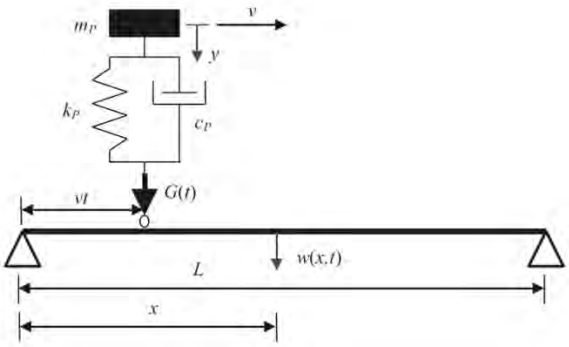

Results of the MSD Model

For the MSD model the maximum accelerations for the three cases are:

- 1 giant jogger → $a_{max} = 14.76$ m/s^2
- 5 jogger pairs → $a_{max} = 13.75$ m/s^2
- 10 single joggers → $a_{max} = 13.10$ m/s^2

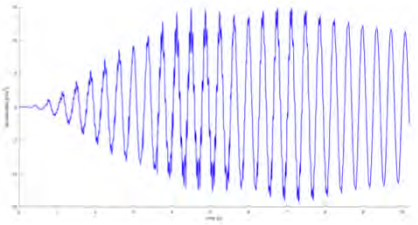

(a) 1 giant jogger

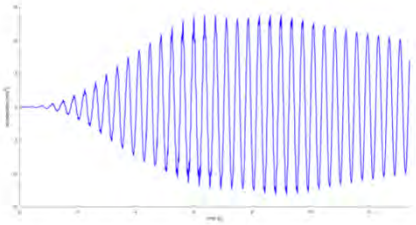

(b) 5 jogger pairs

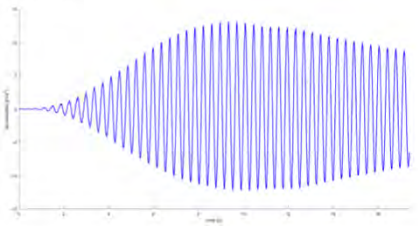

(c) 10 single joggers

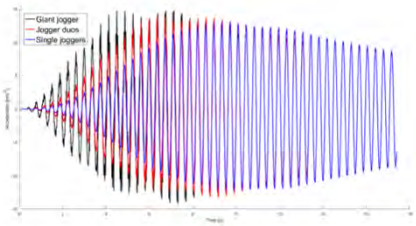

(d) all three load cases

Figure 10.2: acceleration due to the **MSD** model for three different distributions of 10 joggers (NOTE: the time axis of the three cases differ)

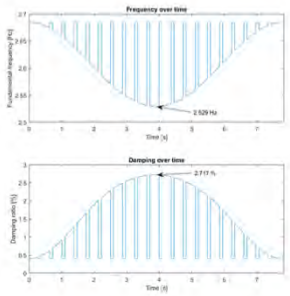

(a) 1 giant jogger

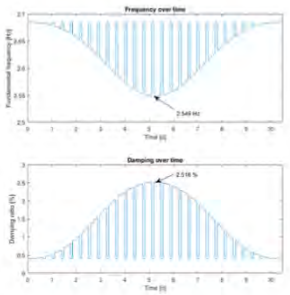

(b) 5 jogger pairs

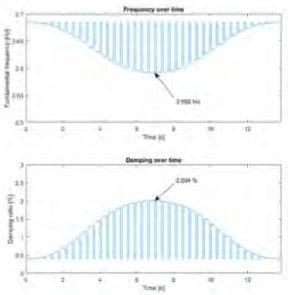

(c) 10 single joggers

Figure 10.3: Damping and Frequency over time for the fundamental mode for three different distributions of 10 joggers according to the **MSD** model, plotted until the last jogger crossed the bridge.

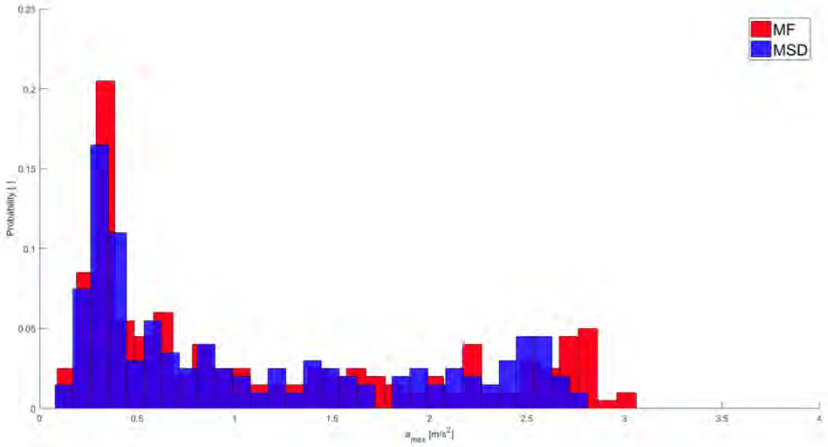

(a) 'fully' stochastic analysis

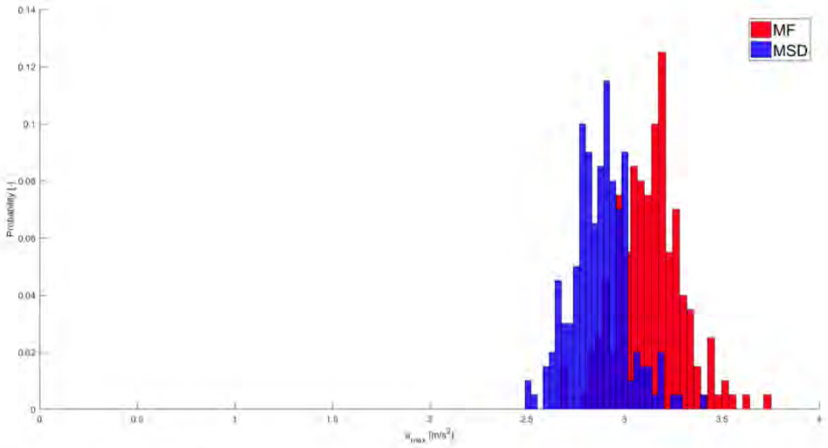

(b) 'human properties' stochastic analysis

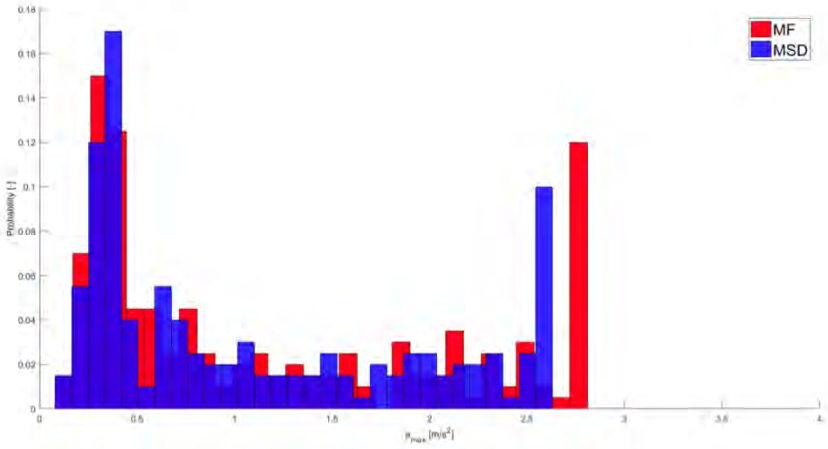

M08

Aravind Ramkumar

Investigation of resin and steel reinforced resin behaviour under quasi-static and cyclic loading in oversized IBCs

The projects deals with the slip resistant behaviour of resin and steel reinforced resin which can be used in injection bolted connection with over-sized hole clearance. The oversize hole clearance in shear connectors of composite structures facilitates the reuse of steel and concrete thus contributing towards a sustainable society. However, due to larger hole clearance, the slip of the connection under cyclic loading becomes critical. In this study, the slip resistant behaviour of these two materials are experimentally found using a custom made test setup with two different hole clearance. Numerical modelling are carried out to validate the test results.using material models for resin and SRR.

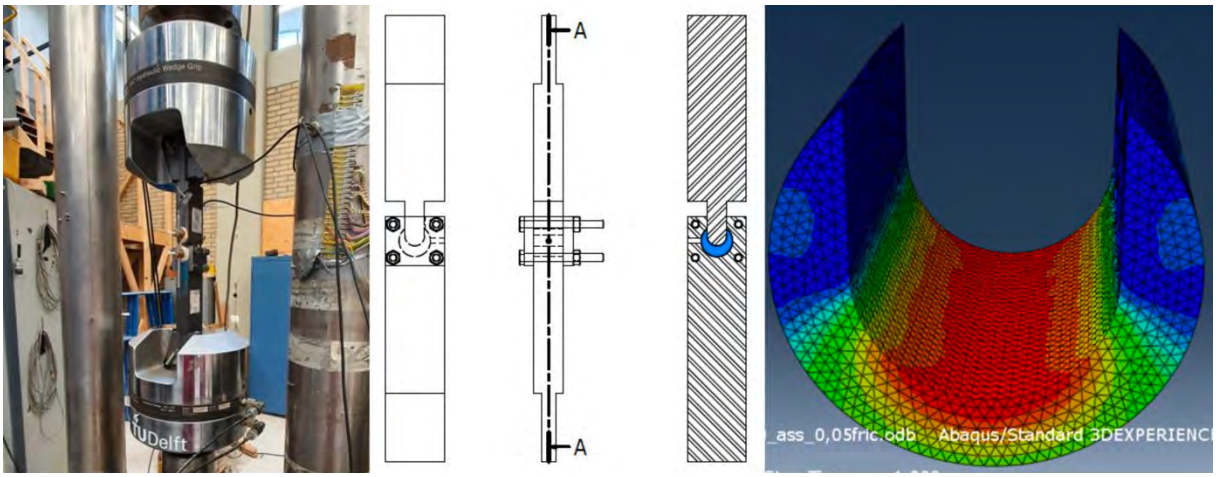

M Sc Thesis description

Injection Bolted Connections (IBC) are connections in which the cavity between the bolts and the plates (hole clearance) is filled with two-component epoxy resin. The oversized hole clearances allow for the reuse of all the structural elements in composite structures. Due to larger hole clearance, the possibility of slip occurrence in the connection is higher and hence there is a need to study the behaviour of resin and steel-reinforced resin (SRR) under cyclic loading. A custom-made setup with 3 and 6 mm oversize that replicates the nominal bearing stress experienced by the resin in a double lap shear joint was used to study the behaviour of the resin/SRR under cyclic loading. The slip obtained from cyclic loading is extrapolated for 5 million cycles to check if maximum slip exceeds the failure criterion of 0.3 mm and slip range exceeds the failure criterion of 0.1 mm over 5 million cycles. Numerical modelling was done to see if the results (initial stiffness) obtained from the experiments can be replicated by the material models for static and one cycle loading with the help of a reasonable friction coefficient between the steel and resin surfaces. Good sets of results were obtained for all the tested stress ranges. On extrapolating to 5 million cycles, resin specimens with 3 mm hole clearance failed at a stress range of 200 MPa and resin specimens with 6 mm hole clearance failed at a stress range of 150 MPa. SRR specimens with 6 mm hole clearance failed at a stress range of 200 MPa. From numerical modelling, a good correlation was found between the force vs displacement curve obtained from the experiments to the curve obtained from the numerical model.

Why Steel?

Steel has been an excellent construction material. However, production of steel results in results in increase of CO_2 emissions into the atmosphere. According to a study conducted by IPCC in 2011, construction industry contributed to about 36% of total CO_2 emissions. Hence, it becomes important to recycle and reuse steel without increasing the product of steel wherever possible. This study was focused on the reuse of composite structures using an over-sized injection bolted shear connection which would replace the existing welded shear studs. When this type of connections is considered, the slip resistant property becomes critical and hence a study was conducted on the slip resistant properties of resin and SRR used to fill the over-sized hole clearance. Hopefully, reuse of steel makes the construction industry move towards a sustainable economy.

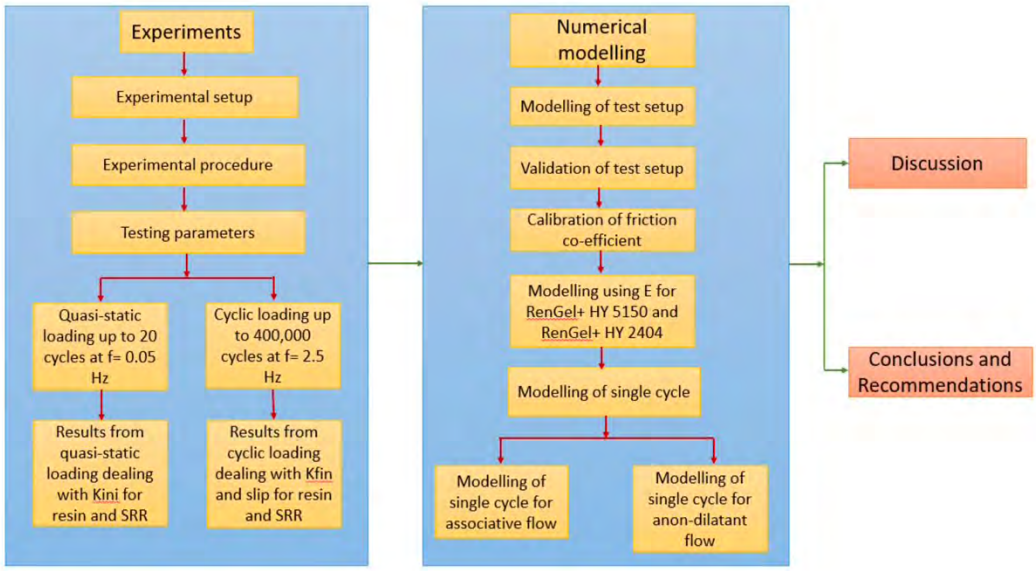

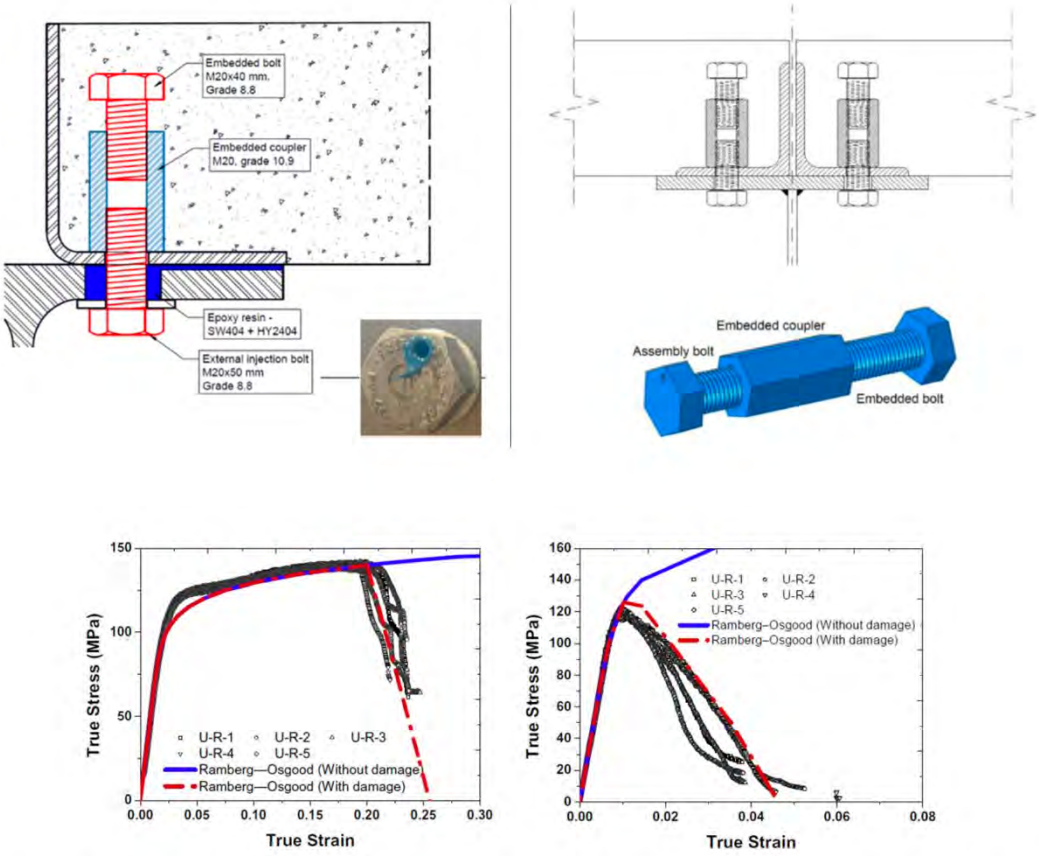

Figure 2.14: Stress-strain relationship of unconfined resin specimens[25] (left). Stress-strain relationship of unconfined steel reinforced resin specimens [25] (right)

Figure 3.17: Completed specimen ready to be tested

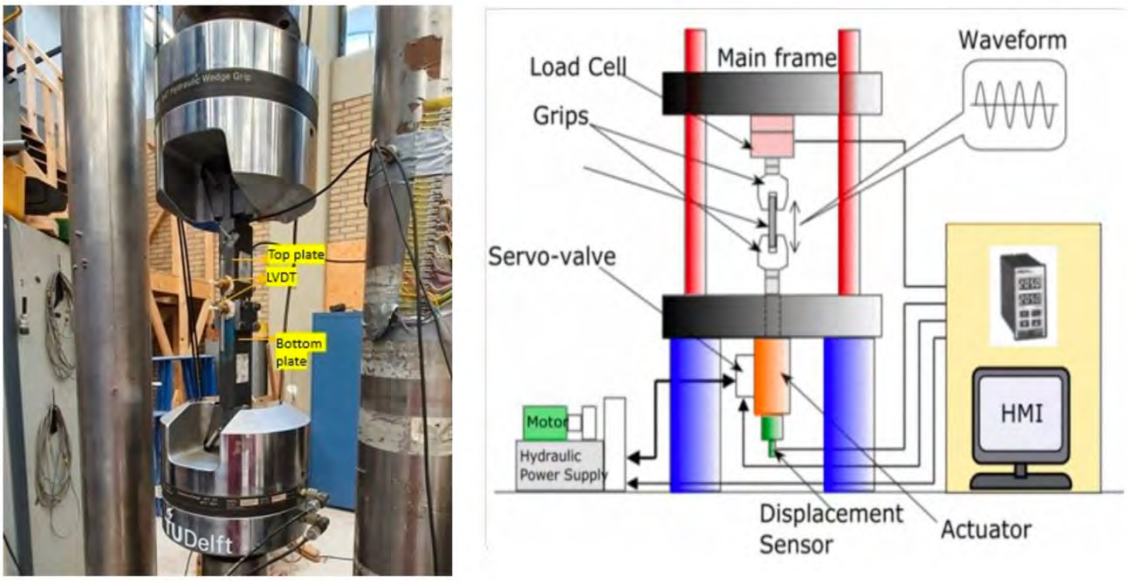

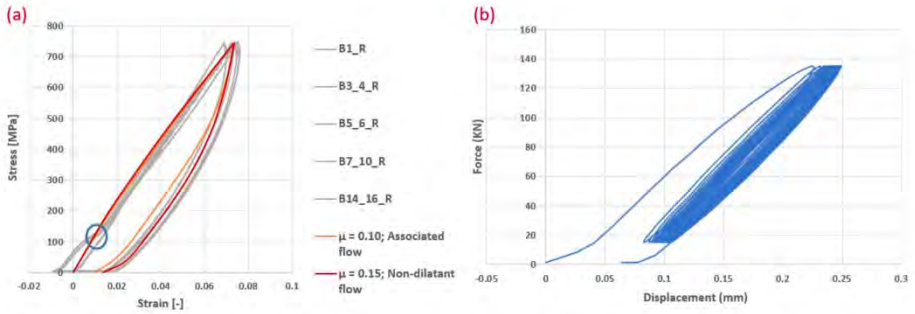

Figure 6.1: (a) Graphs from experiments on resin under monotonic loading indicating stress plateau and graph obtained from FEM modelling [9]; (b) Graph obtained from quasi static experiments from this study

M09

Akram El Kazaz

Numerical investigation for cracks of rib-to-deck welded connection at the crossbeam junction in OSD using XFEM

The thesis numerically investigates cracks caused by fatigue loading at the welded connection between the longitudinal rib and the deck plate at the intersection with the crossbeam. The investigation aims to predict the structural integrity of the OSD with different deck plate thicknesses. This is done using computational fracture mechanics based on LEFM theory integrated with an engineering approach developed to simulate the cracks at this connection.

Thesis summary

The orthotropic steel deck (OSD) is nowadays commonly used due to its advantages, such as its lightweight, short construction time, and high capacity to bear the loads. However, fatigue cracks occur in different welded connections in the OSD. In this study, the rib to-deck-plate connection at the crossbeam conjunction has been analysed. This connection has been considered as a very critical connection due to the high-stress concentration under local wheel loading. In addition, the crack initiating at the weld root and propagating through the deck plate thickness cannot be visually inspected until surface cracks appear when the overlay is removed for the investigation. In the Netherlands, deck plate cracks at rib-to-deck plate connections at the crossbeam constitute a significant proportion of investigated cracks. In this thesis, a numerical investigation of the aforementioned cracks is carried out.

First, XFEM is applied to study fatigue crack propagation using compact tension (CT) specimens. Commercial FE software package Abaqus® is used to build 2D and 3D CT models. The corresponding fatigue crack propagation is calculated in the direct cyclic step with strain energy release rate calculated using the virtual crack closure technique (VCCT). A good match is found between analytical calculation and 2D XFEM modeling. For 3D fatigue crack propagation, the number of cycles calculated from the automated crack propagation approach, using the low cycle fatigue step provided by Abaqus®, shows high sensitivity to element sizes, specifically the used element sizes through the thickness of the CT.

Second, 3D crack propagation is applied to OSD with a *20 mm* deck plate. For this detail, the fatigue crack initiation under compressive stress states is caused by the local loading on the deck plate. A hypothesis of changing the loading sign from compression to tension to subject the initial crack zone to tension is proposed so that this type of crack can propagate using automated XFEM. This assumption is made because high residual stresses normally exist in the welded connections and fatigue crack can propagate even under compressive stresses induced by loading. Before carrying out crack propagation calculation using VCCT, the stationary crack states were analysed using FEM and XFEM for cracks inserted with different angles. The SIFs obtained from FEM and XFEM are the same; in addition, that the SIF obtained when the detail is loaded in tension or compression has the same absolute value. Subsequently, the propagating crack analysis is carried out as a small initial crack with a depth of *0.5 mm* is inserted and Paris' law parameters C and m of $1 \cdot 10^{-13}$ and *3.0* were selected respectively. The obtained results of strain evolution as a function of loading history came close to that from the experiment with a difference of *7.75%* for the initial strain value and *10.95 %* for the maximum one. Moreover, the predicted crack shape, angle, and rate were all validated with similar crack shapes obtained from experiments in various literature. As for the crack propagation behaviour in the thickness direction, the crack arresting took place at around *75%* of the deck thickness and an angle with the vertical axis of around 30^{o}.

Finally, the deck thicknesses of *16 mm* and *10 mm* were considered. Their results converged in terms of the crack propagation behaviour with real test specimens from the literature. It is also found that the *16 mm* and *20 mm* cases had a common crack propagation behaviour in the thickness direction as the crack arrest occurred at around *75%* of the deck thicknesses, while for the *10 mm* deck case the crack developed more dangerously by penetrating through the deck plate leading to a through-thickness crack. The approach proposed by this thesis proved to be valid for predicting the crack behaviour for the considered OSD deck plate thicknesses. Thus, the structural integrity of the detail can be assessed. This proved that for the *16 mm* and *20 mm* deck plates, the structural integrity is acceptable, while the *10 mm* deck safety is not confirmed.

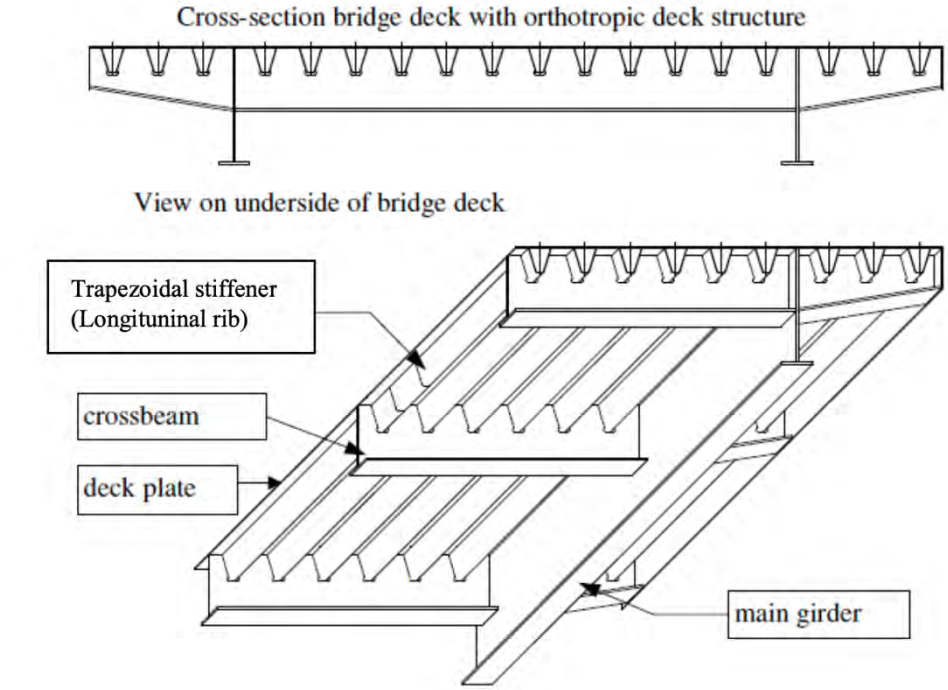

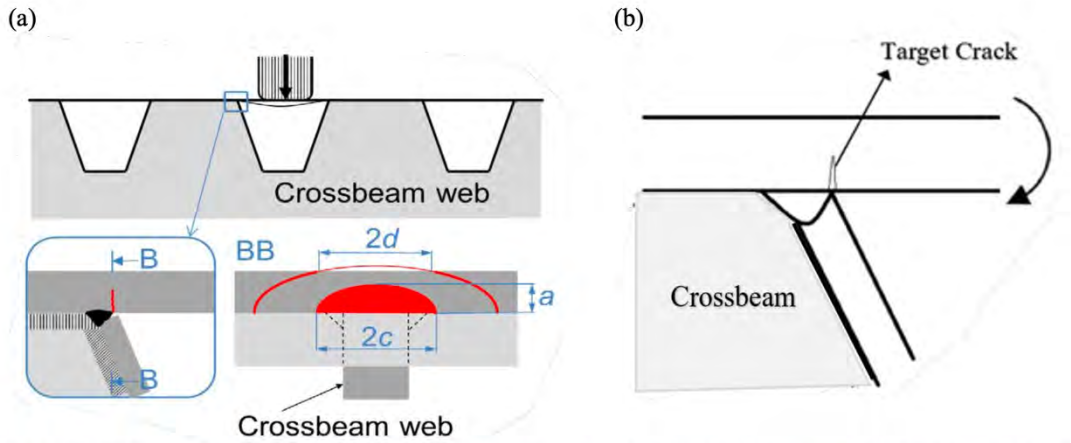

Figure 1.2: OSD deformation due to wheel load. (a) Transverse wheel load positions and OSD cross-section deformation shape. (b) Internal forces due to loading with the targeted crack.

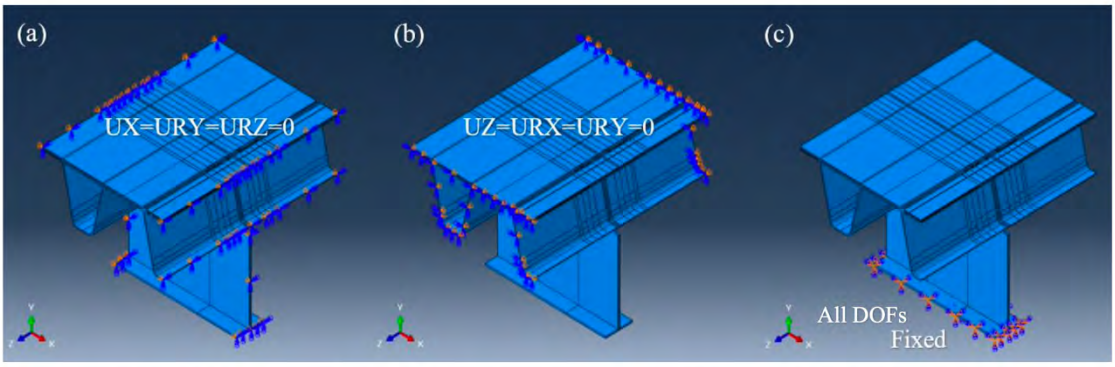

Figure 4.5: FE model boundary conditions. (a) Longitudinal & symmetry side. (b) Front & backside. (c) Crossbeam flange.

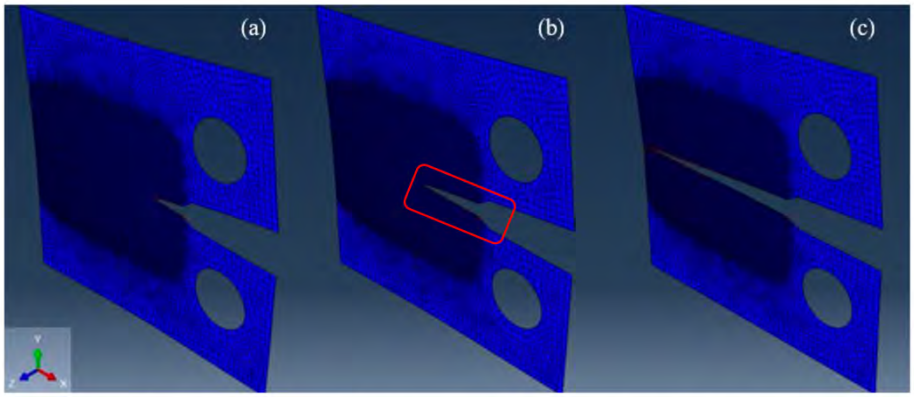

Figure 3.7: 2D-XFE model output (STATUSXFEM). (a) Deformed model at initial flaw length (5 mm). (b) Deformed shape at crack length 11 mm. (c) Deformed shape at final crack length (30 mm)

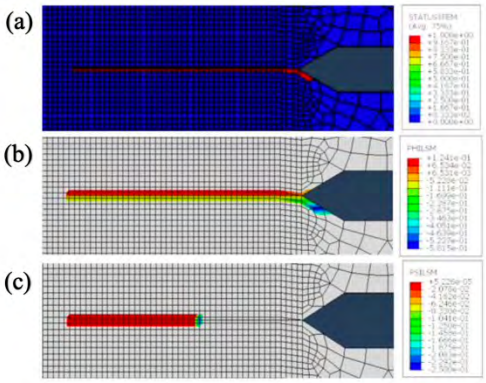

Figure 3.8: 2D-XFEM (undeformed) model output. (a) STATUSXFEM. (b) Level set value phi (PHILSM). (c) Level set value psi (PSILSM).

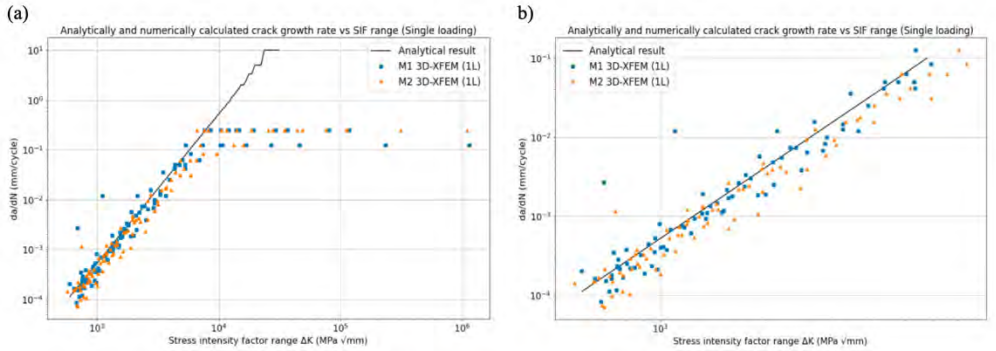

Figure 3.20: Crack growth rate vs SIF range for 3D single-loaded XFE model

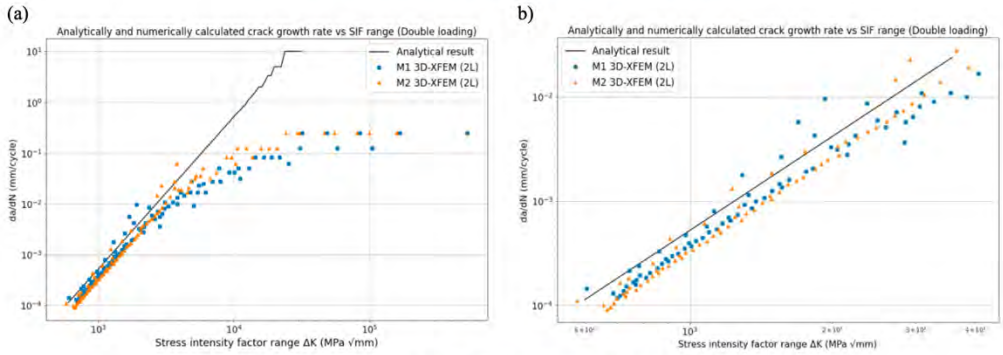

Figure 3.21: Crack growth rate vs SIF range for 3D double-loaded XFE model

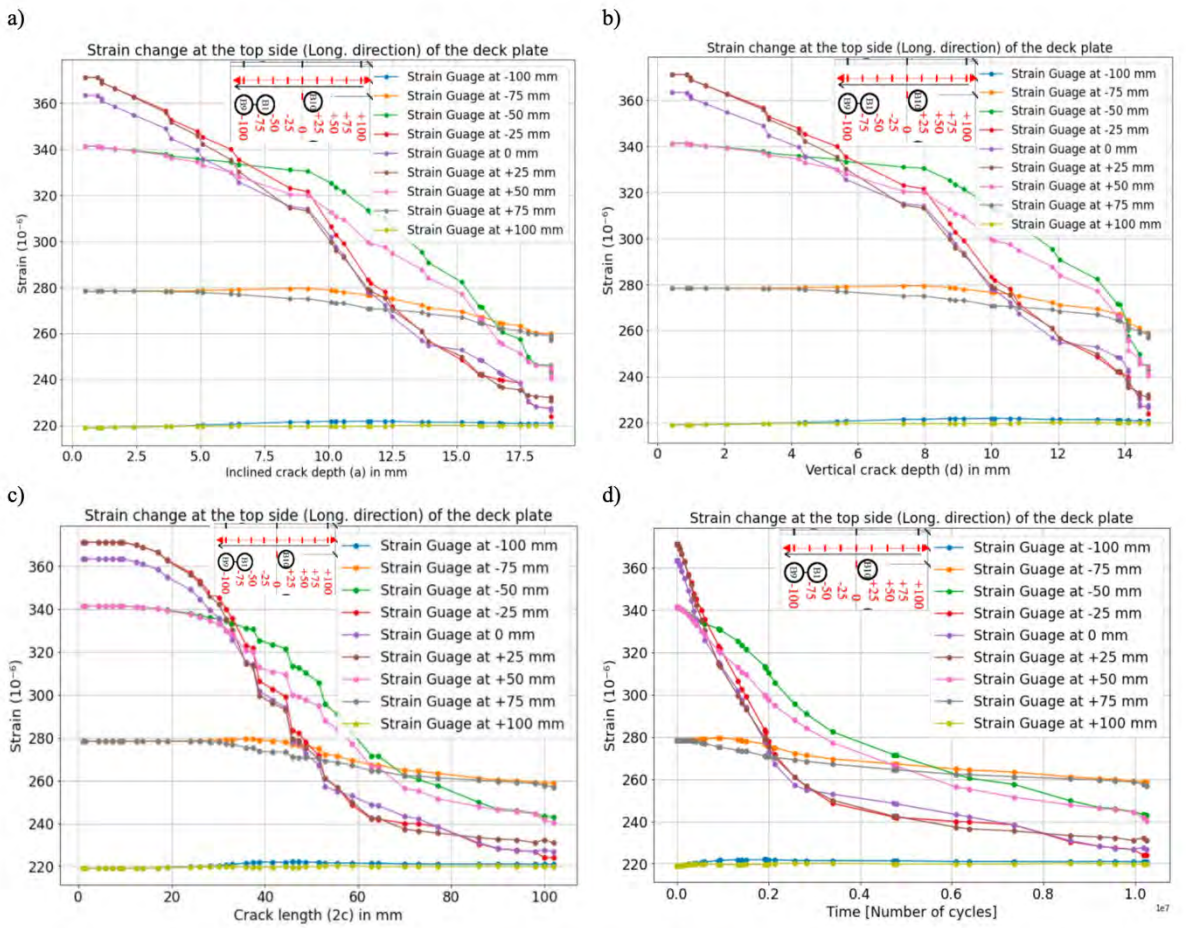

Figure 4.29: FEA strain drop at the top side (longitudinal path) of the deck plate vs;
(a) Actual crack depth [a]. (b) Vertical crack depth [d]. (c) Crack length [2c]. (d) Time [Number of cycles].

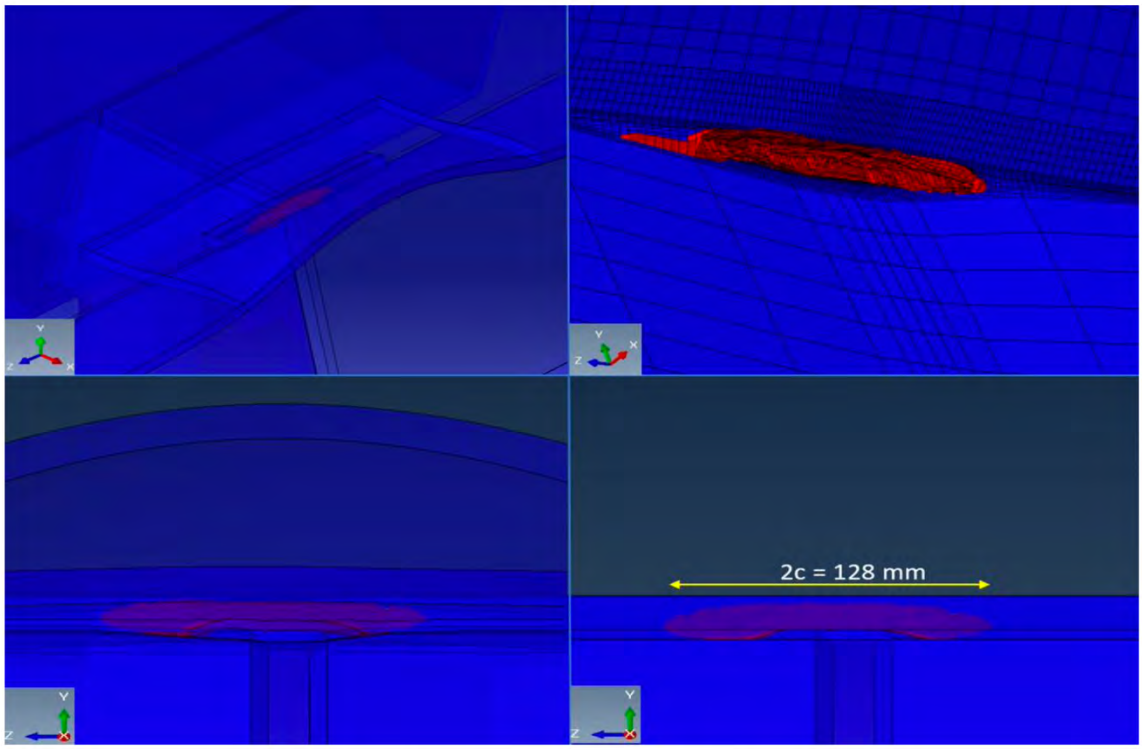

Figure 5.5: Different views of the deformed and undeformed 16 mm OSD

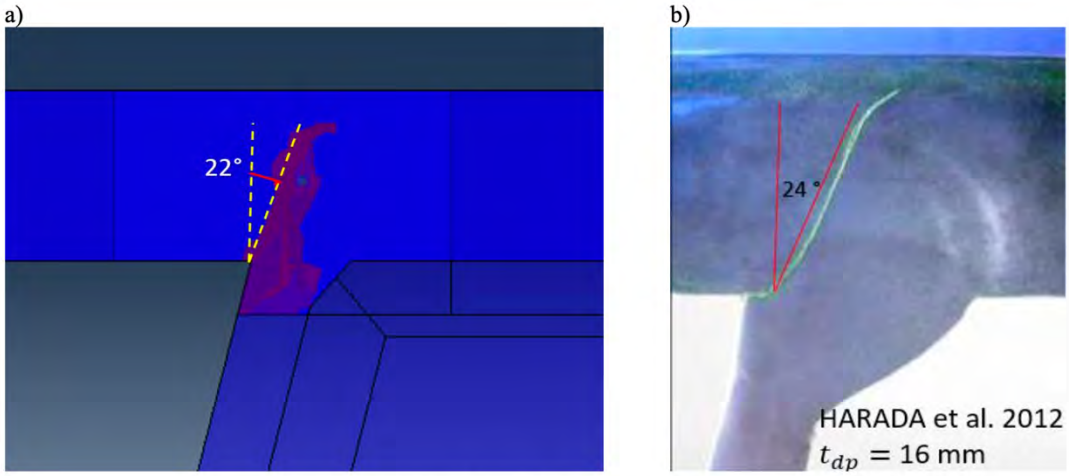

Figure 5.6: Fatigue crack in XFEA and experiment by Harada et al [40]

M10

Jeffrey van Hulst

Reliability Assessment of Steel Structural Elements in Wind Excited Buildings

This research investigates how a full reliability assessment of a steel main bearing structure in a wind excited building can be performed. A new method is developed in which wind tunnel measurements, wind speed models and a finite element model of the building are directly linked. This new method makes the application of a reliability-based design a lot more efficient, more accurate and therefore more interesting to use.

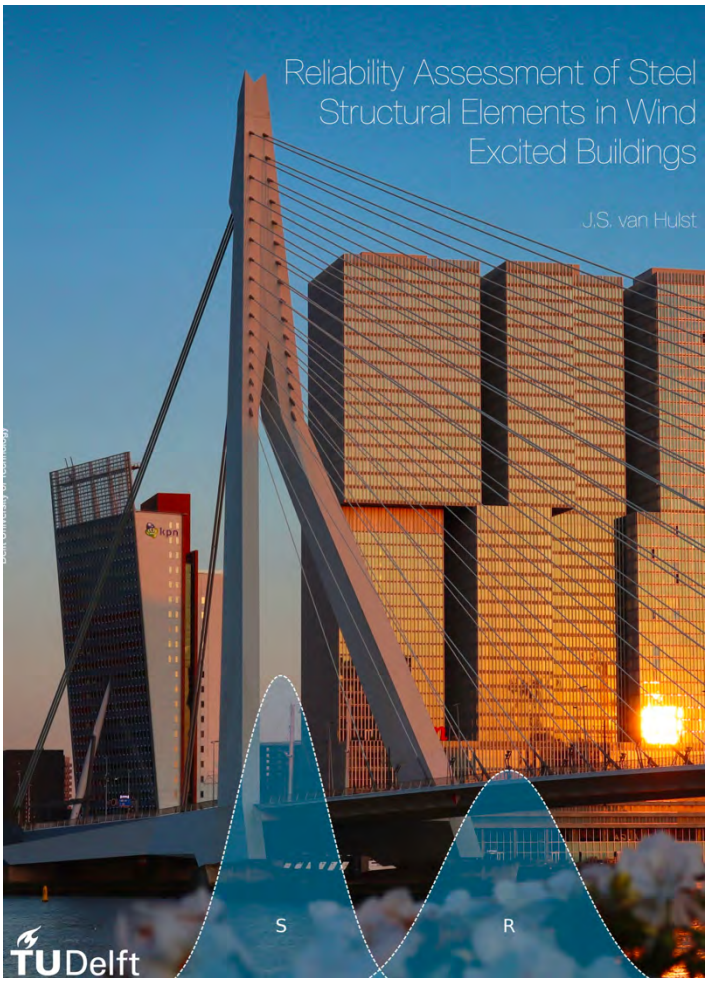

Reliability Assessment of Steel Structural Elements in Wind Excited Buildings

J.S. van Hulst

One of the basic principles of the design of structures is that they must be sufficiently safe and meet the required reliability requirements. In Eurocode NEN-EN 1990 specific minimum reliability index β-values are defined, which depend on a certain reference period and reliability class. To ensure that the structures meet the reliability requirements, partial factors are applied in the Eurocode. The aim is to steer the design to the minimum reliability requirements in a relatively simple way without a complete reliability assessment. Since such a reliability assessment is much more complex and requires more time and knowledge of the engineer. This research investigates how the reliability of a steel main bearing structure in a wind excited building can be determined, taking into account all uncertainties on both the resistance and load side. A new method is developed in which wind tunnel measurements, wind speed models and a finite element model of the building can be directly linked. This is an improvement on recent studies. With this method it is possible to determine the load effects of the wind in specific elements of the building. This can then be used to determine the reliability of the steel main bearing structure in a wind excited building.

First of all, all probabilistic models concerning the resistance side of the reliability assessment are identified by means of an extensive literature study. In this way all material properties and uncertainties are included in the reliability assessment. In addition, wind speed models, boundary layer wind tunnel pressure measurements and a FEM of the case study building are used. A wind load effect model quantifies the forces that occur in the structure due to the given wind load (based on the wind tunnel research) on the structure. This wind load effect model consists of several deterministic $(_r,\ ,h)$ and stochastic parameters as input; think of basic wind velocity and associated sampling uncertainties $_v$, terrain roughness factor $_r(h)$, model uncertainty χ and finally the peak load effects $\hat{G}_X$ and associated sampling uncertainties $\hat{C}_X$. All these data and models are linked to each other to determine the peak load effects $\hat{G}_X$ and associated sampling uncertainties $\hat{C}_X$ in various elements of the case study building.

To further use the wind load effects in the reliability assessment, extreme value theory must be applied to determine the extreme value distributions of these peak load effects. It should be taken into account that the extremes extracted from the data are independent and identically distributed. This study has shown that the application of the block method, in combination with the use of the autocorrelation and reversed univariate method - to determine the correct block duration - works very well. A generalized extreme value distribution without the application of a certain threshold value will result in a non- conservative tail of the distribution. Note that this tail is the most important part of the whole distribution and must therefore be described well. In almost all cases, the extremes in the tail are best described by a Gumbel distribution. This distribution is characterised by the straight tail and, in combination with the addition of a certain threshold value, it is the best way to describe the data including the tail. The decision of a good threshold value can be based on a visual approach of the Quantile-Quantile plot (quantiles of the data vs quantiles of the fit). To keep the effects of sampling uncertainties as low as possible, it is recommended to use as large a data set as possible. To quantify the sampling uncertainties, the bootstrap method is used in combination with the variation of the Cook-Mayne fractile. It is clearly visible that when a smaller block duration t can be used and thus more extreme values remain for fitting, the sampling uncertainties become smaller. In addition, the choice of threshold value also influences the size of the sampling uncertainties; with a higher threshold value, the uncertainty will also increase. A good balance must be achieved between describing the data well with a correct threshold value and not making the threshold value too high in order to reduce the sampling uncertainties.

To demonstrate that the method works, it is applied to a case study building. This case study building is initially designed in a deterministic Eurocode manner. Next, the reliability of a number of elements of the steel main bearing structure is extensively determined. For this particular case study building, it is evident that the design can be further optimised compared to the Eurocode design. In conclusion, this method shows that the possibilities in the field of a reliability-based design are certainly worthwhile for the further optimisation of a structure. And the use of this new method in which all data and models can be linked makes the application of a reliability-based design a lot more efficient, more accurate and therefore more interesting to use.

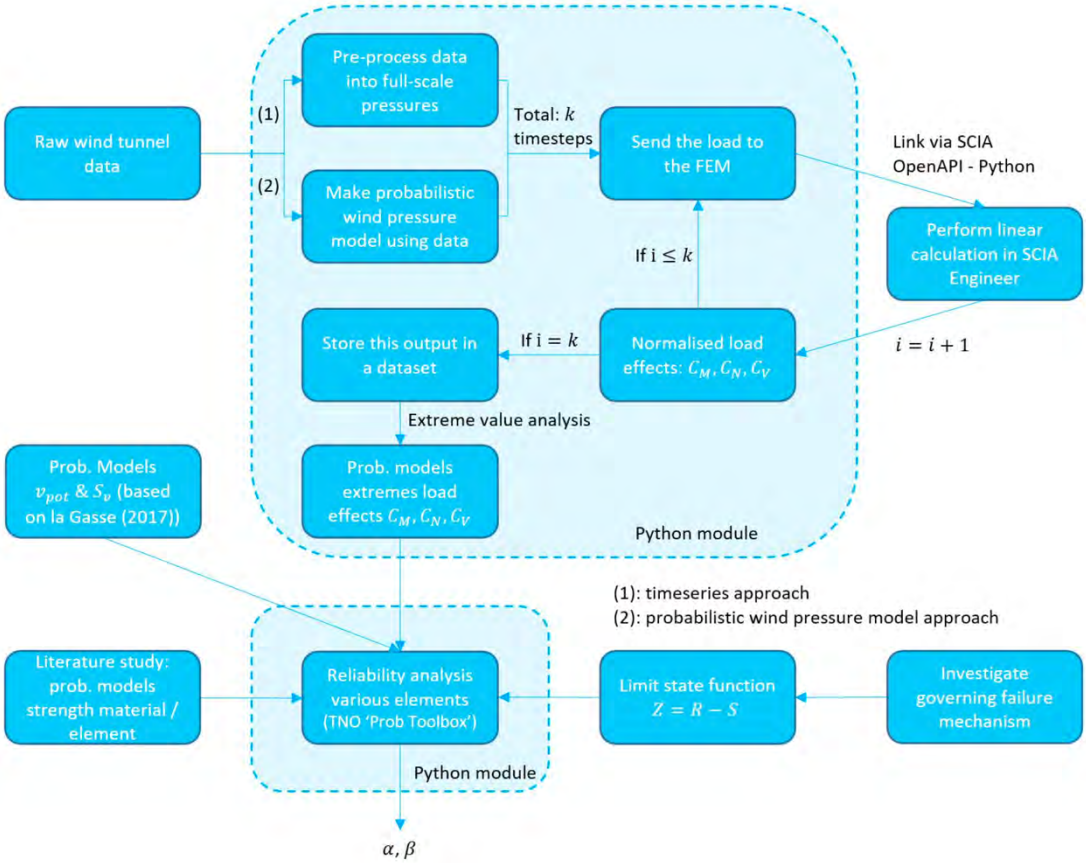

Figure 6.1: Method overview of the reliability assessment procedure in this study

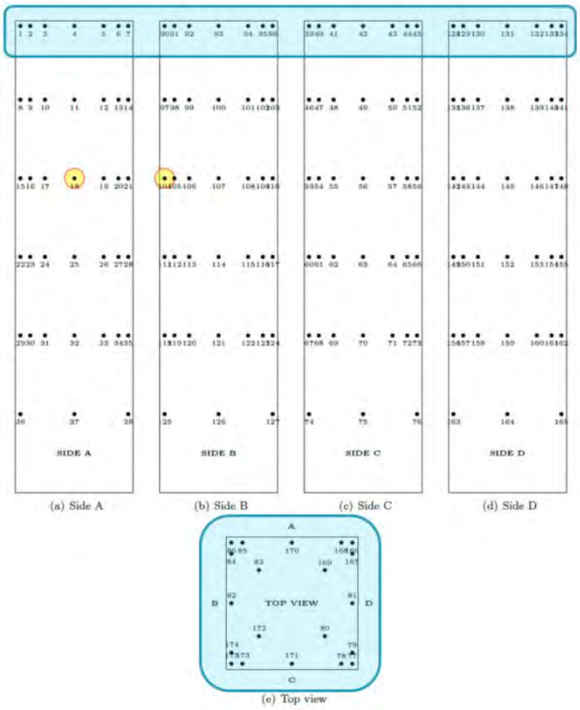

(a) Side A (b) Side B (c) Side C (d) Side D

(e) Top view

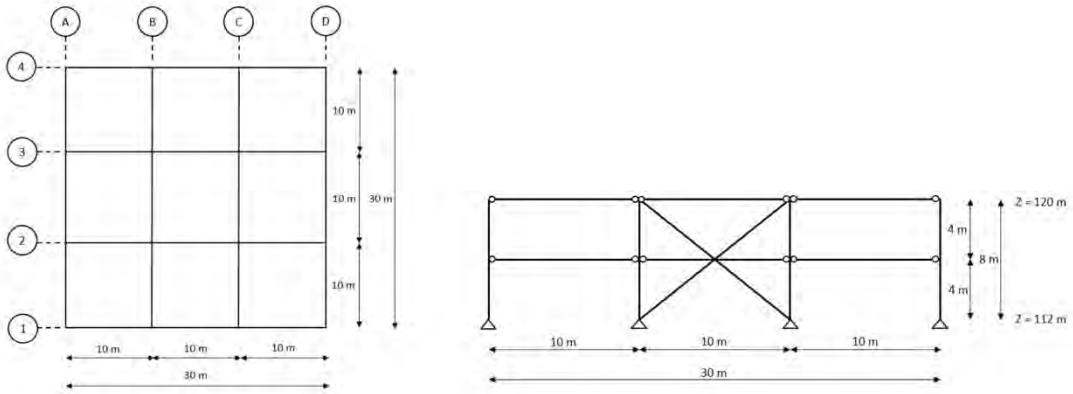

(a) Case study building plan view

(b) Case study building side view

Figure 10.2: Plan and side view of the case study building

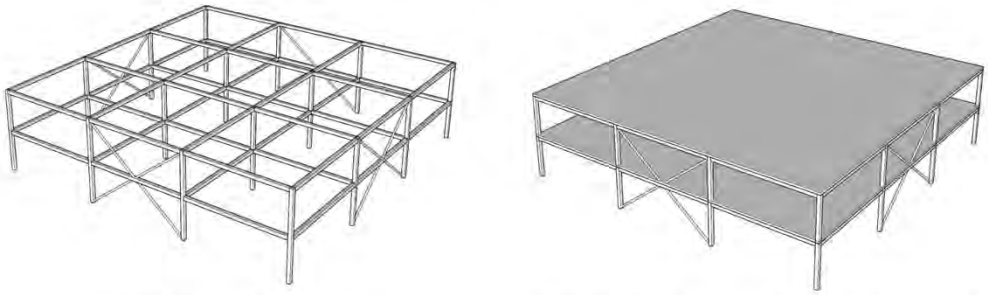

(a) Steel main bearing structure

(b) Steel main bearing structure (including the floor and roof)

Figure 10.3: 3d model of the case study building

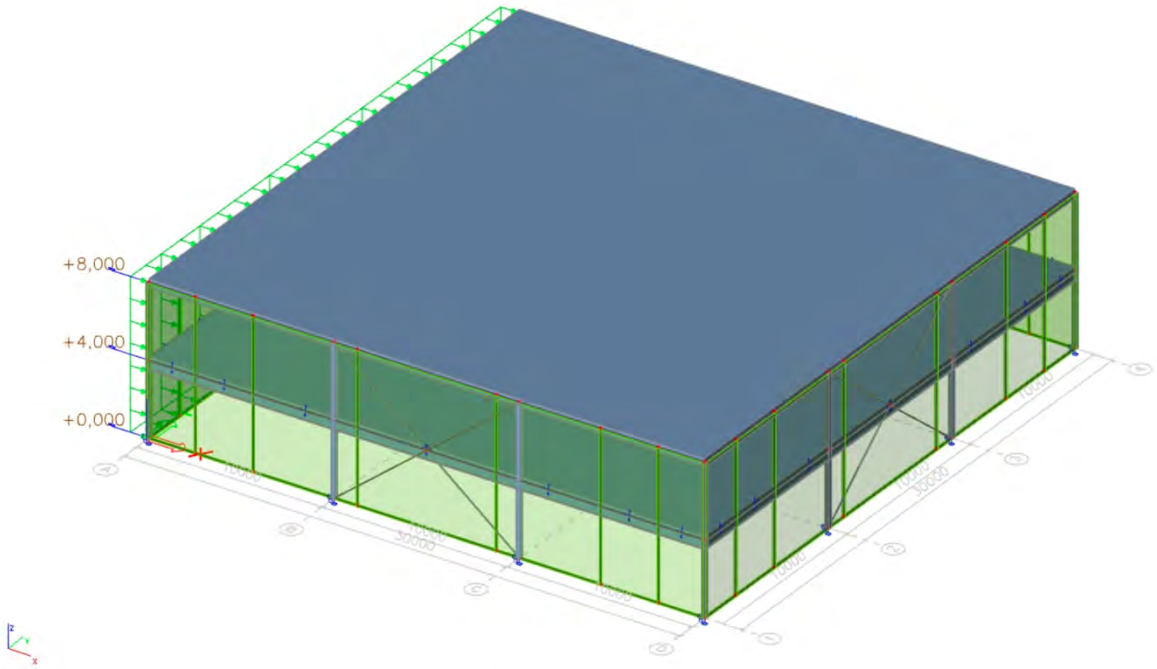

Figure C.1: Render of the Case Study Building in the SCIA FEM

12.2.4. Internal column (S13)

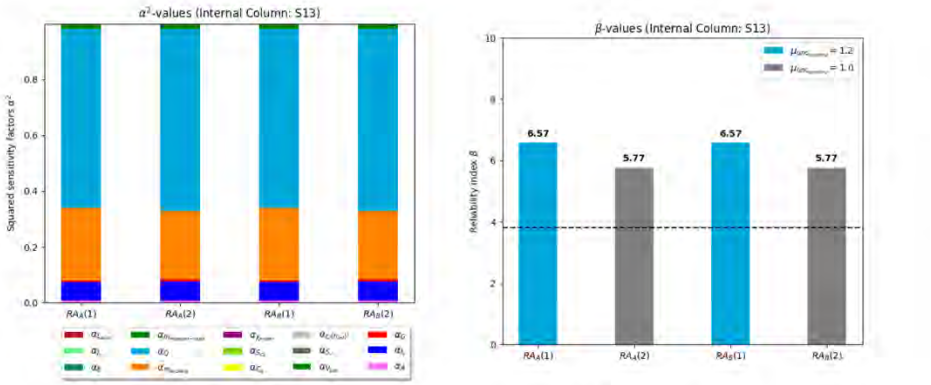

(a) Sensitivity factors α^2 (b) Reliability index values β

Figure 12.4: Sensitivity factors α^2 of the stochastic variables and β-values of the reliability assessment for internal column (S13) with HEA200 profile (deterministic Eurocode design). (A) v_{pot}: Type I GEV (Gumbel) and load effects based on timeseries, (B) v_{pot}: Type III GEV (Weibull) and load effects based on timeseries, (1) $\mu_{m_{buckling}} = 1.2$, (2) $\mu_{m_{buckling}} = 1.0$

	Internal Column (S13)				
u.c. = 0.89	Profile	$RA_A(1)$	$RA_A(2)$	$RA_B(1)$	$RA_B(2)$
Eurocode Design ⟶	HEA200	6.57	5.77	6.57	5.77
	HEA180	5.53	4.69	5.53	4.69
	HEA160	4.39	3.50	4.39	3.50
	HEA140	2.66	1.57	2.66	1.57

Table 12.8: Optimisation of profile for Internal column (S13) based on reliability assessment including both probabilistic action and resistance models

12.2.5. External column (S2)

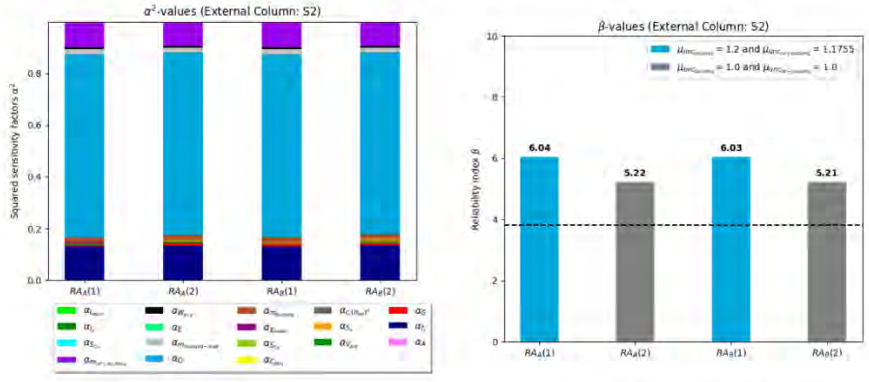

(a) Sensitivity factors α^2 (b) Reliability index values β

Figure 12.5: Sensitivity factors α^2 of the stochastic variables and β-values of the reliability assessment for external column (S2) with HEA220 profile (deterministic Eurocode design). (A) v_{pot}: Type I GEV (Gumbel) and load effects based on timeseries, (B) v_{pot}: Type III GEV (Weibull) and load effects based on timeseries, (1) $\mu_{m_{buckling}} = 1.2$ and $\mu_{m_{lat-buckling}} = 1.1755$, (2) $\mu_{m_{buckling}} = 1.0$ and $\mu_{m_{lat-buckling}} = 1.0$

	External Column (S2)				
u.c. = 0.68	Profile	$RA_A(1)$	$RA_A(2)$	$RA_B(1)$	$RA_B(2)$
Eurocode Design ⟶	HEA220	6.04	5.22	6.03	5.21
	HEA200	4.76	3.89	4.75	3.88
	HEA180	3.37	2.39	3.36	2.38

Table 12.9: Optimisation of profile for External column (S2) based on reliability assessment including both probabilistic action and resistance models

means a net decrease of 10 % in material for this element.

12.2.6. Corner column (S1)

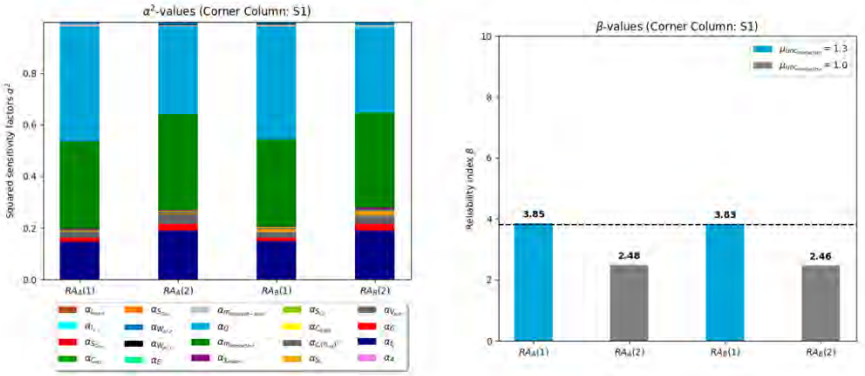

(a) Sensitivity factors α^2

(b) Reliability index values β

Figure 12.6: Sensitivity factors α^2 of the stochastic variables and β-values of the reliability assessment for corner column (S1) with HEA220 profile (deterministic Eurocode design). (A) v_{pot}: Type I GEV (Gumbel) and load effects based on timeseries, (B) v_{pot}: Type III GEV (Weibull) and load effects based on timeseries, (1) $\mu_{m_{interaction}} = 1.3$, (2) $\mu_{m_{interaction}} = 1.0$

	Corner Column (S1)				
u.c. = 0.66	Profile	$RA_A(1)$	$RA_A(2)$	$RA_B(1)$	$RA_B(2)$
	HEA240	5.06	3.83	5.05	3.81
Eurocode Design →	HEA220	3.85	2.48	3.83	2.46
	HEA200	2.40	0.84	2.38	0.82

Table 12.10: Optimisation of profile for Corner column (S1) based on reliability assessment including both probabilistic action and resistance models

M11

Sayantan Pandit

Finite element modelling of open longitudinal stiffener to crossbeam connection in OSD bridges for hot-spot stress determination

The project encapsulates numerical investigation of simple and complex welded connections using finite elements, followed by numerical analyses of OSD bridges, to determine hot-spot stress for fatigue assessment. The aim of my thesis was to improve the modelling technique with shell elements, to obtain accurate hot-spot stress in comparison to the solid element model to save computational time.

Key words: Fatigue, Hot-spot stress, FEM, OSD

Cover Image - Haringvlietbrug: http://www.haringvlietbrug.nl/

Summary of Project:

The phenomenon of fatigue in orthotropic steel deck (OSD) bridges is a predominant problem in the steel industry because of complexity of the stress prediction methods. In the past, many researchers have studied the fatigue behaviour of various connections in OSDs via experiments and Finite Element Modelling (FEM) techniques. In the present research, the connection of open stiffener to crossbeam at the location of cope hole in OSDs has been be studied. Structural hot-spot stress (SHSS) method using surface stress extrapolation has been used to investigate the cracks in stiffener in the longitudinal direction and cracks in crossbeam.

FEM is extensively used for analysing OSDs. In engineering applications, 2D shell elements are widely used instead of 3D solid elements for analysis due to less computational cost. The welds are generally not modelled with shell elements for fatigue assessment of welded structures. In this study, large difference of stresses is obtained by shell and solid elements for both simple and complex fillet welded details and also for the OSD. This difference in structural hot-spot stress (SHSS) is reduced by the application of three weld modelling techniques with shell elements: (i) the IIW approach, (ii) the Eriksson's approach and (iii) a combination of IIW and Eriksson's approaches. All the three methods are based on increasing the thickness of shell elements at the weld region which are easy to be applied in practice. The dependence of SHSS on mesh size and element type has also been investigated in this thesis.

A parametric study is performed first on simple and then on complex fillet welded details to check whether the weld modelling technique can be applied to different geometries, loading and boundary conditions. The solid element model of the complex detail is initially validated with experimental strain measurements. Then, SHSS values from other numerical models are compared with the solid element model. Representative load cases are investigated, followed by load combinations. The weld modelling method with shell elements gave good consistency in the ratio of hot-spot stress compared to the solid element model for these details. The deformations are also investigated for all load cases and load combinations. The combined weld modelling technique with shell elements accurately replicated the weld stiffness of the solid model for both in-plane and out-of-plane load cases.

As a final step in checking the consistency of SHSS ratios between shell elements with welds and solid elements in the application of OSDs, a parametric investigation is performed. This study involved two geometric variants of OSD with different load positions. These two variants were based on design of existing bridges in The Netherlands with relatively thin plates and newly designed ones with thicker plates. The parametric study is divided into two parts. The first part is based on representative load cases. The second part is based on influence lines for determination of critical loading positions having maximum and minimum hot-spot stress. For both these studies, the weld modelling approaches with shell elements gave a good match of SHSS compared to solid models. The SHSS results from shell model with welds are more consistent compared to the regular shell model without weld.

From the preliminary parametric study on OSD, it was found that after weld modelling with shell elements using the combined approach of IIW and Eriksson, less scatter is observed in the SHSS ratios. The coefficient of variation (CV) in SHSS ratio for crossbeam is 6.8% and that for stiffener is around 5.1% which is low. The SHSS values are computed based on the stress perpendicular to weld toe.

From the detailed parametric study, the mean value of SHSS ratio is 1.07 (range: 0.99-1.15) for the crossbeam and 1.02 (range: 0.98-1.10) for the stiffener. The CV of SHSS ratio is 5.4% for the crossbeam and 4% for the stiffener. The stress profiles are also investigated at the critical locations of OSD. The shell model with the combined weld modelling approach is in good agreement with not only SHSS but also with the stress at a distance far away from the stress concentration when compared to the solid model. The deformations are also very similar for both the numerical models. Thus, it is concluded that the combined weld modelling technique using the IIW and the Eriksson's approach with shell elements could be used for accurate fatigue life assessment using hot-spot stress method where the measure of accuracy is with respect to the solid element model.

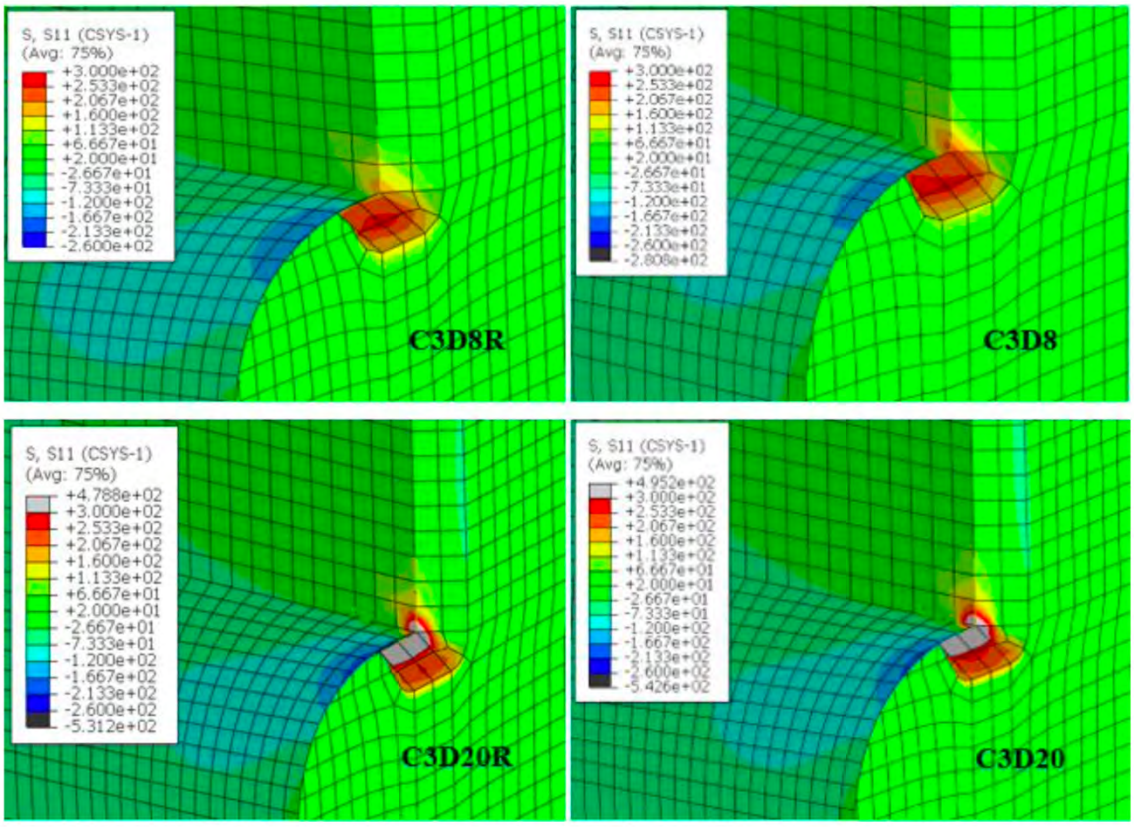

Figure 4.13: Contour plots of stress (S11) for solid models with different element types having same scale

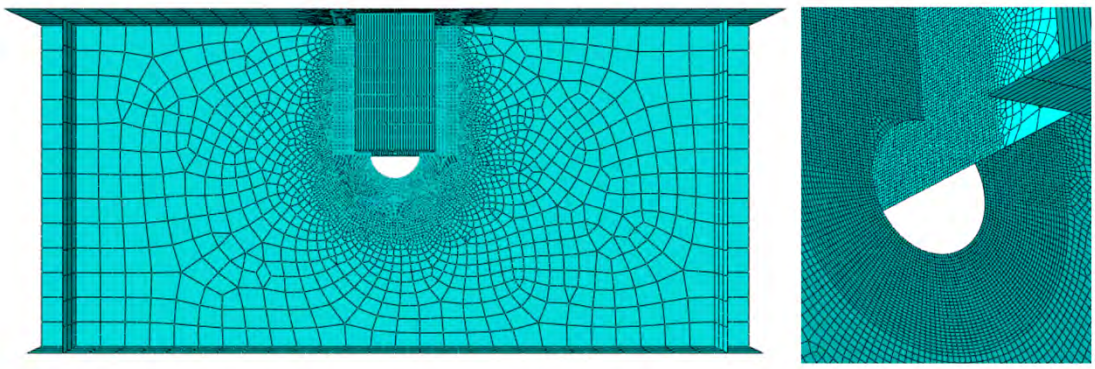

Figure 4.16: Detail with shell elements having a mesh size of 2 mm

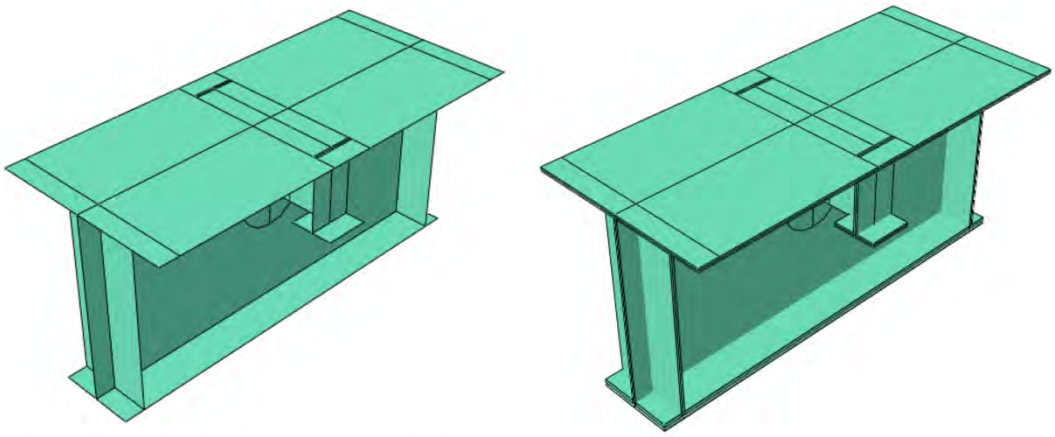

Figure 4.17: Shell element model using mid-plane geometry

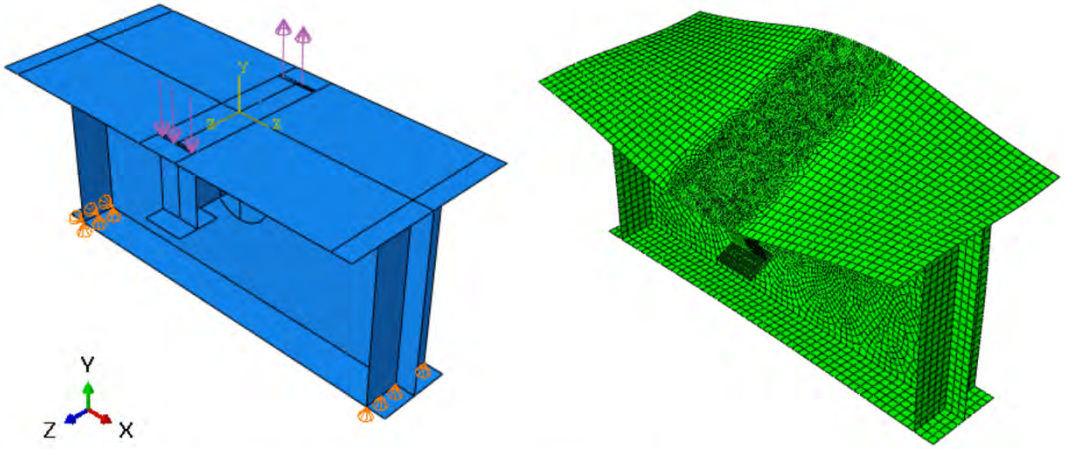

Figure 4.23: Out-of-plane behaviour of the crossbeam: loading and deformed mesh

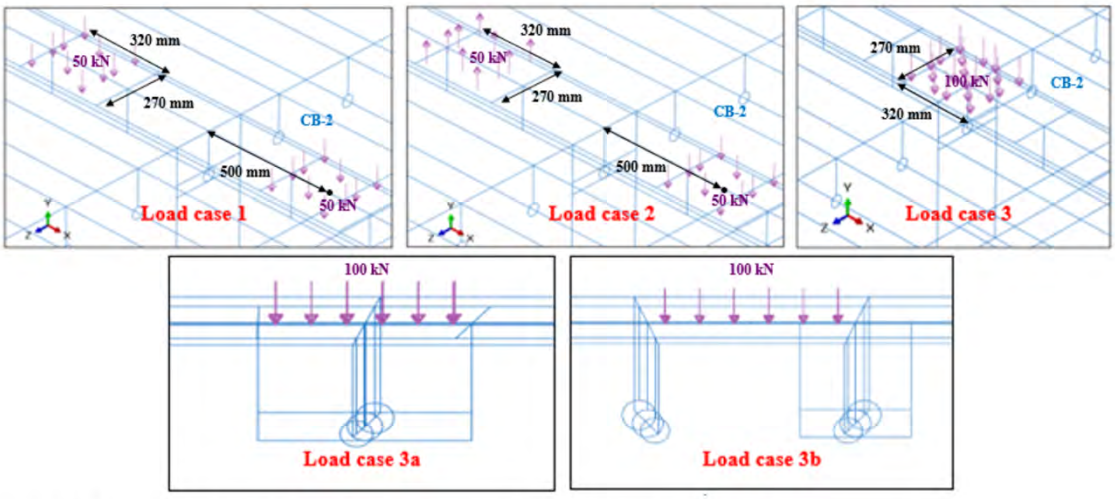

Figure 6.2: Middle crossbeam of the OSD parametric model with the three different load cases

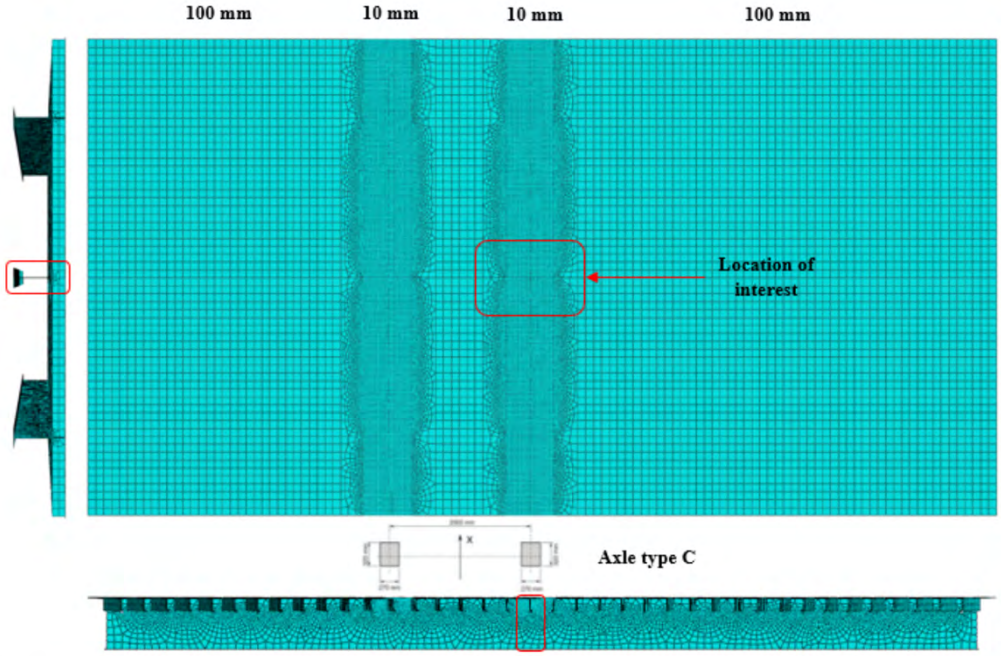

Figure 6.7: Global mesh of the OSD parameter model

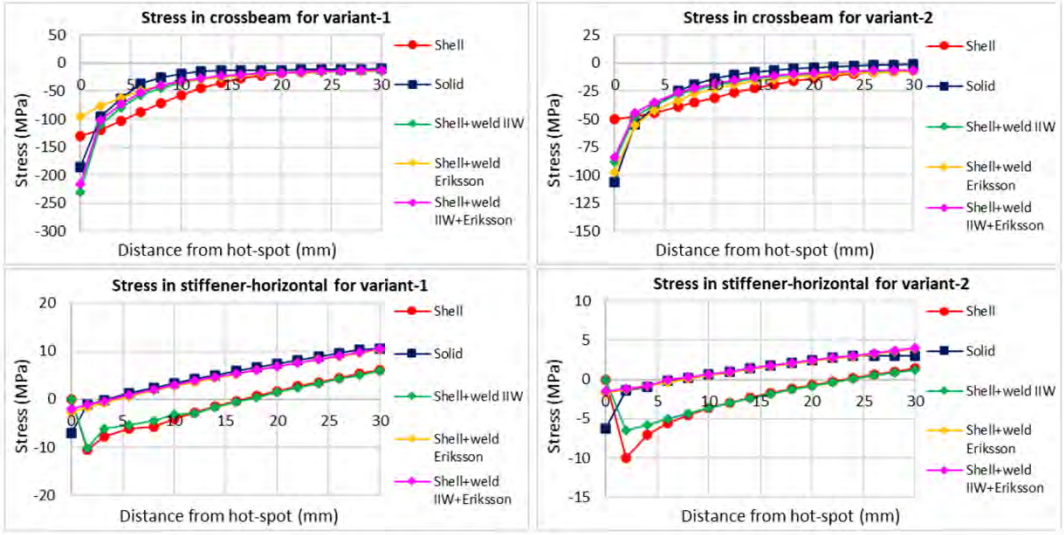

Figure 6.28: Stress distribution perpendicular to weld toe under LC-2

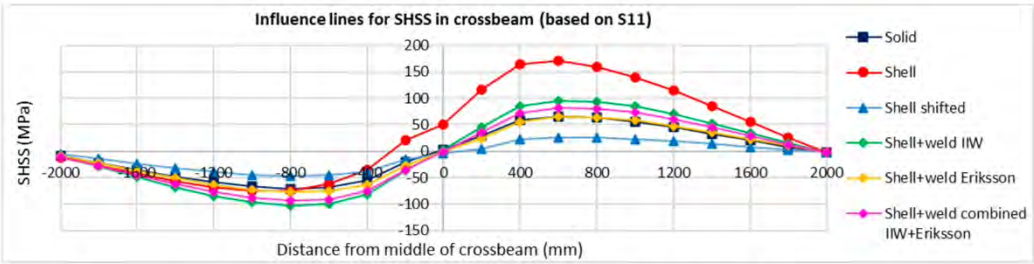

Figure 6.35: SHSS influence lines of crossbeam for variant 1 (old OSD) and axle load path 1 based on type-c calculation

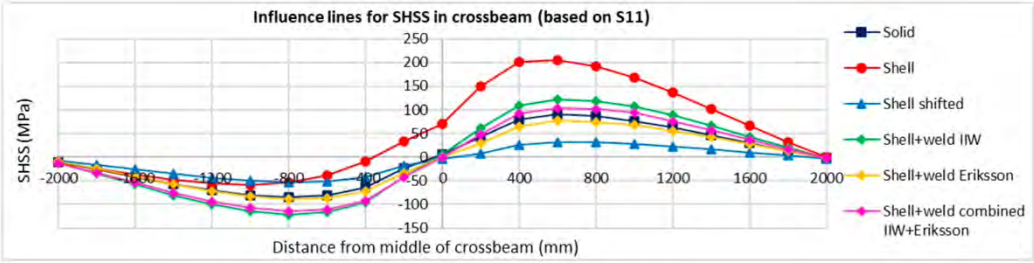

Figure 6.36: SHSS influence lines of crossbeam for variant 1 (old OSD) and axle load path 1 based on type-b calculation

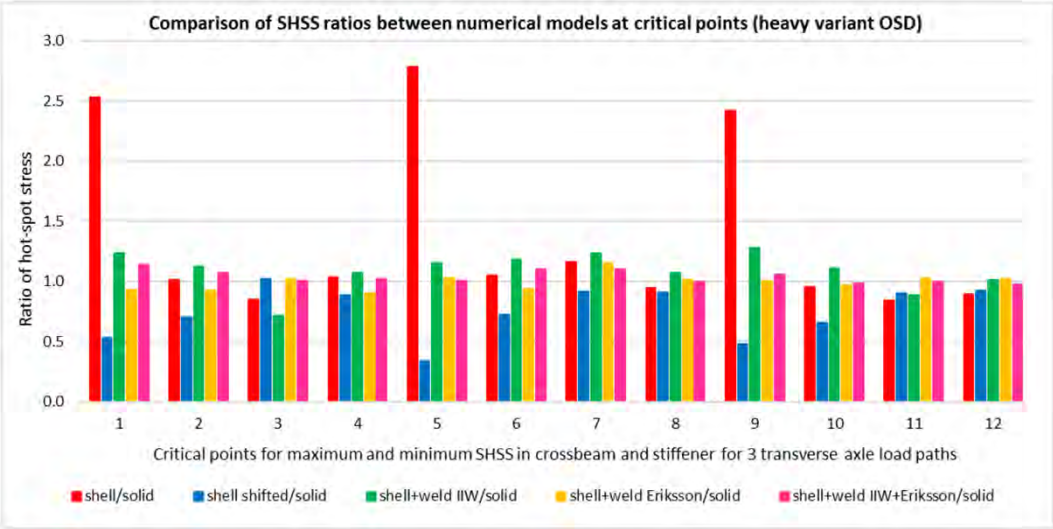

Figure 6.66: Histogram of SHSS ratio for different numerical models of heavy variant OSD based on stress perpendicular to weld toe

M12

Thijs van Gelderen

Truss topology optimization with reused steel elements (vakwerk topologie optimalisatie met hergebruikte stalen elementen)

Hergebruik van staal kan een belangrijke bijdrage leveren aan het verlagen van de CO_2 uitstoot in de bouw. Hergebruik brengt echter veel uitdagingen met zich mee waardoor het in de praktijk nog weinig wordt toegepast. In deze master thesis heb ik een ontwerp tool ontwikkelt die 2D vakwerkconstructies kan ontwerpen met een database van stalen (her)gebruikte elementen. Met deze tool heb ik geprobeerd één van de uitdagingen van ontwerpen met hergebruik te tackelen; namelijk het complexe ontwerpproces. Elk element heeft een individuele lengte en doorsnede en moet zo in de nieuwe constructie worden geplaatst dat deze efficient is. In dit onderzoek heb ik dit bereikt door een bestaande topologie optimalisatie methode, de ground structure method, aan te passen en uit te breiden. De parametrische tool is ontwikkelt in Python en kan meerdere verschillende ontwerpen genereren waarin wordt gestreefd naar een zo hoog mogelijk hergebruik percentage, zo laag mogelijk materiaal volume en een zo hoog mogelijke uitnuttingsgraad van de stalen elementen. Staal is een geschikt materiaal voor hergebruik vanwege de homogene materiaal eigenschappen, mogelijkheden voor demonteren en herconstructie en behoud van kwaliteit. Stalen constructies worden zelden gesloopt vanwege constructieve gebreken. Redenen voor sloop zijn meestal herontwikkeling van het gebied of gebrek aan functionaliteit van het gebouw.

Ontwerptool voor her

Het is van belang dat goede documentatie van gebouwen beschikbaar moet zijn voor componentenhergebruik. Zo wordt duidelijk als een parametrische studie is opgezet voor discrete topologie-optimalisatie (TO) met (her)gebruikte elementen. In dit masteronderzoek is een tool ontwikkeld die vakwerkconstructies kan ontwerpen met een set gebruikte staalelementen. Maar dat heeft zo zijn grenzen.

ir. T.P. van Gelderen, ir. C.A. Slui en ir. P. Lagendijk

Thijs van Gelderen is afstudeer-stagiair bij Aronsohn in Rotterdam en studeerde af op het onderwerp 'parametrisch ontwerpen' aan de Technische Universiteit Delft. Paul Lagendijk is constructief ontwerper bij Aronsohn. Casimir Sluiwas bij Aronsohn raadgevend ingenieur, nu is Slui BIM-adviseur bij FORM in Wateringen. Afstudeercommissie Thijs van Gelderen: drir. M.A.N. Hendriks (voorzitter), ir. L.P.L. van der Linden en ir. S. Pasterkamp.

De bouw is verantwoordelijk voor meer dan 30% van de globale CO_2-uitstoot. Materialen hebben hierin een groot aandeel, de productie van beton en staal draagt bij aan 10% van de wereldwijde uitstoot.
Klimaatverandering dringt aan tot het gebruik van groene energie voor productie en tot recyclen en hergebruik van constructies en elementen. Doordat staal magnetisch en makkelijk te scheiden is van ander afval, wordt meer dan 90% van al het staal gerecycled. Tweederde van het geproduceerde staal komt echter nog van ruwijzer. Daarnaast is voor recyclen veel energie benodigd en leidt maar tot marginale reducties in CO_2-uitstoot. Hergebruik van stalen elementen vereist minder energie en zou daarom een grote bijdrage kunnen leveren aan een circulaire economie.

Hergebruik constructies en componenten

Hergebruik kan worden onderverdeeld in drie categorieën: adaptief, systeem- en componenthergebruik. Adaptief hergebruik wordt vaak toegepast op erfgoedconstructies: verouderde of ongebruikte gebouwen worden geschikt gemaakt voor nieuwe doeleinden. Systeemhergebruik impliceert hergebruik van volledige constructies die uit elkaar worden gehaald en op andere locatie in elkaar worden gezet. Componenthergebruik betekent het hergebruiken van separate elementen: deze categorie is het meest complex en best toepasbaar voor materialen met homogene materiaaleigenschappen, zoals staal. Separaat hergebruik brengt veel vraagstukken met zich mee, een daarvan betreft kosten. Het demonteren van constructies, elemententransport en (her)construeren met nieuwe verbindingen vereist veel arbeid. Dit is kostbaar en maakt gebruik van nieuwe materiaal daarom vaak economisch aantrekkelijker. Een markt moet ontstaan voor de verkoop van elementen uit bestaande gebouwen. Een combinatie van deze markten schaarste van ruwijzer met hoge staalprijzen, kan hergebruik financieel aantrekkelijker maken.
Kwaliteitsgarantie en opslag van elementen zijn opgaven die de aannemer kunnen weerhouden van het toepassen van hergebruikt staal. De kwaliteit van staal is echter in de meeste

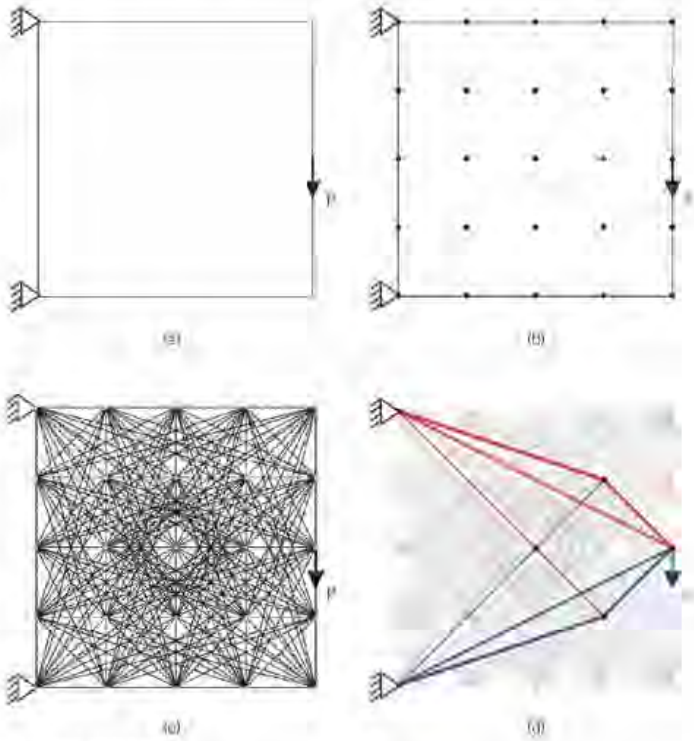

1, Ground Structure Method.

gebruik componenten

2. *Optimalisatieschema.*

gevallen nog goed gebouwen worden meestal gesloopt vanwege gebieds(her)ontwikkeling functionele gebreken of slecht onderhoud. Efficiënt hergebruik van constructies of componenten is afhankelijk van goede documentatie van beschikbaarheid. Platforms als Madaster en New Horizon zijn opgericht om gegevens te verzamelen over materialen en elementen in bestaande gebouwen wat toepasbaarheid van hergebruik zou moeten vergroten.
Ontwerpen met hergebruik van elementen brengt een nieuw *level* van complexiteit met zich mee. In een traditioneel ontwerpproces worden afmetingen van elementen bepaald aan de hand van de geometrie van het ontwerp. Wanneer dit proces wordt toegepast met gebruikte elementen leidt dit al snel tot overgedimensioneerde ontwerpen: het ontwerpproces moet worden omgekeerd waarbij de geometrie wordt bepaald door beschikbare elementen.

Constructieve optimalisatie

Recyclen en hergebruiken zijn twee manieren om de hoeveelheid nieuw materiaal in nieuwe constructies te verminderen. Een derde manier is topologie-optimalisatie waarbij materiaalvolume van de draagconstructie wordt geminimaliseerd. Onderscheid kan worden gemaakt tussen discrete en continuüm topologie-optimalisatie. In de discrete vorm wordt connectiviteit, aantal en positie van elementen geoptimaliseerd. In continuüm optimalisatie wordt de positie van materiaal/element geoptimaliseerd.

Onderzoek

In deze master thesis is discrete topologie-optimalisatie gecombineerd met hergebruikte elementen. Een tool is ontwikkeld die vakwerkconstructies kan ontwerpen met een set gebruikte stalen elementen. De tool is geprogrammeerd in Python waarbij de *ground structure method*[1] van Dorn (1964) is gebruikt als basis voor de optimalisatiemethode. Rekentijd kan worden gereduceerd door *member adding* uit het *member adding schemel*[2] in te schakelen.

Ground structure method

De eerste ontwikkelde discrete topologie-optimalisatiemethode is de *ground structure method*. Een ontwerpdomein wordt gespecificeerd met randvoorwaarden en krachten,

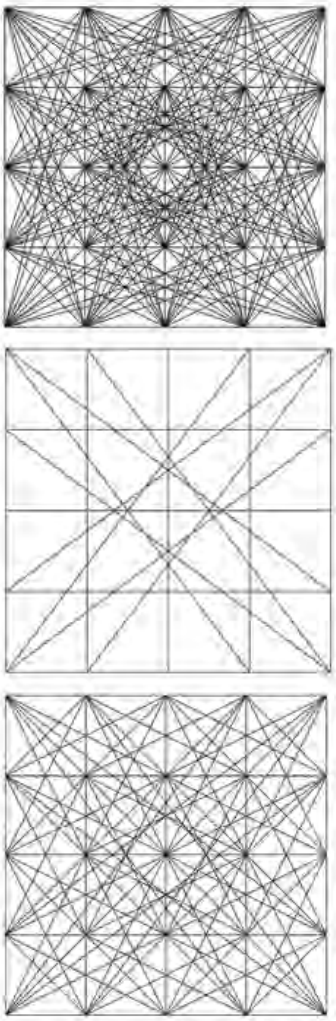

3. *Potentiële memberlijst (PML) (a), gefilterde PML (b), gefilterde PML met tolerantie voor kleine afwijking van lengte (c).*

Enkele websites aanbod tweedehands bouwmateriaal

- Oogstkaart.nl, gratis aanbod.
- Repurpose.nl, adviesbureau.
- SGS.nl, adviesbureau, beslisbomen voor commercieel certificaat in plaats van DoP-certificaat.
- Newhorizon.nl (Material Balance), tussenpersoon, 'gratis aanbod', met commercieel contact met marktpartijen.
- Gebruiktebouwmaterialen.nl, gratis aanbod.
- Madaster.nl, claimen bestanden te hebben van gebouwde projecten aan de hand van BIM-informatie. Abonnementsvorm. Onduidelijk hoe informatie is opgebouwd en is feitelijk bedoeld voor vastgoedontwikkelaars en vooral -beheerders.

en wordt gevuld met knopen zichtbaar in *afbeelding 1(a)* en *afbeelding 1(b)*. *Afbeelding 1(c)* laat alle mogelijke elementen zien tussen de knopen die samen een potentiële memberlijst (PML) vormen. Het oppervlak van elk element wordt geoptimaliseerd waarna een constructie wordt getoond in *afbeelding 1(d)* die voldoet aan evenwicht en maximale druk- en trekspanningen met minimaal volume.

Ontwerptool gebruikte elementen

De optimalisatie bestaat uit een aantal iteratiestappen met als doel het staalvolume te minimaliseren en het percentage hergebruikte elementen en de uitnuttingsgraad van hergebruikte profielen te maximaliseren. Een overzicht van het optimalisatieschema is gegeven in *afbeelding 2*. Topologie wordt geoptimaliseerd met de ground structure method (1) waarna zoveel mogelijk elementen zo efficiënt mogelijk worden vervangen uit een database met elementen voor hergebruik (2), de constructie wordt herberekend (3) en getoetst op efficiëntie, hergebruik percentage en maximale unity check (4). Een *penalty*-systeem is ontwikkeld dat inefficiënte en nieuwe elementen bestraft, wat voorkomt dat deze terug keren in het ontwerp in de volgende en/of opvolgende iteraties. Constructies die voldoen aan alle eisen worden gepresenteerd aan de gebruiker (6).
Geometrische informatie van hergebruikte elementen wordt in de geoptimaliseerde constructie geïmplementeerd door het vervangen van elementen. Voordat de optimalisatie begint, wordt echter al informatie verwerkt in de potentiële memberlijst (PML). De PML in *afbeelding 3(a)* wordt gefilterd met beschikbare lengte(s) uit een database. Alleen elementen met lengtes die beschikbaar zijn, worden beschouwd in *afbeelding 3(b)*. De lengte mag echter wel een stukje afwijken, elementen mogen net te kort of net te lang zijn wat resulteert in een PML met meer mogelijke elementen in *afbeelding 3(c)*.
De optimalisatietool bevat veel verschillende parameters, zoals voor waarden van penalty's. Door de parameters te variëren, kunnen verschillende ontwerpen worden gegenereerd. De beste combinatie van parameters is subjectief: een opdrachtgever kan een ontwerp prefereren met minste volume, minste aantal elementen of hoogste percentage hergebruikte elementen.

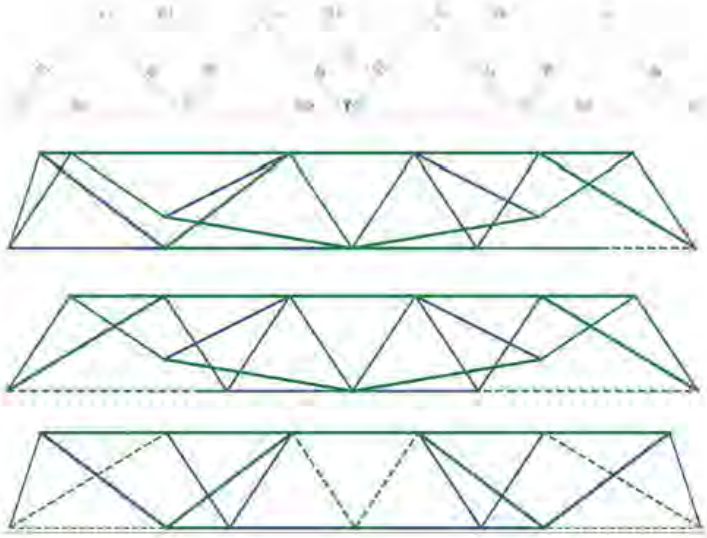

Design	Volume dm³	Members (Elements)	Reuse %	Average UC	Average UC Reused Elements
1	106	32	97	0.73	0.73
2	94	29	90	0.79	0.77
3	94	29	76	0.81	0.75
SCIA	79	14	-	0.96	-

4. Voorbeeldberekening vakwerkligger (L = 22 m, h = 3 m), tweezijdig scharnierend opgelegd met een centrale, verticale puntlast van 355 KN. Groene lijn: 0,75 < UC < 1,0. Blauwe lijn: 0,35 < UC < 0,75. Gestippelde groene lijn = nieuw element.

Beperkte omvang

De tool is effectief voor ontwerpdomeinen met beperkte omvang. Wanneer de grootte van het ontwerpdomein toeneemt en daarmee het aantal knopen en mogelijke elementen, dan neemt de complexiteit snel toe en effectiviteit van de ontwerptool af.
Een voorbeeld (*afb. 4*): een vakwerkligger met een overspanning van 22 m en constructiehoogte van 3 m, scharnierend opgelegd aan beide zijden met een puntlast van 355 KN in het midden in verticale richting. De beschikbare dataset bevat acht profieldoorsnedes (van 400 mm² tot 800 mm²) met verschillende lengtes (van 3,2 m tot 6,0 m), in totaal 62 elementen. De maximale toegestane trek- en drukspanning zijn respectievelijk 355 en 248 N/mm² wat resulteert in ontwerpen met veel elementen. De constructies zijn uitsluitend getoetst op druk en trek, er zijn geen restricties op overlappende en kruisende elementen.
Na het doorlopen van de optimalisatie zijn elf verschillende ontwerpen gevonden waarvan drie zijn gepresenteerd waarbij de boven- en onderrand enkele overlappende elementen bevat. Volumes in dm³ staal.
Een standaardontwerp in SCIA met nieuwe elementen bestaande uit zeven driehoeken leidt tot een volume van 79 dm³. Dit ontwerp

Literatuur
1. W.S. Dorn, R.E. Gomory en H.J. Greenberg, 'Automatic Design of Optimal Structures', *Journal de Mecanique* Vol. 3 (maart), 1964.
2. H. Liuwei, M. Gilbert en X. Song, *A Python script for adaptive layout optimization of trusses*, Springer Nature, Cham (CH) 2019.

Foto's: Kees Hummel

5. De renovatie van Hoogstraat 168-172 in Rotterdam, project met hergebruik van staalprofielen.

is vergeleken met de ontwerpen met hergebruikte elementen. Volumetoename kon worden gelimiteerd tot 19% in het ontwerp met 90% hergebruik waarbij 29 van de 62 beschikbare elementen verwerkt zijn in het ontwerp.

Conclusies

De ontwikkelde tool is voor kleine ontwerpdomeinen geschikt om het complexe ontwerpproces met (her)gebruikte elementen te vereenvoudigen. Verschillende ontwerpen kunnen worden gegenereerd waarbij efficiëntie en hergebruikpercentage wordt gemaximaliseerd.
Topologie-optimalisatie resulteert in ontwerpen met minder volume ten opzichte van standaardontwerpen. Gecombineerd met hergebruikte elementen valt of staat dit met de geschiktheid, hoeveelheid en diversiteit van profieldoorsneden van de beschikbare elementen.
In het voorbeeld in dit artikel met beperkte beschikbaarheid, kon het volume niet worden gereduceerd. De volumetoename ten opzichte van standaardontwerpen met nieuwe elementen kon nog meer worden beperkt.
Zeer efficiënte ontwerpen konden worden gegenereerd met een gemiddelde unity check dichtbij de maximale unity check.
Dit benadrukt het belang van goede gebouwdocumentatie beschikbaar voor hergebruik.
Gegevens van bestaande gebouwen worden echter niet zomaar vrijgegeven.
Om de toepasbaarheid van de ontwerptool te vergroten, moet worden onderzocht of knik, knoopinstabiliteit, eigengewicht, doorbuigingseisen, en restricties op overlappende en kruisende elementen kunnen worden toegevoegd.
Het analyseren van een reductie in opgeslagen CO_2 en energie en een kostenberekening ten opzichte van ontwerpen met nieuwe elementen kan meer inzicht geven in de aantrekkelijkheid van ontwerpen met hergebruikte elementen. •

M13

Koen Gribnau

Shear force in bolted connections for hybrid steel FRP bridges due to traffic, temperature and fatigue loading

To extend the lifespan of bridges with deck problems, the deck can be replaced with an FRP deck. Before this solution can be applied, the relevant static and fatigue forces on the bolted connectors must be investigated. 55 existing girder and arch bridges have been modelled to investigate the shear forces in the connectors. The results show that when replacing the bridge deck, the shear force in the connectors is one of the aspects to be considered.

Fibre reinforced polymers (FRP) can be a solution for future bridge renovation when only the deck of the bridge needs replacement. In these cases the deck is replaced with an FRP sandwich panel deck. The main advantages are a high strength-to-weight ratio which is beneficial for the ever heavier lorries and the fast installation which prevents hindrance. To connect the FRP deck with the steel superstructure, bolted connectors are used. One of the aspects that needs to be investigated before the bolted connectors can be applied are the relevant loads on the bolted connectors. The focus of this thesis will be to investigate the relevant static and fatigue forces on the connectors.
55 existing girder and arch bridges have been selected from a database of Rijkswaterstaat. For each bridge an appropriate FRP deck has been designed with an analytical method. The bridges are modelled in SOFiSTiK to investigate the shear forces in the connectors. The layout of the bolted connectors is kept constant for all bridges, as well as the transverse stiffness of the connector. The shear forces are calculated with a linear analysis. Before the static and fatigue analyses, first the hybrid interaction of the model is investigated. The hybrid interaction is the amount of horizontal forces transferred between the FRP deck and the steel superstructure. Hybrid interaction is beneficial as it increases the strength of the structure. Two models of a generic bridge have been investigated, the first is the standard model which is supposed to use hybrid interaction. The second model is an adjusted version to create a non-hybrid model. Three parameters are investigated: the deflection, the slip and the longitudinal stress over the height of the beam. The results show that hybrid interaction is created with the bolted connectors in the standard model.
In the static analyses two loads are investigated: traffic loads and temperature loads. The shear forces in the longitudinal direction are investigated as this is the governing direction. Before the loads are applied on the existing bridges, first a generic bridge has been investigated to gain knowledge over three bridge parameters. First the facing laminate of the FRP deck is changed. Second the direction of the webs of the FRP deck, and this also changes the connector layout due to feasibility. Third the expansion coefficient of the resin is changed. For traffic loads mainly the direction of the webs influences the shear forces in the connectors. For temperature loading the shear forces are largely depending on the expansion coefficient of the laminate, the close the expansion coefficient to the expansion coefficient to the steel superstructure, the lower the shear forces. The existing bridges that have been investigated resulted in a large scatter in results. The layout of the superstructure of the bridge influences the facing laminate and the number of connectors, which influences the maximum shear forces in the connectors. For both traffic and temperature loads, the connectors close to the supports experience the highest shear forces.
Besides the static loading, also fatigue is investigated. The shear forces in the connectors are calculated for one bridge, namely the approach bridge Nieuw Vossemeer. This bridge is one of the heaviest loaded bridges in the static analyses and it is according to expect judgement facing deck problems. Two aspects are investigated in the fatigue analysis, first the magnitude and second the type of load cycles. The magnitude is important as this needs to be below the slip resistance of the bolted connectors. The type of load cycles is important as this is related to how damaging the load cycle is. Because there are no S-N curves for bolted connectors between an FRP deck with a steel superstructure, the damage cannot be calculated. The R-ratio is used to investigate the type of load cycles. To calculate the R-ratio of a load cycle, the minimum shear force is divided by the maximum shear force. The resulting number expresses the type of load cycle. For the results, distinction has been made between the connectors close to the supports and connectors in the lengthwise middle of the bridge span. Both the magnitude as the type of loading is different.
Finally, it is concluded that the shear forces in the connectors is one of the aspects to be considered when designing a bridge with hybrid interaction between the FRP deck and steel superstructure. A large scatter of shear forces can be expected, depending on the bridge layout. Incorrect deck design can result in unnecessary high shear forces. The connector layout can be optimised to make the design more cost efficient.

Timeline of constructed bridges

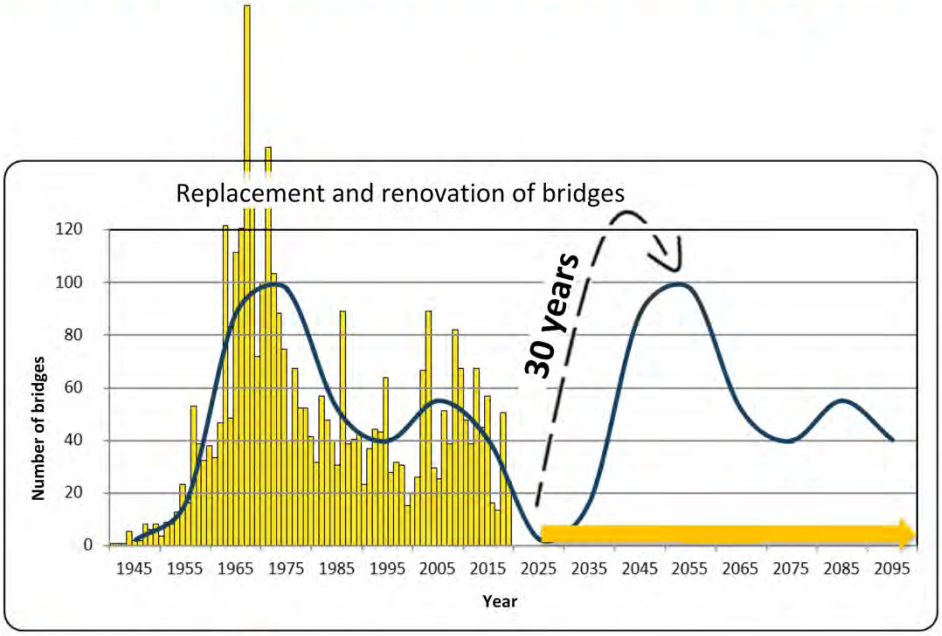

Rijkswaterstaat

Shear force in bolted connections for hybrid steel-FRP bridges

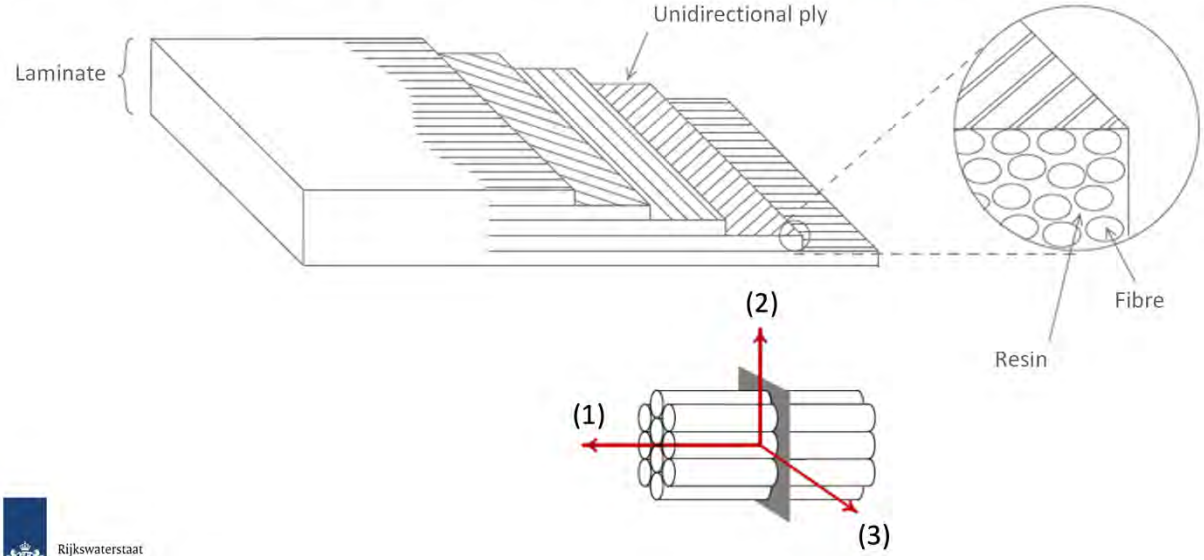

Rijkswaterstaat

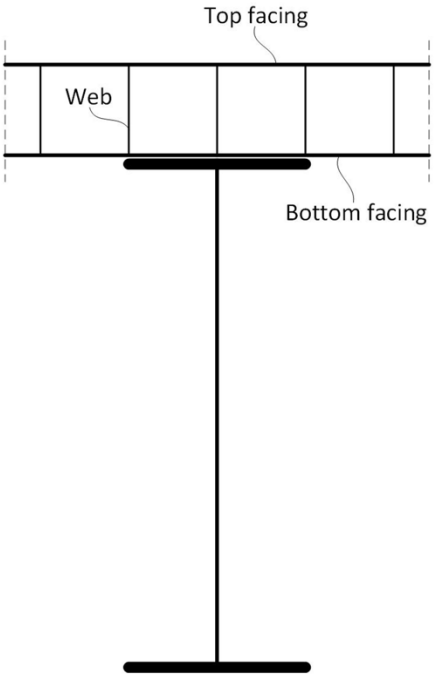

R-ratio distribution

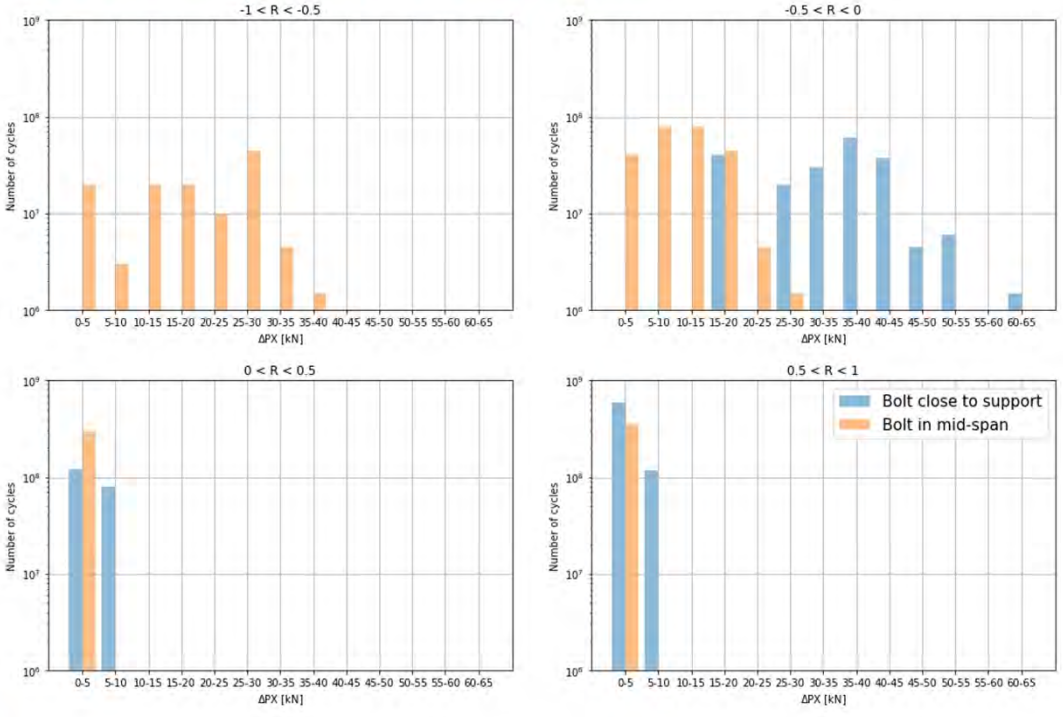

Multiple lorries

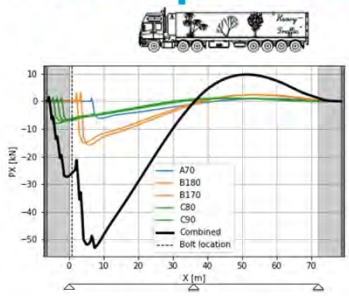

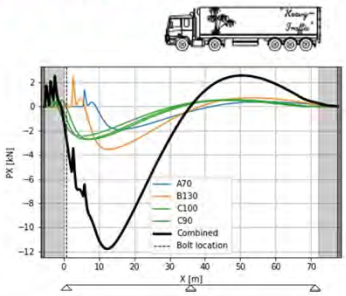

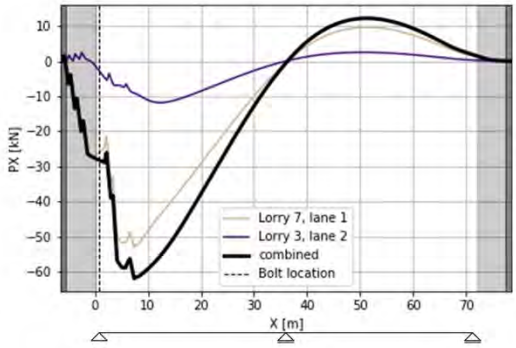

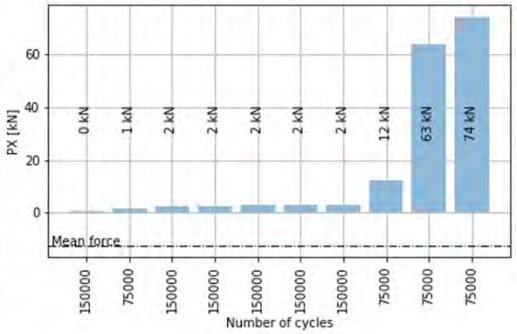

Rijkswaterstaat

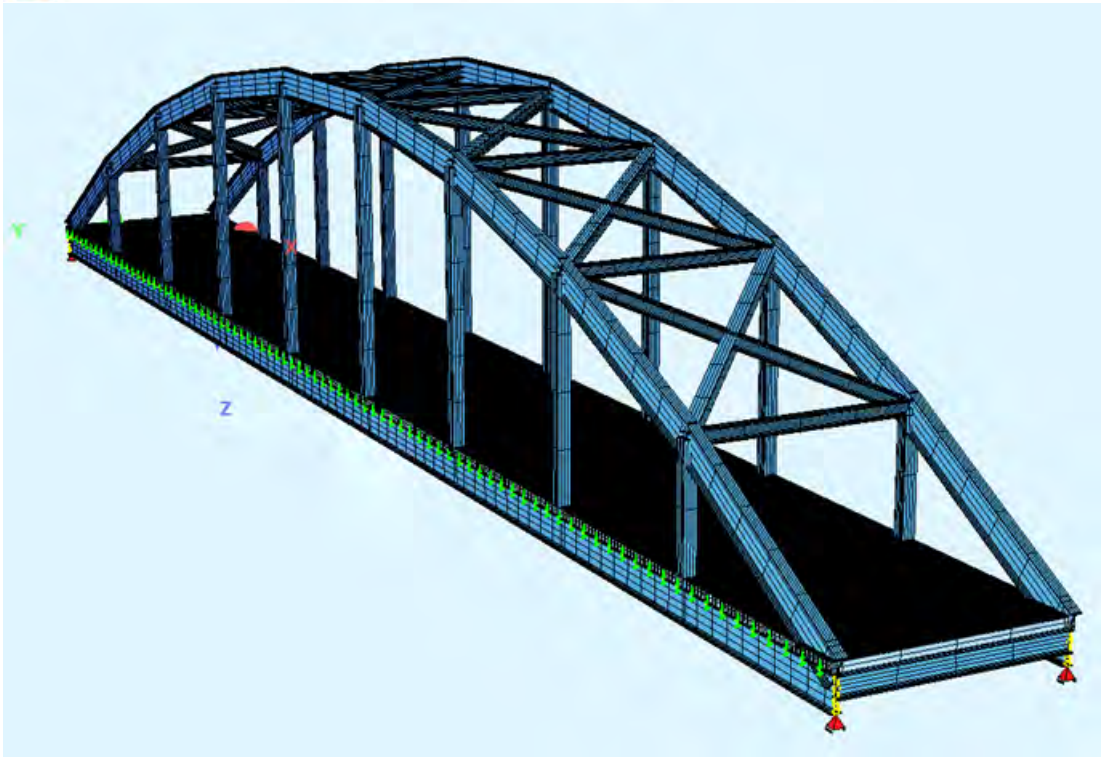

M14

Mees Wolters

Novel mesoscale modelling method for complex composite geometries – Applied onto wrapped composite joints of circular hollow sections

The wrapped composite joint shows promise to replace conventional welded joints in tubular structures subject to fatigue loads, improving its fatigue performance considerably. To understand these complex joints numerical simulations are performed. A methodology is proposed which enables the creation of complex composite laminates on the mesoscale level. The resulting mechanism based tool enables to track damage onset and evolution within the wrapped composite joint with high-fidelity.

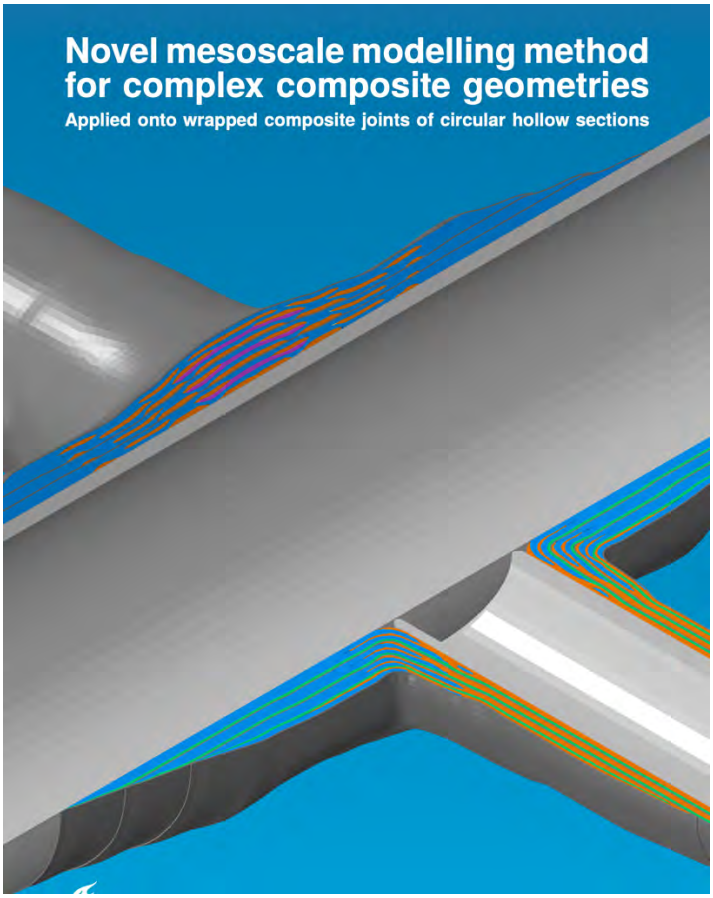

M15

Tim Kapteijn

Feasibility study into the application of wrapped FRP joints on large diameter monopile dolphins – A study into the bending moment capacity of the wrapped pile splice

Fatigue resistant Wrapped Fibre Reinforced Polymer (wFRP) joints may have large potential in replacing the welded tubular connections in marine structures where design is governed by the fatigue limit state (FLS). In large diameter monopile dolphins the structural dimensions exceed the sizes for which spirally welded tubes can be produced. The monopile dolphin is designed with steel cans of 3 meter length connected by fatigue sensitive circumferentially butt welded splice joints. Application of an uniaxial wFRP joint on this large diameter monopile dolphin may greatly improve the utilisation in fatigue limit state allowing an overall steel thickness reduction. Design calculations indicate a potential steel material reduction of 40%. Additional benefits are a reduced coating area and improvement of the local buckling resistance of the large diameter steel tube. Experimental results on small scale uniaxial wFRP joint specimens indicate outstanding performance instatic bending, reaching 100% of the plastic bending moment capacity of the steel section. Preliminary FEA underpredicts the wrapped joint performance, but tuning the steel-FRP interface parameters result in a good fit of FEA with experimental results. In upscaling the small scale wrapped joint FE model a reduction in bending moment capacity compared to the plastic bending moment capacity of the steel section is observed. More research is needed on this size effect for uniaxial wFRP joints prior to application in full scale monopile dolphins.

Feasibility study into the application of wrapped FRP joints on large diameter monopile dolphins

A study into the bending moment capacity of the wrapped pile splice

Fatigue resistant Wrapped Fibre Reinforced Polymer (wFRP) joints may have large potential in replacing the welded tubular connections in marine structures where steel design is governed by the fatigue limit state (FLS). In large diameter steel monopile dolphins the structural dimensions exceed the sizes for which spirally welded tubes can be produced. The monopile dolphin is designed with steel cans of 3 meter length connected by fatigue sensitive circumferentially butt welded splice joints. Application of an uniaxial wFRP joint on this large diameter monopile dolphin may greatly improve the utilisation in fatigue limit state allowing an overall steel thickness reduction. As steel has a significant carbon footprint, reducing the amount of steel in monopile dolphin design by considering innovative connection technologies is of interest. Figure 1 indicates a typical load case for monopile dolphins.

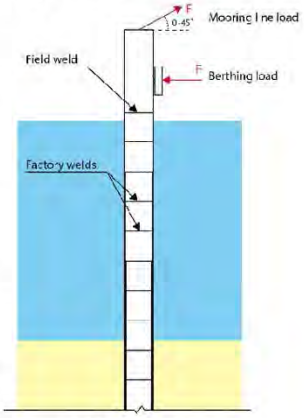

Figure 1 Monopile dolphin typically loaded in bending

To realize these steel savings in monopile design, the bending moment capacity of the wFRP joint should be sufficient. An experimental campaign on small scale specimen ($\emptyset 168.3 - 5$) is set up to assess the bending capacity of a wFRP joint. The 4-point-static-bending test set-up and finite element model is presented in Figure 2. The specimen is painted white to obtain surface strains with 3D digital image correlation. By tuning the model parameters of the steel-FRP interface a very good fit is obtained between the experimental static bending results and the finite element model in Abaqus.

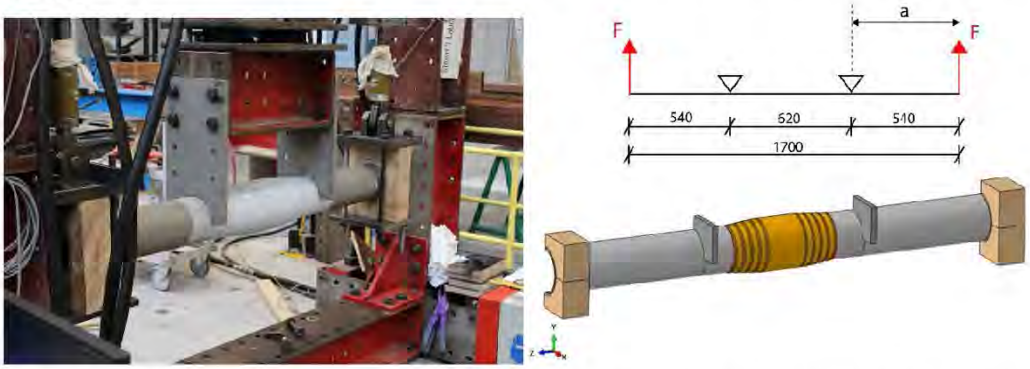

Figure 2 Left: 4-point-bending test set-up in the Stevin laboratory at the Delft University of Technology. On the right the finite element model is shown using symmetry to reduce computational time.

For small scale welded pile splices the uniaxial Wrapped Fibre Reinforced Polymer (wFRP) joint may be a serious alternative considering the static bending moment capacity. With a relatively short wrapping length a high bending moment capacity is reached. Based on the strong size effect observed in upscaling the wFRP joint Finite Element (FE) model, application of the uniaxial wFRP joint on a single splice in a large diameter monopile dolphins seems unfeasible with current joint design. For the reference structure 40% of the steel material can be saved by an overall thickness reduction when all welded pile splices are replaced by a wFRP joint, but considering the needed overlap lengths in order to transfer bending moments this solution converges to a monopile dolphin totally wrapped by FRP.

Tim Kapteijn – Master thesis - Structural Engineering - Delft University of Technology

M16

Lars Bogers

Application of a plug & play connection as a beam-to-column connection in a steel frame

Onderzoek naar de sterkte en stijfheid van een plug & play verbinding en identificatie van de kritieke onderdelen van de verbinding en evaluatie voor herbruikbaarheid.

Application of a plug & play connection as a beam-to-column connection in a steel frame

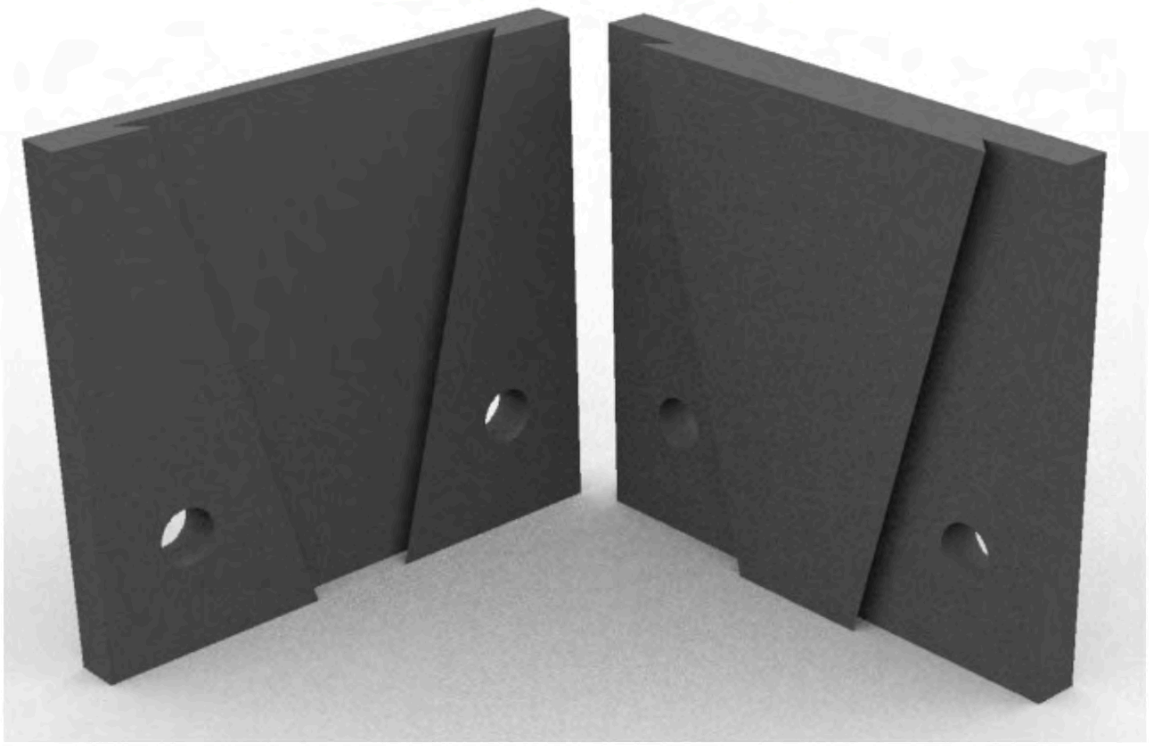

Abstract

A steel frame is designed which is expandable and reducible at any time. In order to reduce the assembly and disassembly time of the frame a new type of beam-to-column connection is proposed, a so-called plug & play connection. The design codes cannot be used for the estimation of the structural perfor- mance of this connection. Therefor the following objective is defined:

What is the structural performance of the plug & play connection and how can the connection be reusable?

In the state of art the benefits and problems plug & play connections offer over traditional steel connections is given. A case study of a steel frame, which consists of stacked units with fixed dimensions, is described. For this case study a global analysis is performed to investigate the possible internal forces on the plug & play connection.

With the results obtained from the state of art and the global analysis an initial design is made. This initial design assumes a perfect fitted connection. Both the stiffness of a column major and minor axis joint is investigated for a hogging, sagging and out-of-plane bending moment. For all cases the joint is classified as semi-rigid. The inclined parts of both socket and plug will yield for all cases and the highest plastic strain will occur in the inclined parts of the connection. The thin base plate of the socket causes that the socket shows a bending deformation for all displacement cases, this bending deformation makes that the plug will be easier to pull the plug out of the socket, which reduces the stiffness.

So an optimized design is checked for the minor axis case. For this optimized design the base plate thickness of the socket is increased in order to prevent the bending deformation of the socket. This optimized design also includes tolerances. The optimized design has removed the bending deformation of the socket. For a downwards displacement slip will occur, as a consequence of the tolerances, before contact between plug and socket is initiated. No slip will occur for an upwards or out-of-plane displacement as the bolt will be immediately in tension. So for the downwards case the initial stiffness is depending on the contact between plug and socket, while for the upwards and out-of-plane displacement the initial stiffness is provided by only the bolts. For all cases the stiffness is increased compared to the initial design.

The final step is to evaluate the re-usability of the connection. The plastic deformation has to be limited in order to be able to reuse the connection. For the upwards and out-of-plane case, in the optimized design, no plastic strain occurs in the inclined parts of the connection when the moment is below the elastic moment resistance. This is because the elastic moment resistance is only provided by the bolts. For the downwards case there is plastic deformation in the inclined parts. However, increasing the thickness of the plug has reduced the maximum plastic strain compared to the initial design. So when the moments on the connection are below the elastic moment resistance the connection should be reusable. A visual inspection should prove whether the plug still fits in the socket.

A real test should prove whether the plug & play connection reduces the assembly and disassembly time. If this is the case, then the moments on the joint should below the elastic moment resistance, so the connection could be reused. The joints will not be classified as rigid, so their semi-rigid behaviour should be taken into account in the global analysis.

Figure 3.3: ConXR connection [4]

Figure 3.4: ConXl connection [4]

Figure 3.5: ConX gravity connection [4]

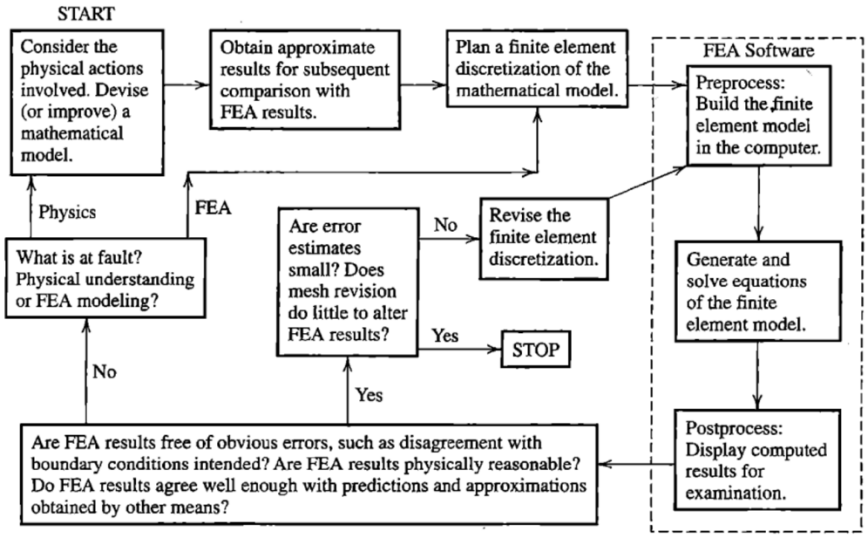

Figure 4.1: Outline finite element analysis [7]

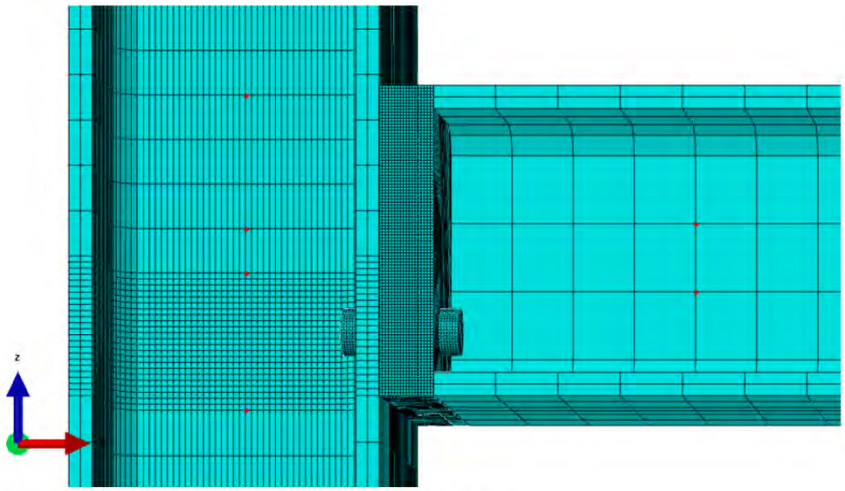

(a) With mesh

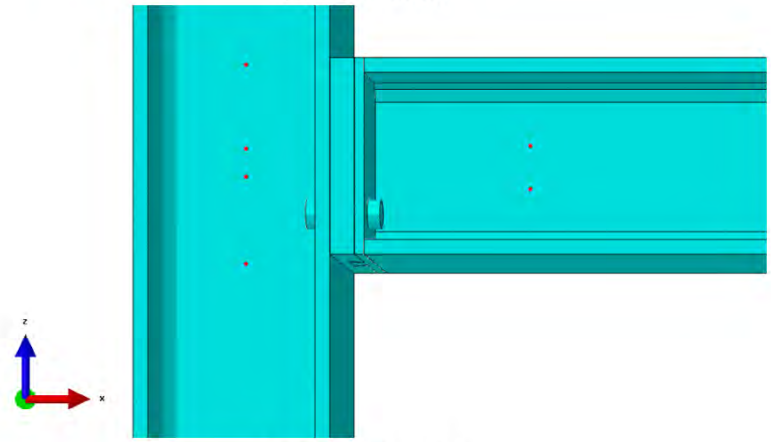

(b) Without mesh

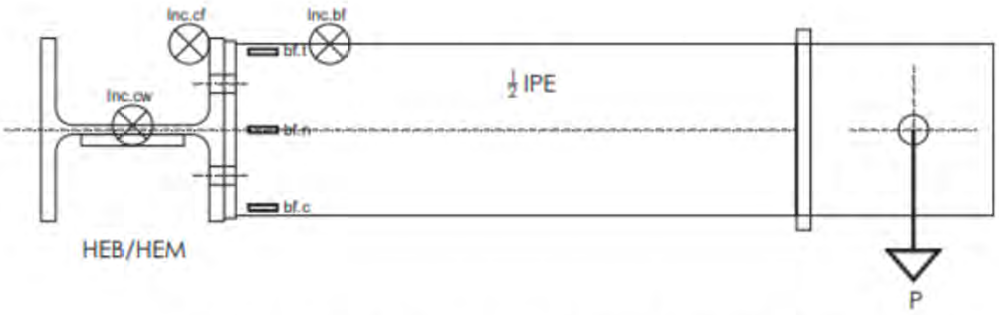

Figure 7.10: Test setup out-of-plane bending [10]

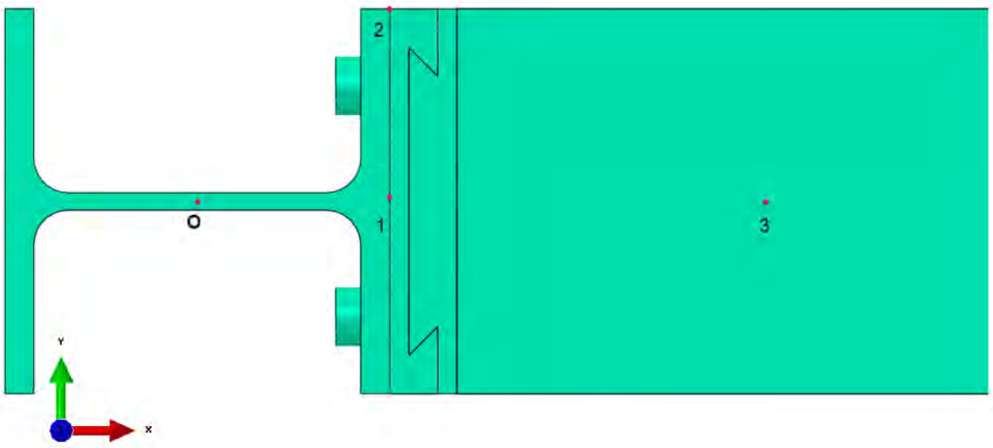

Figure 7.11: Location data point for out-of-plane bending

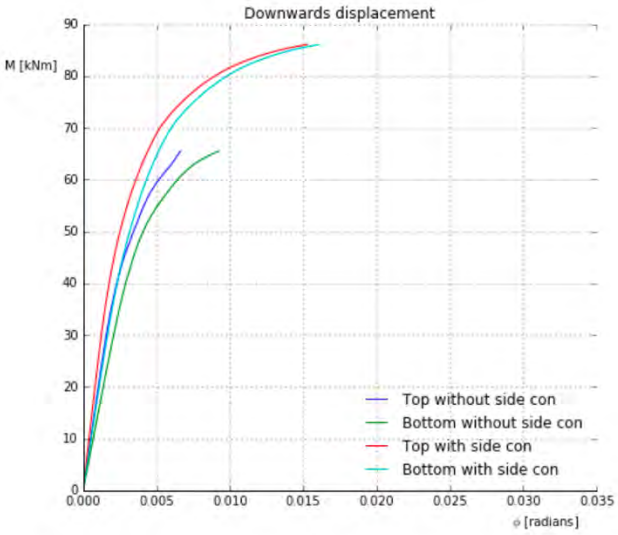

Figure 7.15: $M - \phi$ curve for model with and without side con

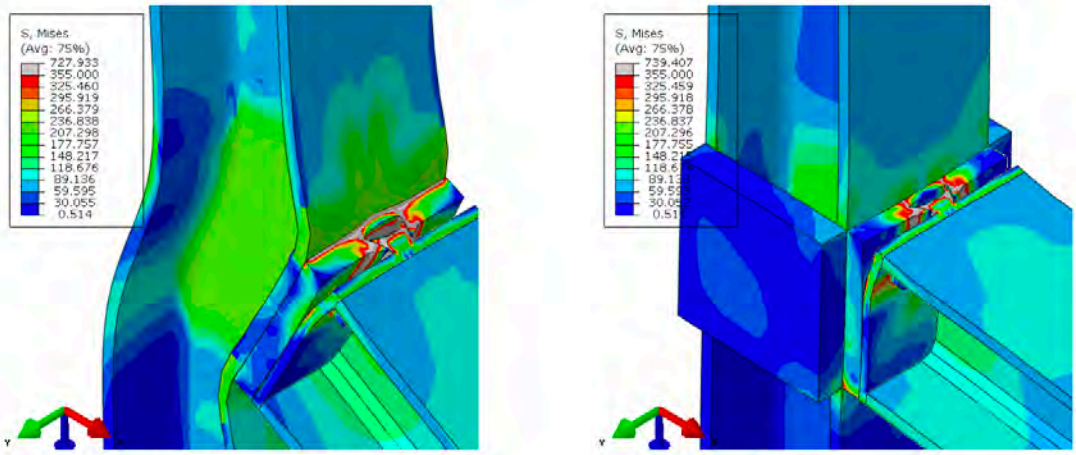

(a) Von Mises (b) Von Mises

Figure 7.25: Von Mises stress (scale factor 20)

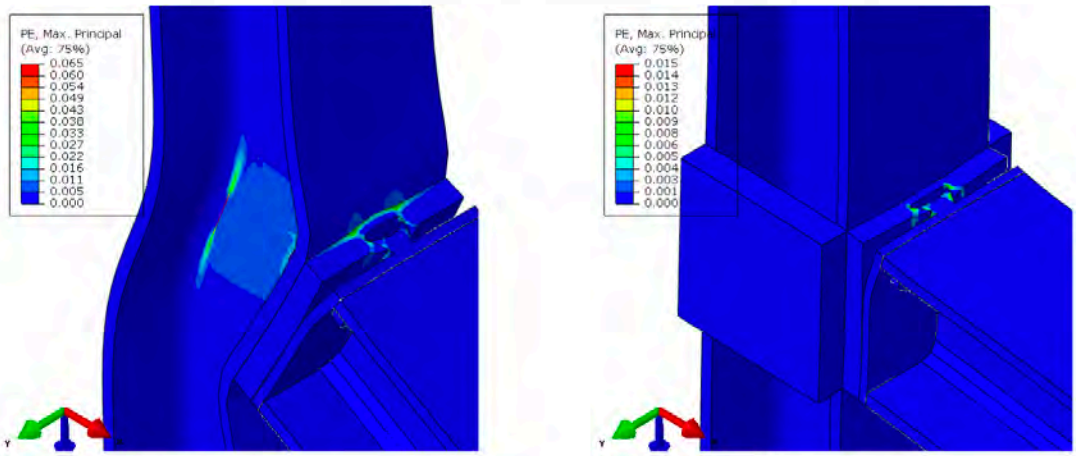

(a) Plastic strain (b) Plastic strain

Figure 7.26: Plastic strain (scale factor 20)

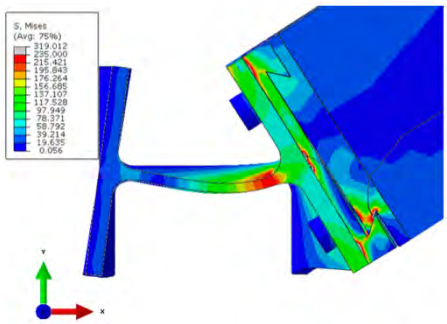

(a) Von Mises (limit legend 235MPa)

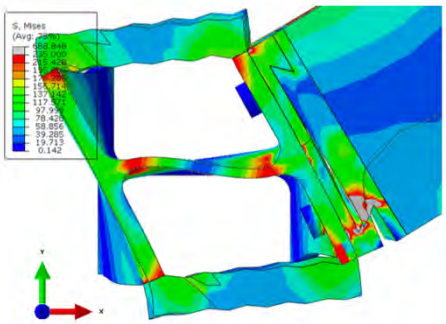

(b) Von Mises (limit legend 235MPa)

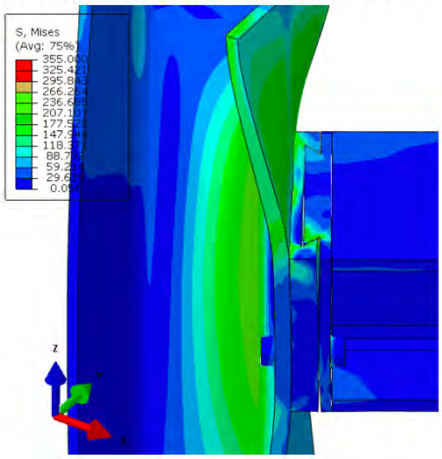

(c) Von Mises (limit legend 355MPa)

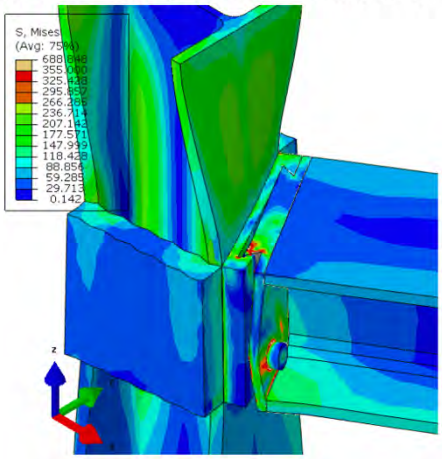

(d) Von Mises (limit legend 355MPa)

Figure 7.31: Von Mises stress (scale factor 20)

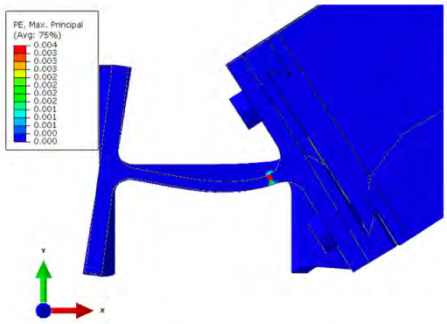

(a) Plastic strain

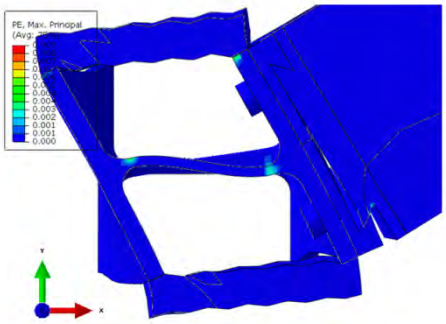

(b) Plastic strain

Figure 7.32: Plastic strain (scale factor 20)

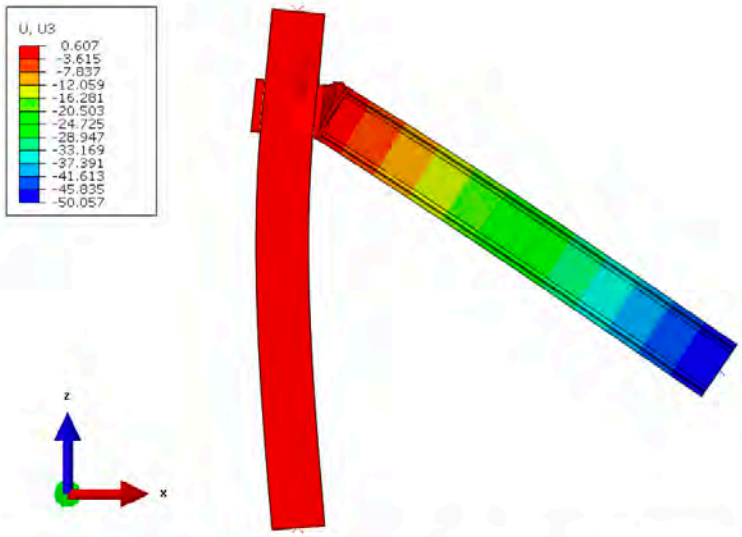

Figure 7.38: Deformed model (scale factor 20) downwards displacement

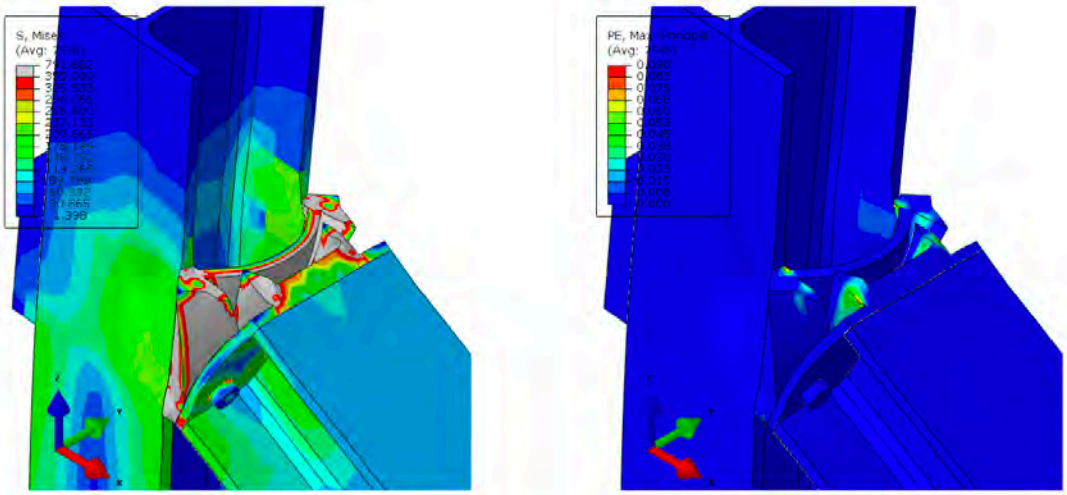

(a) Von Mises stress

(b) Plastic strain

Figure 7.39: Von Mises stress and plastic strain (scale factor 20)